
TÜRKİYE CUMHURİYETİ'NİN YÜZÜNCÜ YILI
Modern Approaches to
Traffic Safety and Sound Insulation
Editor
Kurtuluş ARTIK
BİDGE

BIDGE Publications

Modern Approaches to Traffic Safety and Sound Insulation

Editor: Kurtuluş ARTIK

ISBN: 978-625-372-267-8

Page Layout: Gözde YÜCEL

1st Edition:

Publication Date: 25.06.2024

BIDGE Publications,

Certificate No: 71374

www.bidgeyayinlari.com.tr - bidgeyayinlari@gmail.com

Krc Bilişim Ticaret ve Organizasyon Ltd. Şti.
Güzeltepe Mahallesi Abidin Daver Sokak Sefer Apartmanı No: 7/9 Çankaya / Ankara

Content

CHAPTER I

Improving Accuracy and Reliability in Traffic Accident Severity Analysis Utilizing Robust Logistic Ridge Regression

Kadir Berkhan AKALIN[1]
Arzu ALTIN YAVUZ[2]
Murat KARACASU[3]

Introduction

In transportation and traffic engineering, safety, efficiency, and sustainability are considered the three primary objectives. From a safety perspective, traffic accidents not only impose a significant financial burden but also result in irreparable losses to society. Road design, user behavior, and environmental factors are identified as the primary contributors to traffic accidents (Abdel-Aty & Radwan,

[1] Dr. Research Assistant., Department of Civil Engineering, Eskisehir Osmangazi University, Eskisehir, Turkiye, 26480, Orcid: 0000-0001-6720-5498, kbakalin@ogu.edu.tr
[2] Professor Dr., Department of Statistics, Eskisehir Osmangazi University, Eskisehir, Turkiye, 26480, Orcid: 0000-0002-3277-740X, aaltin@ogu.edu.tr
[3] Professor Dr., Department of Civil Engineering, Eskisehir Osmangazi University, Eskisehir, Turkiye, 26480, Orcid: 0000-0001-9721-0984, muratk@ogu.edu.tr

2000; Akalın, 2016; Akalın, 2023; Candefjord et al., 2021; Delen et al., 2017; Eluru, 2013; González-Sánchez, 2018; Karacasu et al., 2016; Miaou & Lum, 1993; Oh, 2006; Park et. al., 2012).

Traffic safety is defined as the methods and measures employed to mitigate the occurrence of death, injury, and property loss among road users. According to data from the World Health Organization (WHO) in 2018, over 1.25 million deaths and 50 million non-fatal injuries, including permanent disabilities, occur globally as a result of traffic accidents each year. Without proper precautions, road traffic accidents are projected to become the seventh leading cause of death by 2030. These accidents also impose a significant economic burden, with costs estimated at approximately 3% of a country's gross domestic product (GDP) in many nations (WHO, 2018).

Türkiye is among the top 10 countries with the highest number of traffic accident fatalities, with approximately 4,500 fatal accidents occurring annually (Kırmızıoğlu & Tüydeş-Yaman, 2012). In 2016, a total of 1,182,491 traffic accidents were recorded in Türkiye, of which 16% resulted in death or personal injury and 84% resulted in material damage. Approximately 7,300 individuals lost their lives and 304,000 were injured as a result of road traffic accidents (KGM, 2017). According to the WHO, traffic accidents are a leading cause of death among individuals aged between 15 and 29 globally, and 48% of road traffic accidents resulting in death involve individuals aged between 15 and 44 (WHO, 2018).

Various statistical techniques are employed in accident causality studies, and the validity and reliability of the results

obtained from such studies are directly related to the appropriateness of the chosen methods. Logistic regression analysis is a commonly used method for identifying the factors contributing to traffic accidents. However, logistic regression analysis is predicated on the assumption of minimal multicollinearity among explanatory variables, unlike linear regression analysis. In reality, many factors associated with traffic accidents are highly correlated. Therefore, it is necessary to eliminate multicollinearity to obtain valid results. Various techniques can be employed to eliminate multicollinearity. Most factors related to traffic accidents are categorical data, which precludes the use of Pearson or Spearman correlations. In such cases, the strength of the relationship between explanatory variables is calculated using the Cramer V correlation coefficient. Additionally, some observations within accident data sets may be outliers, which can significantly impact logistic regression results. These outliers can lead to inaccurate estimates of the factors contributing to the accident and their effects. To address this issue, robust methods that are resistant to hypothetical distortions and minimize the effect of outliers have gained popularity in recent years.

Several studies have employed logistic regression techniques in order to investigate the factors that contribute to traffic accidents. Shibata & Fukuda (1994) employed unconditional multiple logistic regression to evaluate the impact of potential risk factors of drivers on accident severity. Karacasu, Ergül & Altın-Yavuz (2014) utilized logistic regression and discriminant analysis methods in their study of the contributing factors to traffic accidents. Balagh, Naderkhani & Makis (2014) applied a stochastic logistic regression model to provide a more comprehensive assessment of driving conditions and

a more accurate estimation of highway collisions during winter conditions. Jia et al. (2018) used logistic regression to determine the influence of attitudinal and low-carbon factors on behavioral intentions of commuting mode choice. Thigpen & Handy (2018) employed binary logistic regression to investigate the factors influencing driver's licensing of young adults in the US. Fitch et al. (2019) used logistic regression to investigate the relationship between the road environment, cycling attitudes, and usual travel mode to school among teenagers. Tay, Barua & Kattan (2009) conducted research to identify the factors contributing to hit-and-run incidents in fatal crashes. Xu et al. (2012) used logistic regression to determine and predict the factors affecting the seriousness of accidents occurring at crossroads. Mujalli, Al-Masaeid & Alamoush (2023) used clustering techniques and SVMs to analyze crashes on rural and suburban highways in Jordan.

This study aims to introduce two novel versions of logistic regression analysis, which are commonly used in the field of traffic research and are better suited to the data structure, in order to accurately estimate the factors contributing to traffic accidents in Antalya, Türkiye. Firstly, a conventional logistic regression analysis, which is commonly employed in literature, is discussed. Secondly, a robust logistic regression analysis, which is effective in handling outliers in the data set, is presented. Finally, the logistic ridge regression used in case of multicollinearity between explanatory variables is introduced.

As a result of the analysis, it has been determined that there is a high correlation between the factors and that the accident data include outliers. For this reason, robust logistic ridge regression

analysis is proposed to determine the factors that cause traffic accidents.

The structure of the paper is as follows: In Section 2, the theoretical background of the methods for classical logistic regression, robust logistic regression, and robust logistic ridge regression are introduced. Section 3 provides a description of the study area and dataset. Section 4 presents the analysis results, and Section 5 contains discussion and conclusion.

Theoretical Background of the Methods

Multivariate statistical methods convert the data structure into a simpler form and provide appropriate solutions to the problem's structure. In this study, traffic accident data from Antalya, one of the largest cities in Turkey and a major tourist destination with heavy traffic, was analyzed to determine which variables influence accidents. The accident type is considered with two classes: fatal and injury. The logistic regression method gives reliable results in classification. There are many logistic regression methods that can be used depending on the data structure. Some are briefly introduced in this section.

Logistic Regression

The classification problem is a process of statistical decision-making, where the researcher has two options: determining the variables that provide discrimination by examining the distinguishing characteristics of the groups, and assigning individuals to groups using these distinctive functions. Logistic regression analysis is appropriate for situations where the groups are known in advance. The primary purpose of logistic regression

analysis is to explain the causal relationship between independent variables and the dependent variable, similar to other regression methods (Eluru, 2013; Hair et al., 1995; Shankar and Mannering, 1996).

Logistic regression analysis is commonly employed to evaluate the significance of traffic accident risk factors when the dependent variable is binary in nature (Xu et al., 2012; Tay, Rifaat & Chin, 2008; Yan et al., 2005). Logistic regression is a regression technique that examines the connection between an explanatory variable or variables and a discrete response variable. Binary logistic regression is particularly useful when the dependent variable represents a dichotomy. It can also be employed to assess the connection between the dependent variable and associated independent variables (Lemeshow & Hosmer, 2000). In logistic regression, the independent variables can be either categorical or continuous. The logistic regression model predicts the likelihood of the dependent variable taking one of its possible values. In the case where the dependent variable is dichotomous, the logistic regression model can be defined as follows:

$$P(Y = 1|X = x) = \pi(x) = \frac{e^{x_\beta}}{1+e^{x_\beta}} \quad (1)$$

where X is independent variable matrix and β is unknown parameter vector.

In logistic regression analysis, it is necessary to apply transformation in order to take the values of the dependent variable to [0,1]. Logit transformation is stated as

$$logit\ \pi(x) = \ln\left(\frac{\pi(x)}{1-\pi(x)}\right) = X\,\beta \quad (2)$$

In this transformation, $\pi(x)$ indicates the probability of occurrence of an event, and $1-\pi(x)$ indicates the probability of an event not occurring. The ratio of $\frac{\pi(x)}{1-\pi(x)}$ is called as the odds ratio (OR) and is used to interpret the coefficients in logistic regression analysis.

When an independent variable x_i increases by one unit while holding all other factors constant, the odds increase by a factor e^{β_i}. This means that the OR is equal to e^{β_i}. The factor reflects the extent to which the odds of the outcome increase (OR greater than 1) or decrease (OR less than 1) with a one-unit increase in the corresponding independent variable. For categorical independent variables, the ORs provide a means to compare accident risks between different levels in this study (Xu et al., 2012; Lemeshow & Hosmer, 2000; Tay, Barua & Kattan, 2009).

Robust Logistic Regression

In practice, some observations obtained for the variable of interest may have values that are significantly larger or smaller than the rest of the data, and are inconsistent with the remainder of the dataset. Such observations are defined as outliers or anomalies. An outlier or anomaly is a rare observation that shows a significant deviation from the other members of the sample or is inconsistent with the rest of the data set. Outliers or anomalies can exist in many different fields and be caused by a wide variety of reasons such as instrumental error, human error, natural deviations in populations and also fraudulent behavior. These observations are called anomalies for categorical data. Anomalies are deviations from expected patterns in a dataset that do not follow a clear definition of

normal behavior. In a basic two-dimensional dataset, anomalies can be visualized as illustrated in Figure 1. The dataset is composed of two normal regions, N_1 and N_2, where the majority of observations are located. However, observations that are significantly distant from these regions, such as points o_1 and o_2, as well as those in region O_3, are considered as anomalies (Singh & Upadhyaya 2012).

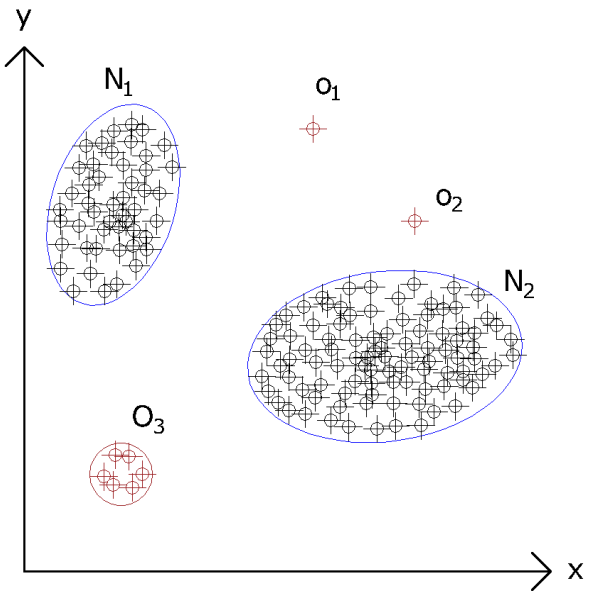

Figure 1: An illustration of anomalies in a two-dimensional data set as a simple example

The results obtained from the logistic regression model established for a data set containing an anomaly value may not reflect the truth. Anomalies cause model assumptions to fail. In the case that the data set does not contain an outlier value, the parameter estimates obtained by the maximum likelihood estimation (MLE) method are efficient, but they are lost if there are anomalies (Imon & Hadi, 2008). The parameter estimates obtained in this case do not

reflect reality. For this reason, it is necessary to examine and determine the anomalies in detail. Anomaly detection is a very important step in data analysis and that has been researched in different research areas and application areas. Anomaly detection has been used to detect and, if necessary, removed outliers in datasets. Numerous methods for anomaly detection have been developed, but the majority of these methods are designed to handle numerical data. Limited approaches exist for detecting anomalies in categorical datasets. In many road accident applications, the data objects are described using qualitative (categorical) attributes. Normally distributed attribute value frequency (NAVF) method is a simple yet fast and effective, and one of the efficient methods to detect outliers in categorical data. Results of this algorithm show that this requires lesser processing time while maintaining good outlier detection accuracy when compared with other existing techniques (Reddy, Babu & Govardhan, 2013). In this study, NAVF method was used for anomaly detection. The NAVF algorithm is as follows:

- Initially, all data points are labeled as non-outliers in the NAVF algorithm.
- Then, the normalized frequency value ($f(x_{ij})$) of each attribute value for each point x_i is calculated.
- Next, AVF value as the frequency score of each record x_i is calculated:

$$AVF\ Score\ (x_i) = F_i = \frac{1}{m}\sum_{j=1}^{m} f(x_{ij}) \quad (3)$$

Furthermore, the mean and standard deviation values of xi are determined. If any object frequency is less than three standard

deviations of the mean (mean-3 sd) then this model treats those objects as outliers. This method calculates target numbers of outliers itself based on the frequency. The method uses AVF score formula to find AVF score, but no target numbers of outliers is required (Reddy, Babu & Govardhan, 2013).

In logistic regression analysis, the probabilities of obtaining 0-1 values for the dependent variable are modeled. However, the presence of outliers in the data set can have an impact on these probabilities. Robust methods are techniques that enhance the reliability and validity of results obtained from statistical methods by minimizing the effect of outliers and assumptions disruption. In this study, a robust logistic regression model is utilized. The Bianco-Yohai (Bianco & Yohai, 1996) estimator or M-estimator which is proposed as a method for robust logistic regression is defined as follows:

$$\beta_n = argmin \sum_{i=1}^{n} \phi(Y_i, \pi(x_i'\beta)) \quad (4)$$

$d_i(\beta)$ is variance of β in function $\phi(Y_i, \pi(x_i'\beta)) = \tilde{n}(d_i(\beta)) + \tilde{n}_0(\pi(x_i'\beta))$ and $\tilde{n}(t)$ is restricted function (Hobza, Pardo & Vajda, 2012).

The logistic ridge regression method is obtained through the constrained maximum likelihood method and is formulated as follows:

$$\hat{\beta}_{LRR} = \left[X'\widehat{W}X + kI\right]^{-1}\left[X'\widehat{W}X\hat{\beta}_{MLE}\right] \quad (5)$$

In Equation (5), k (where $k > 0$) represents the bias constant, and its significantly influences the performance of the ridge estimator (Hoerl & Kennard, 1970).

Robust Logistic Ridge Regression

As in simple linear regression analysis, logistic regression also assumes that the independent variables are uncorrelated. The relationship between the independent variables is referred to as multicollinearity (Montgomery, Peck & Vining, 2001). When multicollinearity is present, there are several important issues such as loss of the minimum variance feature of estimators, an increase in the variance of the regression coefficients, and a high R^2 value of the model. Additionally, the variance of the regression coefficients can approach infinity and the sign of the coefficient estimates can differ from theoretical predictions. Furthermore, all or most of the independent variables may not be statistically significant. To address these issues, the ridge regression method proposed by Hoerl & Kennard (1970) is widely used. The use of the ridge estimator in logistic regression is reported by Dufy & Santer (1989).

In the event that the data set contains both outliers and multicollinearity among independent variables, it is recommended to use the robust logistic ridge regression method, instead of the MLE for logistic regression analysis. This is because the robust logistic ridge regression method is better equipped to handle both the presence of outliers and multicollinearity in the data, and can provide more robust and reliable results.

The robust logistic ridge regression estimator (RLRR) proposed by Croux & Haesbroeck (2003) is given in Equation (6).

$$\hat{\beta}_{RLRR} = \left[X'\widehat{W}^{*}X + k^{*}I\right]^{-1}\left[X'\widehat{W}^{*}X\hat{\beta}_{WBY}\right] \quad (6)$$

where, $\widehat{W}$ is the matrix with diagonal elements $\hat{\pi}_i(x)[1-\hat{\pi}_i(x)]$ and $\hat{\beta}_{WBY}$ is weighed Biancho-Yohai estimator. $\hat{\beta}_{RLRR}$ estimator is iteratively calculated.

It is important to investigate the presence of multicollinearity among the explanatory variables prior to applying the robust logistic ridge regression method. Correlation analysis is a statistical technique that is used to examine the linear relationship between two variables, or the relationship of one variable with multiple other variables, and to quantify the degree of this relationship. In correlation analysis, it is generally preferred that both variables be continuous and follow a normal distribution. The correlation coefficient, denoted as "r", ranges between -1 and +1, and its value depends on the variables being studied. Various correlation coefficients can be used to determine the relationship between quantitative or qualitative variables as summarized in Table 1.

Table 1: Correlation coefficient measurement methods according to variable types

Method	**Variables**	**Range**
Pearson's Correlation Coefficient	continuous *(normally distributed)*	-1 and +1
Spearman's Rank Correlation Coefficient	ordinal and continuous	-1 and +1
Kendall's Correlation Coefficient	ordinal	-1 and +1
Phi Correlation Coefficient	binary	-1 and +1
Cramer's V Correlation Coefficient	categorical	0 and +1
Lambda Correlation Coefficient	ordinal	-1 and +1

In this study, the linear relationship between explanatory variables was examined by Cramer V Correlation Coefficient because of all variables considered were classifiable and most of them had more than two levels. Cramer V Correlation Coefficient calculated as below:

$$V = \sqrt{\frac{\chi^2}{{\chi^2}_{max}}} = \sqrt{\frac{\chi^2}{N(k-1)}} \quad (7)$$

where χ^2 is the Pearson chi-square statistic, N is the sample size, k is the lesser number of categories.

Cramer's V correlation is a measure similar to the Pearson correlation coefficient. However, while Pearson correlation is utilized to assess the strength of linear relationships, Cramer's V is applied to evaluate correlations in tables with more than two rows and two columns. Cramer's V correlation ranges between 0 and 1, as displayed in Table 2. A value near 0 implies a minimal association between variables, while a value near 1 indicates a robust association (Osborn, 2006).

Table 2: Relationships for different cramer's v correlation coefficient values

Cramer's V Correlation Coefficient	**Relationship**
$V \geq 0.25$	Very strong relationship
$0.25 > V \geq 0.15$	Strong relationship
$0.15 > V \geq 0.10$	Moderate relationship
$0.10 > V \geq 0.05$	Weak relationship
$0.05 > V \geq 0.01$	Negligible relationship
$V = 0$	No relationship

Study Field and Data Description

In this study, a comprehensive dataset comprising of information pertaining to 24,249 serious traffic accidents that occurred in the province of Antalya between January 2013 and December 2017 were collected from the Antalya Security General Directorate. These accidents were reported incidents that resulted in injury or fatality. The dataset includes information on a variety of factors related to the accidents such as the drivers, passengers, vehicles, road conditions, and environmental factors. The variables and their levels are presented in Table 3. The dependent variable, Y, denotes the type of accident and is binary in nature:

$$\boldsymbol{Y} = \begin{cases} 0, & \text{The accident results in at least one injury} \\ 1, & \text{The accident results in at least one fatality} \end{cases} \quad (8)$$

Table 3: Variables notation and description

Variable	Notation	Description
Dependent variable		
Accident Type	Y	0=Injury; 1=Fatality
Independent variable		
Crash Site	X_1	1=Residential Area; 2=Rural Area
Road Type	X_2	1=Divided Road; 2=One-way; 3=Two-way Undivided; 4=Other
Pavement Type	X_3	1=Asphalt; 2=Bituminous Surface or Chip seal; 3=Concrete; 4=Concrete Blocks; 5=Gravel Surface; 6=Unpaved Surface
Road Class	X_4	1=State Road; 2=Quarter; 3=Street; 4=Parking Lot; 5=Other; 6=City Road; 7=Driveway; 8=Detour; 9=Connection Road; 10=Village Road

Horizontal Geometry	X_5	1=Alignment; 2=Ordinary Curve; 3=Dangerous Curve
Vertical Geometry	X_6	1=Uncurved; 2=Ordinary Slope; 3=Dangerous Slope; 4=At The Top
Junction Geometry	X_7	1=Three Legs T; 2=Three Legs Y; 3=Four Legs; 4=Roundabout; 5=Overpass/Underpass; 6=Other; 7=Grade Crossing; 8=Not Available or Unproper
Crossing	X_8	1=Controlled; 2=Uncontrolled; 3=School Crossing; 4=Pedestrian Crossing; 5= Not Available or Unproper
Other Parameters	X_9	1=Narrow Lane; 2=Narrow Bridge; 3=Over bridge; 4=Under bridge; 5=Over Culvert; 6=Speed Bump; 7=Tunnel; 8=None
Weather	X_{10}	1=Clear; 2=Foggy; 3=Rainy; 4=Snowy; 5=Sleet; 6=Strong Wind
Road Surface	X_{11}	1=Dry; 2=Wet; 3=Snowy; 4=Icy; 5=Puddle; 6=Other
Accident Pattern	X_{12}	1=Head-on Collision; 2=Rear-End Collision; 3=Side-on Collision; 4=Side-to-Side Collision; 5=Hitting a Parked Car; 6=End-to-End Pileup; 7=Multiple-Vehicle Collision; 8=Hitting a Fixed Object; 9=Pedestrian Collision; 10=Animal Collision; 11=Overturn; 12=Run-off-Road Accident; 13=Fall out of Vehicle; 14=Object fall from vehicle
Number of Vehicles Involved	X_{13}	1=One; 2=Two; 3=More Than Two
Sidewalk	X_{14}	1=Available; 2=Unavailable
Shoulder	X_{15}	1=Available; 2=Unavailable
Lane Line	X_{16}	1=Available; 2=Unavailable

Traffic Light	X_{17}	1=Available; 2=Damaged; 3=Unavailable
Lighting	X_{18}	1=Available; 2=Damaged; 3=Unavailable
Obstacle	X_{19}	1=Available; 2=Unavailable

The study area, Antalya province, and its geographical location is given in Figure 2. Additionally, the figure includes map images that demonstrate the spatial distribution of the accident locations within the region. As depicted in the figure, the incidence of accidents is concentrated in the central region of the study area and spread throughout the city.

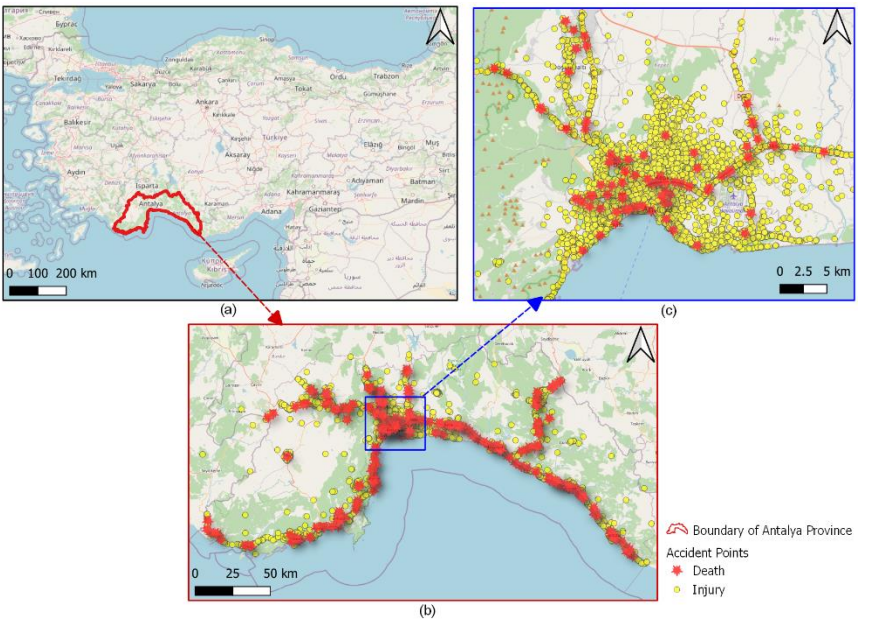

Figure 2: Map of the study field: a) Location of Antalya Province, b) Accident spots throughout the city, c) Accident spots in the city center

The distribution of the accident pattern by type, as well as the text clouds for fatal and injury accidents, is presented in Figure 3. The text clouds display the most frequently occurring data in the largest font, providing a visual representation of the accident patterns. The figure indicates that fatal accidents frequently result from pedestrian collisions (25.80% of all fatal accidents), while injury accidents are commonly caused by side-on collisions (41.74% of all fatal accidents).

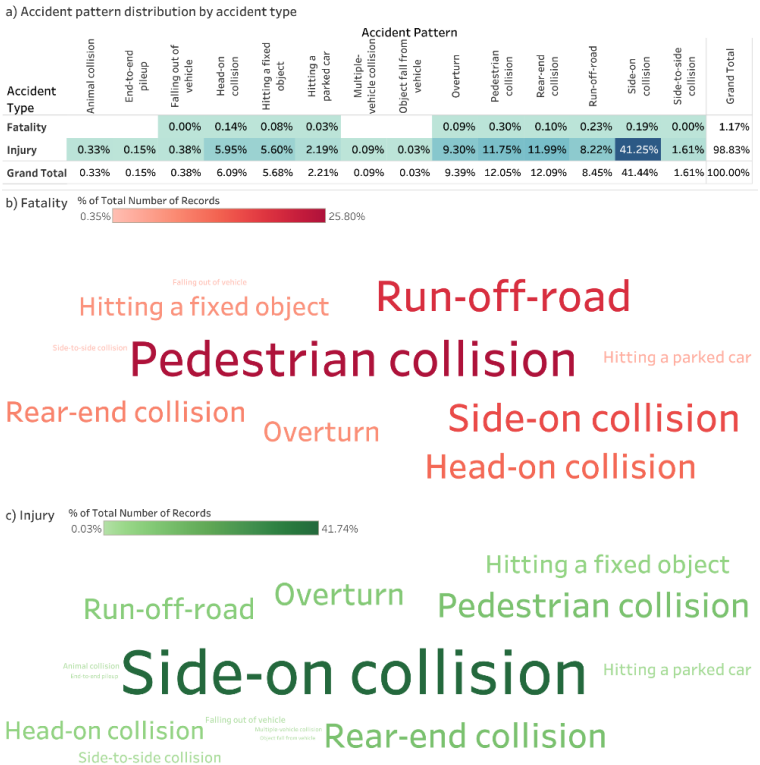

Figure 3: Accident pattern distribution by accident type: a) Distribution of accidents, b) Text cloud for fatal accidents, c) Text cloud for injury accidents

Crosstabs of independent variables such as horizontal and vertical geometry, pavement type and road surface, area and lighting condition according to accident types are given in Figure 4. As can be understood from here, in terms of road geometry and regardless of the accident type (fatal or injury), most of the accidents occurred on alignment and uncurved roads. Similarly, regardless of the type of accident, a significant proportion of accidents happened on dry asphalt roads. In addition, it is reported that a higher percentage of fatal accidents (38.87%) occurred in rural areas where lighting is unavailable, while a majority of injury accidents (64.90%) occurred in urban areas where lighting is available.

a) Crosstab of horizontal and vertical geometry by accident type

Horizontal Geometry	Vertical Geometry	Accident Type: Fatality	Accident Type: Injury
Alignment	Uncurved	66.78%	81.70%
	Top of curve	0.71%	0.14%
	Ordinary slope	7.77%	7.35%
	Dangerous slope		0.10%
Ordinary curve	Uncurved	8.13%	4.61%
	Top of curve		0.05%
	Ordinary slope	9.19%	4.09%
	Dangerous slope	0.35%	0.09%
Sharp curve	Uncurved	1.77%	0.52%
	Top of curve		0.03%
	Ordinary slope	3.89%	1.06%
	Dangerous slope	1.41%	0.26%
Grand Total		100.00%	100.00%

b) Crosstab of pavement type and road surface by accident type

Pavement Type	Road Surface	Accident Type: Fatality	Accident Type: Injury
Asphalt	Dry	84.81%	85.50%
	Icy		0.06%
	Other		0.18%
	Puddle		0.09%
	Snowy		0.05%
	Wet	10.95%	8.70%
Chipseal	Dry	1.06%	1.17%
	Other		0.01%
	Wet	0.35%	0.19%
Gravel	Dry	0.71%	0.28%
	Other		0.01%
	Puddle		0.00%
	Wet		0.05%
Paving stone	Dry		0.20%
	Wet		0.01%
Stabilized	Dry	0.71%	3.18%
	Puddle		0.00%
	Wet	0.35%	0.23%
Unpaved	Dry	1.06%	0.07%
	Puddle		0.00%
	Wet		0.02%
Grand Total		100.00%	100.00%

c) Crosstab of area and lighting condition by accident type

Area	Lighting	Accident Type: Fatality	Accident Type: Injury
Residential	Available	35.34%	64.90%
	Damaged	1.06%	1.40%
	Unavailable	14.84%	18.48%
Rural	Available	8.48%	3.85%
	Damaged	1.41%	0.46%
	Unavailable	38.87%	10.90%
Grand Total		100.00%	100.00%

Figure 4: Crosstabs by accident type: a) Horizontal and vertical geometry, b) Pavement type and road surface, c) Area and lighting condition

Data Analysis Results

In this study, a forward-stepwise (conditional) method was utilized to develop the logistic regression model and to identify the independent variables that significantly contribute to explaining the dependent variable. The goodness-of-fit test results of the logistic regression model, including the overall significance and validity of the variables, are presented in Table 4.

Table 4: Logistic regression analysis goodness-of-fit test results

Goodness-of-Fit Test	Value
Cox & Snell R^2	0.719
Nagelkerke R^2	0.959
Hosmer & Lemeshow	1.000

The Hosmer-Lemeshow test statistic is utilized to perform an overall significance test of the model. A value closer to 1 for this test statistic suggests a better fit for the model. Additionally, Cox & Snell and Nagelkerke R^2 statistics, which demonstrate the proportion of independent variables to the dependent variable, are performed within the context of study. The Cox & Snell and Nagelkerke R^2 values are 71.9% and 95.9%, respectively. Based on the analysis, the established model for traffic accidents is considered generally significant. Estimated coefficients from the logistic regression analysis and related statistics on the significance tests of the parameters in Table 5. In the binary logistic regression model, the first dependent variable (0=Injury) was selected as the reference category. This means that the effect of the independent variables on the reference category was used as a basis for comparison to evaluate the effect of the independent variables on the other dependent variables.

Table 5: Logistic regression analysis results

Variables		**Estimate**	**Std. Error**	**Z Value**	**Pr(>|Z|)**	**OR**
Intercept		14.862	356.651	0.042	0.967	2848757.152
Crash Site	Residential Area	0.248	0.220	1.126	0.260	1.281
Road Type	Divided Road	0.174	0.594	0.293	0.769	1.190
	One-way	0.982	0.693	1.416	0.157	2.670
	Two-way Undivided	0.095	0.591	0.161	0.872	1.100
Pavement Type	**Asphalt**	**3.134**	**0.756**	**4.146**	**0.000**	**22.961**
	Bituminous Surface or Chip Seal	**3.392**	**0.910**	**3.729**	**0.000**	**29.716**
	Concrete	12.429	31.258	0.020	0.984	249846.430
	Concrete Blocks	**3.427**	**0.943**	**3.632**	**0.000**	**30.778**
	Gravel Surface	1.703	1.023	1.665	0.096	5.490
Road Class	State Road	0.121	0.889	0.137	0.891	1.129
	Quarter	1.771	0.914	1.937	0.053	5.876
	Street	1.063	0.868	1.224	0.221	2.894
	Parking Lot	14.759	45.511	0.010	0.992	2568212.296
	Other	15.334	37.760	0.018	0.985	4566931.851
	City Road	-0.126	1.063	-0.118	0.906	0.882
	Driveway	12.194	56.433	0.015	0.988	197661.000
	Detour	0.562	1.356	0.414	0.679	1.754
	Connection Road	11.007	55.157	0.013	0.990	60304.940
Horizontal Geometry	Alignment	0.343	0.297	1.153	0.249	1.409
	Curvy Road	0.124	0.295	0.420	0.674	1.132
Vertical Geometry	Uncurved	0.495	0.755	0.655	0.512	1.640
	Ordinary Slope	0.650	0.762	0.853	0.394	1.915
	Dangerous Slope	0.279	0.897	0.311	0.756	1.322
Junction Geometry	Three Legs T	0.466	0.263	1.768	0.077	1.593
	Three Legs Y	1.453	1.010	1.439	0.150	4.278
	Four Legs	**0.762**	**0.269**	**2.831**	**0.005**	**2.142**
	Roundabout	0.508	0.294	1.728	0.084	1.662
	Overpass or Underpass	10.609	71.315	0.020	0.984	40515.311
	Other	0.049	0.429	0.115	0.908	1.051
	Grade Crossing	10.460	44.969	0.009	0.993	34892.845
Crossing	Controlled	-0.132	1.112	-0.119	0.905	0.876
	Uncontrolled	11.115	12.661	0.011	0.991	67182.966
	School Crossing	-0.483	1.034	-0.467	0.640	0.617
	Pedestrian Crossing	-0.124	0.215	-0.577	0.564	0.884
Other Parameters	**Narrow Lane**	**-0.981**	**0.473**	**-2.076**	**0.038**	**0.375**
	Narrow Bridge	11.230	36.871	0.006	0.995	75327.671
	Over Bridge	**-1.410**	**0.543**	**-2.598**	**0.009**	**0.244**
	Under Bridge	-1.216	1.028	-1.183	0.237	0.296
	Over Culvert	-1.851	1.121	-1.652	0.099	0.157
	Speed Bump	**-2.126**	**1.079**	**-1.971**	**0.049**	**0.119**
	Tunnel	-0.472	0.740	-0.638	0.524	0.624
Weather	Clear	-13.906	74.432	-0.008	0.993	0.000
	Foggy	-14.804	74.432	-0.009	0.993	0.000
	Rainy	-13.971	74.432	-0.008	0.993	0.000
	Snowy	-2.036	96.636	-0.001	0.999	0.131
	Sleet	-0.119	44.979	0.000	1.000	0.887
Road Surface	Dry	-14.608	57.622	-0.017	0.986	0.000
	Wet	-14.324	57.622	-0.017	0.987	0.000

	Snowy	-1.826	18.563	-0.001	0.999	0.161
	Icy	0.179	17.704	0.000	1.000	1.196
	Puddle	-0.857	17.726	-0.001	1.000	0.424
Accident Pattern	Head-on Collision	-15.845	20.998	-0.008	0.994	0.000
	Rear-End Collision	-14.484	21.998	-0.007	0.994	0.000
	Side-On Collision	-14.513	21.998	-0.007	0.994	0.000
	Side-to-Side Collision	-13.745	21.998	-0.007	0.995	0.000
	Hitting a Parked Car	-15.197	21.998	-0.007	0.994	0.000
	End-to-End Pileup	-0.506	23.986	0.000	1.000	0.603
	Multiple-Car Accidents	-0.127	24.625	0.000	1.000	0.880
	Fixed Object Hit	-15.346	29.998	-0.007	0.994	0.000
	Pedestrian Collision	-16.871	29.998	-0.008	0.994	0.000
	Animal Collision	-0.888	29.543	0.000	1.000	0.411
	Overturn	-14.876	29.998	-0.007	0.994	0.000
	Run-off-Road	-15.565	29.998	-0.007	0.994	0.000
	Falling out of Vehicle	-15.691	29.998	-0.008	0.994	0.000
Number of Vehicles Involved in The Accident	**One**	**1.011**	**1.402**	**2.514**	**0.012**	**2.748**
	Two	0.396	0.275	1.442	0.149	1.486
Sidewalk	**Available**	**0.395**	**1.165**	**2.388**	**0.017**	**1.484**
Shoulder	Available	-14.099	82.218	-0.017	0.986	0.000
Lane Line	Available	0.138	1.032	0.134	0.893	1.149
Traffic Light	Available	-0.379	0.204	-1.853	0.064	0.685
	Damaged	0.184	0.373	0.493	0.622	1.202
Lighting	Available	0.232	0.164	1.414	0.157	1.262
	Damaged	-0.086	0.431	-0.199	0.842	0.918
Obstacle	Available	9.532	82.055	0.016	0.987	13798.749
Correct Classification Rate		*0.124*	**Bold expressions specify statistically significant coefficients at the 95% confidence level.**			

In statistical modeling, the Pr(>|z|) column is commonly used to report the p-value associated with the z value column. The p-value is a measure of the probability of observing a result as extreme as, or more extreme than, the observed result under the null hypothesis. In this case, the null hypothesis is that the coefficient of the corresponding independent variable is equal to zero. If the p-value is smaller than the chosen significance level, it suggests that the variable is statistically significant, indicating that the corresponding coefficient is unlikely to be zero. In the model results, estimated coefficients with a p-value less than 0.05 in the 95% confidence interval were considered statistically significant.

As presented in Table 5, the p-values for the variables related to pavement type (asphalt, bituminous surface or chip seal, concrete blocks), junction geometry (four legs), other parameters (narrow lane, over bridge, speed bump), number of vehicles involved in the accident (one), and sidewalk (available) were found to be less than 0.05, indicating that these variables are statistically significant. Using the last level of the categorical independent variables as a reference category, the OR for the pavement type (asphalt) variable was determined to be 22.961, indicating that accidents occurring on asphalt roads lead to 22.961 times more deaths than accidents on the unpaved roads when other variables are fixed. This result seems reasonable since driving on unpaved roads tends to be slower, and drivers may exercise more caution. Furthermore, the OR for the junction geometry (four legs) variable was found to be 2.142, indicating that accidents on a four-way road may result in deaths 2.142 times more than accidents occurring on a road without intersections.

When Table 4 and Table 5 are evaluated together, the logistic regression model demonstrates statistical significance, yet the presence of numerous statistically insignificant model coefficients indicates potential modeling errors. In addition, the accuracy of the model (correct classification rate) is estimated to be only 12.4%, which indicates that the model may not be sufficient to determine the factors affecting traffic accidents. To mitigate the risks of such limitations, it is advisable to examine the validity of the data. As all explanatory variables in this study were categorical, we employed the NAVF method to determine outliers. Specifically, we calculated

attribute value frequency (AVF) scores for all observations using the RStudio and demonstrated box plot in Figure 5.

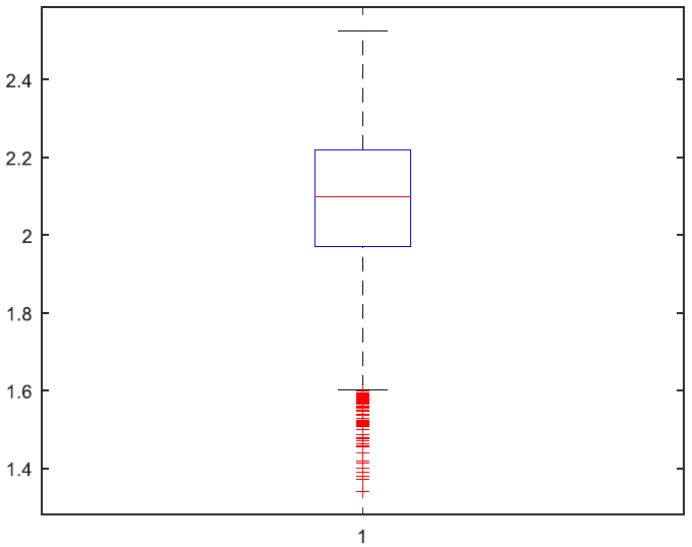

Figure 5: Box plot for logistic regression analysis

The NAVF method classifies observations with an AVF score below the mean-3sd threshold as anomalies. As shown in Figure 5, several anomalies were detected in the data set. Given the presence of outliers, we applied robust logistic regression analysis and results of this analysis is given in Table 6.

Table 6: Robust logistic regression analysis results

Variables		**Estimate**	**Std. Error**	**Z Value**	**Pr(>|Z|)**	**OR**
Intercept		8.922	56.651	0.157	0.875	7497.752
Crash Site	**Residential Area**	**1.248**	**0.249**	**5.005**	**0.000**	**3.483**
Road Type	Divided Road	0.174	0.809	0.216	0.829	1.191
	One-way	**1.983**	**0.864**	**2.294**	**0.022**	**7.266**
	Two-way Undivided	0.095	0.801	0.119	0.905	1.100
Pavement Type	**Asphalt**	**3.137**	**0.716**	**4.384**	**0.000**	**23.039**
	Bituminous Surface or Chip Seal	**3.395**	**0.882**	**3.850**	**0.000**	**29.824**

	Concrete	**4.446**	**0.753**	**5.904**	**0.000**	**85.305**
	Concrete Blocks	**3.430**	**0.882**	**3.891**	**0.000**	**30.891**
	Gravel Surface	1.705	1.157	1.473	0.141	5.500
Road Class	State Road	0.122	1.011	0.120	0.904	1.129
	Quarter	1.773	1.198	1.480	0.139	5.888
	Street	1.064	0.903	1.179	0.239	2.897
	Parking Lot	**3.775**	**1.380**	**2.736**	**0.006**	**43.578**
	Other	**5.351**	**1.608**	**3.327**	**0.001**	**210.780**
	City Road	-0.126	1.163	-0.108	0.914	0.882
	Driveway	**2.211**	**0.937**	**2.360**	**0.018**	**9.121**
	Detour	0.563	1.255	0.448	0.654	1.755
	Connection Road	**3.024**	**1.501**	**2.015**	**0.044**	**20.581**
Horizontal Geometry	Alignment	0.343	0.271	1.266	0.205	1.409
	Curvy Road	0.124	0.302	0.410	0.682	1.132
Vertical Geometry	**Uncurved**	**1.495**	**0.757**	**1.974**	**0.048**	**4.461**
	Ordinary Slope	0.651	0.765	0.850	0.395	1.917
	Dangerous Slope	0.279	0.895	0.312	0.755	1.322
Junction Geometry	Three Legs T	0.466	0.359	1.299	0.194	1.594
	Three Legs Y	1.455	0.973	1.495	0.135	4.284
	Four Legs	**1.763**	**0.300**	**5.868**	**0.000**	**5.828**
	Roundabout	0.508	0.334	1.524	0.128	1.663
	Overpass or Underpass	**1.625**	**0.390**	**4.163**	**0.000**	**5.079**
	Other	0.050	0.423	0.117	0.907	1.051
	Grade Crossing	**1.476**	**0.366**	**4.035**	**0.000**	**4.373**
Crossing	Controlled	-0.132	1.913	-0.069	0.945	0.876
	Uncontrolled	**2.129**	**0.389**	**5.477**	**0.000**	**8.409**
	School Crossing	-0.484	0.707	-0.684	0.494	0.617
	Pedestrian Crossing	-0.124	0.234	-0.530	0.596	0.883
Other Parameters	**Narrow Lane**	**-0.982**	**0.410**	**-2.394**	**0.017**	**0.375**
	Narrow Bridge	**1.745**	**0.744**	**2.346**	**0.019**	**5.725**
	Over Bridge	**-1.411**	**0.560**	**-2.519**	**0.012**	**0.244**
	Under Bridge	-1.217	1.373	-0.886	0.376	0.296
	Over Culvert	-1.853	1.038	-1.785	0.074	0.157
	Speed Bump	**-2.128**	**1.071**	**-1.987**	**0.047**	**0.119**
	Tunnel	-0.472	0.901	-0.524	0.600	0.624
Weather	**Clear**	**-13.921**	**7.017**	**-1.984**	**0.047**	**0.000**
	Foggy	-4.820	4.012	-1.201	0.230	0.008
	Rainy	**-3.986**	**2.032**	**-1.962**	**0.050**	**0.019**
	Snowy	-2.038	1.457	-1.399	0.162	0.130
	Sleet	-0.120	3.493	-0.034	0.973	0.887
Road Surface	**Dry**	**-14.624**	**5.027**	**-2.909**	**0.004**	**0.000**
	Wet	**-14.340**	**5.080**	**-2.823**	**0.005**	**0.000**
	Snowy	-1.828	1.388	-1.317	0.188	0.161
	Icy	0.179	2.154	0.083	0.934	1.196

	Puddle	-0.858	3.569	-0.240	0.810	0.424
Accident Pattern	**Head-on Collision**	**-5.862**	**2.800**	**-2.093**	**0.036**	**0.003**
	Rear-End Collision	**-4.499**	**1.917**	**-2.347**	**0.019**	**0.011**
	Side-On Collision	**-4.529**	**1.537**	**-2.946**	**0.003**	**0.011**
	Side-to-Side Collision	**-3.759**	**1.904**	**-1.974**	**0.048**	**0.023**
	Hitting a Parked Car	**-5.213**	**1.015**	**-5.138**	**0.000**	**0.005**
	End-to-End Pileup	-0.506	2.309	-0.219	0.826	0.603
	Multiple-Car Accidents	-0.128	3.380	-0.038	0.970	0.880
	Fixed Object Hit	**-5.363**	**1.907**	**-2.812**	**0.005**	**0.005**
	Pedestrian Collision	**-6.889**	**2.269**	**-3.037**	**0.002**	**0.001**
	Animal Collision	-0.889	3.477	-0.256	0.798	0.411
	Overturn	**-4.892**	**2.457**	**-1.991**	**0.046**	**0.008**
	Run-off-Road	**-5.582**	**2.426**	**-2.301**	**0.021**	**0.004**
	Falling out of Vehicle	-5.708	3.636	-1.570	0.116	0.003
Number of Vehicles Involved in The Accident	**One**	**1.012**	**0.439**	**2.305**	**0.021**	**2.751**
	Two	0.397	0.405	0.979	0.328	1.487
Sidewalk	Available	0.395	0.222	1.782	0.075	1.485
Shoulder	Available	-4.114	7.491	-0.549	0.583	0.016
Lane Line	Available	0.139	1.188	0.117	0.907	1.149
Traffic Light	Available	-0.379	0.220	-1.726	0.084	0.684
	Damaged	0.184	0.469	0.392	0.695	1.202
Lighting	Available	0.233	0.190	1.226	0.220	1.262
	Damaged	-0.086	0.664	-0.129	0.897	0.918
Obstacle	**Available**	**3.547**	**1.372**	**2.585**	**0.010**	**34.704**
Correct Classification Rate		*0.657*	**Bold expressions specify statistically significant coefficients at the 95% confidence level.**			

Table 6 reveals that 34 variable coefficients are statistically significant at a 0.05 significance level. The standard error values for these coefficients were lower than those found in the initial logistic regression analysis. The resulting model's accuracy rate was 65.7%. Nevertheless, ORs for certain variables, such as road surface, weather, accident pattern, crossing, shoulder, traffic light and lighting were found to contradict theoretical expectations. For

instance, the odds of death from traffic accidents were lower on wet and dry surfaces compared to other surfaces, whereas fatal accidents typically occur on wet surfaces (Edwards, 1998; Theofilatos and Yannis, 2014). Furthermore, the significant coefficients had reversed signs, indicative of multicollinearity among explanatory variables. The classical logistic regression results suggested that the model was generally significant, but the coefficients were meaningless, further raising suspicion of multicollinearity. Therefore, we computed Cramer's V correlation coefficients between the independent variables, as all the explanatory variables were categorical. Figure 6 presents the results, which reveal strong correlations among many independent variables, as indicated in Table 2's definition of a strong linear relationship as a Cramer's V correlation coefficient greater than 0.15.

	V1	**V2**	**V3**	**V4**	**V5**	**V6**	**V7**	**V8**	**V9**	**V10**	**V11**	**V12**	**V13**	**V14**	**V15**	**V16**	**V17**	**V18**	**V19**
V1	1.000																		
V2	0.105	1.000																	
V3	0.093	0.138	1.000																
V4	**0.813**	**0.308**	**0.268**	1.000															
V5	**0.273**	0.054	0.042	**0.238**	1.000														
V6	**0.227**	0.091	0.027	**0.194**	**0.479**	1.000													
V7	**0.211**	0.115	0.063	**0.372**	0.141	0.124	1.000												
V8	0.022	**0.200**	0.047	**0.158**	0.088	0.074	**0.258**	1.000											
V9	0.031	0.070	0.069	0.087	0.079	0.095	**0.164**	**0.187**	1.000										
V10	0.134	0.042	0.046	0.141	0.101	0.123	0.046	0.020	0.018	1.000									
V11	0.132	0.029	0.064	0.143	**0.151**	0.128	0.051	0.033	0.025	**0.523**	1.000								
V12	**0.313**	**0.256**	0.105	**0.385**	**0.384**	**0.240**	**0.454**	**0.167**	0.112	**0.158**	**0.150**	1.000							
V13	**0.167**	0.077	0.044	**0.201**	**0.252**	0.142	**0.344**	0.016	0.056	0.076	0.083	**0.996**	1.000						
V14	**0.381**	0.115	0.109	**0.359**	**0.220**	**0.203**	**0.187**	**0.167**	0.068	0.071	0.072	**0.250**	0.122	1.000					
V15	**0.416**	**0.228**	0.139	**0.501**	0.144	0.080	**0.203**	0.064	0.054	0.068	0.066	**0.224**	0.112	0.128	1.000				
V16	**0.258**	**0.367**	**0.191**	**0.466**	0.084	0.051	**0.196**	0.145	0.057	0.049	0.054	**0.205**	0.094	0.048	**0.456**	1.000			
V17	0.070	**0.272**	0.070	**0.186**	0.097	0.087	**0.369**	**0.302**	0.038	0.025	0.022	**0.157**	0.120	0.088	0.088	**0.163**	1.000		
V18	**0.405**	0.106	0.076	**0.359**	**0.224**	**0.193**	0.139	0.134	0.058	0.086	0.081	**0.235**	0.129	**0.345**	**0.157**	0.025	**0.333**	1.000	
V19	0.014	0.036	0.029	0.039	0.014	0.027	0.027	0.005	0.035	0.008	0.019	0.034	**0.015**	0.014	0.028	0.037	0.016	0.023	1.000

Figure 6: Cramer's V correlation coefficients between independent variables

Robust logistic ridge regression analysis was applied to eliminate the problem of multicollinearity and to decrease the effect of the outliers. The results of the analysis are given in Table 7.

Table 7: Robust logistic ridge regression analysis results

Variables		**Estimate**	**Std. Error**	**Z Value**	**Pr(>|Z|)**	**OR**
Intercept		0.402	19.651	0.020	0.984	1.495
Crash Site	**Residential Area**	**0.625**	**0.201**	**3.104**	**0.002**	**1.867**
Road Type	**Divided Road**	**-0.845**	**0.417**	**-2.027**	**0.043**	**0.430**
	One-way	**0.478**	**0.234**	**2.040**	**0.041**	**1.613**
	Two-way Undivided	**0.960**	**0.421**	**2.278**	**0.023**	**2.610**
Pavement Type	**Asphalt**	**0.820**	**0.416**	**1.973**	**0.048**	**2.270**
	Bituminous Surface or Chip Seal	**0.839**	**0.425**	**1.976**	**0.048**	**2.315**
	Concrete	**0.038**	**0.012**	**3.269**	**0.001**	**1.038**
	Concrete Blocks	**0.805**	**0.406**	**1.982**	**0.048**	**2.237**
	Gravel Surface	**0.915**	**0.257**	**3.553**	**0.000**	**2.496**
Road Class	**State Road**	**0.950**	**0.389**	**2.444**	**0.015**	**2.587**
	Quarter	**0.833**	**0.418**	**1.994**	**0.046**	**2.301**
	Street	**0.983**	**0.126**	**7.810**	**0.000**	**2.673**
	Parking Lot	**0.799**	**0.402**	**1.989**	**0.047**	**2.222**
	Other	1.356	1.012	1.340	0.180	3.880
	City Road	0.286	1.001	0.286	0.775	1.331
	Driveway	**0.892**	**0.451**	**1.979**	**0.048**	**2.440**
	Detour	0.865	0.985	0.879	0.379	2.376
	Connection Road	0.916	0.422	**2.173**	**0.030**	**2.499**
Horizontal Geometry	**Alignment**	**-0.373**	**0.123**	**-3.031**	**0.002**	**0.689**
	Curvy Road	**-0.116**	**0.051**	**-2.261**	**0.024**	**0.891**
Vertical Geometry	**Uncurved**	**-0.954**	**0.401**	**-2.376**	**0.017**	**0.385**
	Ordinary Slope	**-0.891**	**0.300**	**-2.967**	**0.003**	**0.410**
	Dangerous Slope	**-0.614**	**0.306**	**-2.007**	**0.045**	**0.541**
Junction Geometry	**Three Legs T**	**0.340**	**0.158**	**2.146**	**0.032**	**1.404**
	Three Legs Y	**0.377**	**0.190**	**1.986**	**0.047**	**1.458**
	Four Legs	**0.688**	**0.290**	**2.371**	**0.018**	**1.989**
	Roundabout	**0.411**	**0.201**	**2.045**	**0.041**	**1.509**
	Overpass or Underpass	**0.301**	**0.152**	**1.989**	**0.047**	**1.352**
	Other	0.011	0.402	0.028	0.977	1.012
	Grade Crossing	**0.269**	**0.137**	**1.967**	**0.049**	**1.308**
Crossing	**Controlled**	**-0.985**	**0.472**	**-2.087**	**0.037**	**0.374**
	Uncontrolled	**0.963**	**0.295**	**3.263**	**0.001**	**2.620**
	School Crossing	**-0.681**	**0.268**	**-2.543**	**0.011**	**0.506**
	Pedestrian Crossing	**-0.283**	**0.120**	**-2.359**	**0.018**	**0.753**
Other Parameters	**Narrow Lane**	**0.772**	**0.341**	**2.264**	**0.024**	**2.164**
	Narrow Bridge	**0.698**	**0.354**	**1.971**	**0.049**	**2.010**
	Over Bridge	**-0.854**	**0.349**	**-2.446**	**0.014**	**0.426**
	Under Bridge	-0.349	0.987	-0.353	0.724	0.706
	Over Culvert	-0.537	0.982	-0.546	0.585	0.585

	Speed Bump	**-0.577**	**0.293**	**-1.970**	**0.049**	**0.562**
	Tunnel	**-0.956**	**0.459**	**-2.083**	**0.037**	**0.384**
Weather	Clear	0.359	0.714	0.503	0.615	1.432
	Foggy	**0.699**	**0.356**	**1.962**	**0.050**	**2.012**
	Rainy	**0.942**	**0.346**	**2.724**	**0.006**	**2.564**
	Snowy	**0.799**	**0.405**	**1.972**	**0.049**	**2.223**
	Sleet	0.188	0.493	0.382	0.703	1.207
Road Surface	Dry	0.193	0.232	0.831	0.406	1.213
	Wet	**0.520**	**0.241**	**2.157**	**0.031**	**1.683**
	Snowy	**0.498**	**0.244**	**2.044**	**0.041**	**1.646**
	Icy	**0.532**	**0.254**	**2.097**	**0.036**	**1.702**
	Puddle	0.153	0.569	0.269	0.788	1.166
Accident Pattern	**Head-on Collision**	**1.599**	**0.812**	**1.968**	**0.049**	**4.946**
	Rear-End Collision	**1.396**	**0.620**	**2.252**	**0.024**	**4.041**
	Side-On Collision	**1.800**	**0.894**	**2.012**	**0.044**	**6.048**
	Side-to-Side Collision	0.498	1.877	0.265	0.791	1.645
	Hitting a Parked Car	-0.009	1.134	-0.008	0.994	0.991
	End-to-End Pileup	**1.248**	**0.608**	**2.053**	**0.040**	**3.484**
	Multiple-Car Accidents	**1.200**	**0.603**	**1.989**	**0.047**	**3.319**
	Fixed Object Hit	0.064	1.157	0.055	0.956	1.066
	Pedestrian Collision	**1.375**	**0.683**	**2.012**	**0.044**	**3.955**
	Animal Collision	0.566	0.989	0.572	0.568	1.761
	Overturn	**1.049**	**0.516**	**2.033**	**0.042**	**2.856**
	Run-off-Road	**1.293**	**0.601**	**2.151**	**0.031**	**3.644**
	Falling out of Vehicle	-0.074	0.933	-0.080	0.937	0.928
Number of Vehicles Involved in The Accident	**One**	**-0.694**	**0.342**	**-2.032**	**0.042**	**0.500**
	Two	**1.276**	**0.651**	**1.962**	**0.050**	**3.584**
Sidewalk	**Available**	**-0.418**	**0.192**	**-2.173**	**0.030**	**0.659**
Shoulder	**Available**	**-0.781**	**0.347**	**-2.248**	**0.025**	**0.458**
Lane Line	**Available**	**0.896**	**0.451**	**1.986**	**0.047**	**2.449**
Traffic Light	**Available**	**-0.529**	**0.152**	**-3.477**	**0.001**	**0.589**
	Damaged	**0.960**	**0.432**	**2.223**	**0.026**	**2.612**
Lighting	**Available**	**-0.247**	**0.120**	**-2.054**	**0.040**	**0.781**
	Damaged	**-0.487**	**0.248**	**-1.961**	**0.050**	**0.614**
Obstacle	**Available**	**1.346**	**0.372**	**3.616**	**0.000**	**3.842**
Correct Classification Rate		*0.876*	**Bold expressions specify statistically significant coefficients at the 95% confidence level.**			

When Table 7 is examined, we observed that 59 of the obtained coefficients for the robust logistic ridge regression model were statistically significant at a 0.05 significance level. The standard error values for these coefficients were lower than those in

the other regression analyses. Moreover, eliminating the effects of multicollinearity and outliers, the ORs in the robust logistic regression analysis revealed expected signs for previously opposing coefficients. Furthermore, we calculated the accuracy rate of the resulting model to be 87.6%, which represents a significant improvement over previous analysis.

Conclusion

The aim of this study is to determine the causes of accident severity using a data set of 24,249 serious traffic accidents from Antalya, Türkiye, utilizing the robust logistic ridge regression technique. The robust logistic ridge regression technique was performed to overcome the limitations of the classical logistic regression and robust logistic regression analysis and to provide more reliable results. By taking into account the multicollinearity and outliers in the dataset, the proposed model was able to identify the significant variables that affect the accident severity more accurately, and the ORs obtained were more consistent with theoretical expectations.

If logistic regression analysis was the only method used in this study, it would have suggested that traffic accident casualties are caused by only a limited number of variables (9 significant parameters). However, the results obtained using this method are significantly different from the actual situation for certain variables. For instance, the risk of casualties in a traffic accident on a narrow lane road was found to be lower compared to accidents caused by other road geometry parameters, although narrow roads are expected to have a higher probability of fatalities due to limited space. Moreover, it was concluded that some important variables such as

weather conditions, road surface conditions, and accident pattern do not have a significant effect on traffic accidents, which is not consistent with the existing knowledge and studies in the literature. The low accuracy of the model (12.4%) and the observed issues can be attributed to the presence of outliers, which classical logistic regression is unable to effectively handle.

After conducting a robust logistic regression analysis that eliminated the effect of outliers, it was found that there were more significant variables (34 parameters) that affected traffic accidents. Although the model shows good performance (65.7% of accuracy rate), upon examination of the ORs, it is observed that some variables, although statistically significant, produce results that are inconsistent with expected outcomes. For instance, the probability of death in a head-on collision is less by a factor of 0.003 compared to death caused by reference variable –an object falling from a vehicle. The trend is similar for rear-end collision, side-on collision, side-to-side collision, hitting a parked car, fixed object hit, pedestrian collision, overturns, and run-off-road accidents when compared to object falling from a vehicle causing deaths. However, percentages of fatalities appear to be higher in pedestrian collision, side-on collision, run-off-road, and head-on collision. These unexpected results are attributed to the multicollinearity among the explanatory variables.

The problem caused by multicollinearity was eliminated through the utilization of robust logistic ridge regression analysis, resulting in an accuracy rate of 86.7%. Additionally, a significant number of factors (59 parameters) affecting the type of accident were identified as significant both statistically and in practical terms.

The research findings revealed that the occurrence of fatal accidents in residential areas was 1.867 times higher than that in rural areas. This result can be attributed to the higher number of vehicles and traffic density in residential areas.

In terms of road types, the highest risk of fatalities is observed on two-way undivided roads where traffic moves in both directions without a physical barrier. This is due to the higher likelihood of speeding and reckless driving, which increases the risk of fatalities by 2.610 times compared to other road types. On one-way roads, the risk of fatalities is 1.613 times higher compared to other road types. However, divided roads have a significant impact in reducing the occurrence of fatal accidents. The risk of fatalities is 2.326 (1/0.430) times lower in the case of traffic accidents that occur on divided roads. Therefore, the utilization of divided roads can significantly reduce the number of fatal traffic accidents.

When considering the type of pavement, it was found that roads with a gravel surface pose the highest risk due to the possibility of skidding and run-off-road. The risk of death from accidents on this type of road is 2.496 times higher than on an unpaved road.

Streets are associated with the highest risk of death compared to other road classes. The risk of death from an accident on a street is 2.673 times higher than on a village road. Considering the statistically significant parameter estimations, the road classes with the highest probability of fatal accidents are state roads, followed by connection roads, driveways, quarters, and parking lots. From here, it can be inferred that the risk of fatal accidents is higher on roads with more traffic congestion.

It was found that sharp curves pose the highest risk of death according to the horizontal geometry. The risk of death on a curvy road is 1.122 (1/0.891) times less than that on a sharp curvy road. On the other hand, the risk is reduced by 1.451 (1/0.689) times on the alignment of road. With regard to vertical geometry, the highest risk of fatal accidents is observed at the top of the vertical curve. This can be attributed to the limited visibility of approaching vehicles from the opposite direction, which increases the risk of death. In comparison, the risk of fatal accidents is 1.848 (1/0.541) times less on dangerous slopes, 2.439 (1/0.410) times less on ordinary slopes, and 2.597 (1/0.385) times less on uncurved roads.

According to the junction geometry, four-legged intersections have the highest risk of fatal accidents. This may be due to inadequate clear sight triangles, red light violations, and right-of-way violations. The risk of death resulting on four-legged intersections is 1.989 times higher compared to the absence of proper geometry. Then, respectively, the highest risks of fatal accidents occur at roundabouts, three-legged Y intersections, three-legged T intersections, overpass or underpass, and grade crossings.

The risk of fatal accidents is 2.674 (1/0.374) times lower on controlled crossings compared to those with improper or no design. Conversely, on uncontrolled roads, the risk of fatal accidents is 2.620 times higher. School way crossings and pedestrian crossings also have a lower likelihood of resulting in death compared to those with improper design. The presence of speed bumps or traffic lights approaching these crossings, along with drivers being more cautious in these areas, are factors that reduce the risk of death.

The probability of fatalities in traffic accidents increases twofold on narrow lane roads and narrow bridges. Presence of speed bumps can reduce the risk of fatal accidents through controlling and calming the flow of traffic. The probability of fatal accidents in areas such as over bridges or tunnels is relatively low due to the lower allowable speeds in these locations.

Fatal accident likelihood was found to be 2.564 times higher on rainy days compared to strong windy days, possibly due to the difficulty of vehicle control in rainy conditions. Similarly, during foggy and snowy days, the risk of fatal accidents doubled compared to strong wind conditions, which could be attributed to drivers being less likely to drive or more cautious in the stormy weather. In rainy, foggy, and snowy weather, vehicle control and traction can significantly impact driving conditions and increase accident risk and severity. Additionally, the risk of fatal accidents is higher on wet, snowy, and icy road surfaces. The results obtained for weather and road surface categories appear to be consistent.

The analysis of accident patterns reveals that side-impact collisions pose the highest risk of fatality. In comparison to the least frequent type of accident, which involves an object falling from a vehicle, the risk of death in side-impact collisions is 6.048 times higher. The following high-risk accidents, listed in order of effect size, head-on collisions, rear-end collisions, pedestrian hits, run-off-road, end-to-end pileup accidents, multiple-car accidents, and overturns. The presence of sidewalks and shoulders has been found to reduce the risk of accidents, whereas the presence of obstacles and lane lines increases it.

Upon examining accidents in terms of causality and severity, this study highlights the importance of utilizing robust logistic ridge regression to obtain more accurate and reliable results compared to robust logistic and classical logistic regression methods. However, the study has certain limitations, such as the lack of additional location based variables in the dataset, as well as factors such as visibility, humidity, or travel purposes. The dependent variable is also limited to binary variables for fatalities and injuries, without accounting for variables for near-miss incidents or property damage. Future studies could improve the dataset by including data from different cities. Furthermore, in contrast to modeling discrete variables as in this study, investigations could focus on factors affecting the total number of accidents or the frequency of accidents for specific severity levels, and discuss measures to reduce accident frequency.

References

Abdel-Aty, M.A. & Radwan A. E. (2000) Modeling traffic accident occurrence and involvement. Accident Analysis and Prevention 32(5): 633-642.

Akalın, K. B. (2016). Investigation of factors affecting tram accident severity with multinomial logit model. Master's thesis. Eskisehir Osmangazi University.

Akalın, K. B. (2023). Investigating Motorcycle Accidents in the Presence of Carriageway Hazards. Academic Platform Journal of Natural Hazards and Disaster Management, 4(2), 98-108.

Balagh, A. K. G., Naderkhani, F., & Makis, V. (2014). Highway accident modeling and forecasting in winter. Transportation research part A: policy and practice, 59, 384-396.

Bianco, A. M., & Yohai, V. J. (1996). Robust estimation in the logistic regression model (pp. 17-34). Springer New York.

Candefjord, S., Muhammad, A. S., Bangalore, P., & Buendia, R. (2021). On Scene Injury Severity Prediction (OSISP) machine learning algorithms for motor vehicle crash occupants in US. Journal of Transport & Health, 22, 101124.

Croux, C., & Haesbroeck, G. (2003). Implementing the Bianco and Yohai estimator for logistic regression. Computational statistics & data analysis, 44(1-2), 273-295.

Delen, D., Tomak, L., Topuz, K., & Eryarsoy, E. (2017). Investigating injury severity risk factors in automobile crashes with predictive analytics and sensitivity analysis methods. Journal of Transport & Health, 4, 118-131.

Duffy, D. E., & Santner, T. J. (1989). On the small sample properties of norm-restricted maximum likelihood estimators for logistic regression models. Communications in Statistics-Theory and Methods, 18(3), 959-980.

Edwards, J. B. (1998). The relationship between road accident severity and recorded weather. Journal of Safety Research, 29(4), 249-262.

Eluru, N. (2013). Evaluating alternate discrete choice frameworks for modeling ordinal discrete variables. Accident Analysis & Prevention, 55, 1-11.

Eluru, N., Bhat, C. R., & Hensher, D. A. (2008). A mixed generalized ordered response model for examining pedestrian and bicyclist injury severity level in traffic crashes. Accident Analysis & Prevention, 40(3), 1033-1054.

Fitch, D. T., Rhemtulla, M., & Handy, S. L. (2019). The relation of the road environment and bicycling attitudes to usual travel mode to school in teenagers. Transportation research part A: policy and practice, 123, 35-53.

González-Sánchez, G., Maeso-González, E., Olmo-Sánchez, M. I., Gutiérrez-Bedmar, M., Mariscal, A., & García-Rodríguez, A. (2018). Road traffic injuries, mobility and gender. Patterns of risk in Southern Europe. Journal of Transport & Health, 8, 35-43.

Hair, J., Rolphe, E., Ronald, L. & William, C. (1995). Multivariate Data Analysis with Readings. Prentice Hall International Editions.

Hobza, T., Pardo, L., & Vajda, I. (2012). Robust median estimator for generalized linear models with binary responses. Kybernetika, 48(4), 768-794.

Hoerl, A. E., & Kennard, R. W. (1970). Ridge regression: Biased estimation for nonorthogonal problems. Technometrics, 12(1), 55-67.

Imon, A. R., & Hadi, A. S. (2008). Identification of multiple outliers in logistic regression. Communications in Statistics-Theory and Methods, 37(11), 1697-1709.

Jia, N., Li, L., Ling, S., Ma, S., & Yao, W. (2018). Influence of attitudinal and low-carbon factors on behavioral intention of commuting mode choice–A cross-city study in China. Transportation research part A: policy and practice, 111, 108-118.

Karacasu, M., Ergül, B., & Altın-Yavuz, A. (2014). Estimating the causes of traffic accidents using logistic regression and discriminant analysis. International journal of injury control and safety promotion, 21(4), 305-313.

Karacasu, M., Altın-Yavuz, A., Ergül, B., & Akalın, K. B. (2016). Traffic Perception in Eskişehir Province. In IOP Conference Series: Earth and Environmental Science (Vol. 44, No. 5, p. 052063). IOP Publishing.

KGM (2017) Summary of Traffic Accident. General Directorate for Highways of Turkey.

Kırmızıoğlu, E., & Tüydeş-Yaman, H. (2012). Comprehensibility of traffic signs among urban drivers in Turkey. Accident Analysis & Prevention, 45, 131-141.

Lemeshow, S. & Hosmer, D. (2000). Applied Logistic Regression. Wiley Series in Probability and Statistic, Wiley Interscience, 2 Sub Edition, New York.

Miaou, S. P., & Lum, H. (1993). Modeling vehicle accidents and highway geometric design relationships. Accident Analysis & Prevention, 25(6), 689-709.

Montgomery, D. C., Peck, E. A., & Vining, G. G. (2001). Introduction to the Linear Regression Analysis. John Willey and Sons, New Jersey.

Mujalli, R. O., Al-Masaeid, H., & Alamoush, S. (2023). Modeling Traffic Crashes on Rural and Suburban Highways Using Ensemble Machine Learning Methods. KSCE Journal of Civil Engineering, 27(2), 814-825.

Oh, J. T. (2006). Development of severity models for vehicle accident injuries for signalized intersections in rural areas. KSCE Journal of Civil Engineering, 10, 219-225.

Osborn, C. E. (2006). Statistical applications for health information management. Jones & Bartlett Learning.

Park, S., Jang, K., Park, S. H., Kim, D. K., & Chon, K. S. (2012). Analysis of injury severity in traffic crashes: a case study of Korean expressways. KSCE Journal of Civil Engineering, 16(7), 1280.

Reddy, D., Babu, B. R., & Govardhan, A. (2013). Outlier Analysis of Categorical Data using NAVF. Informatica Economica, 17(1).

Shankar, V., & Mannering, F. (1996). An exploratory multinomial logit analysis of single-vehicle motorcycle accident severity. Journal of safety research, 27(3), 183-194.

Singh, K., & Upadhyaya, S. (2012). Outlier detection: applications and techniques. International Journal of Computer Science Issues (IJCSI), 9(1), 307.

Tay, R., Barua, U., & Kattan, L. (2009). Factors contributing to hit-and-run in fatal crashes. Accident Analysis & Prevention, 41(2), 227-233.

Tay, R., Rifaat, S. M., & Chin, H. C. (2008). A logistic model of the effects of roadway, environmental, vehicle, crash and driver characteristics on hit-and-run crashes. Accident Analysis & Prevention, 40(4), 1330-1336.

Theofilatos, A., & Yannis, G. (2014). A review of the effect of traffic and weather characteristics on road safety. Accident Analysis & Prevention, 72, 244-256.

Thigpen, C., & Handy, S. (2018). Driver's licensing delay: A retrospective case study of the impact of attitudes, parental and social influences, and intergenerational differences. Transportation research part A: policy and practice, 111, 24-40.

World Health Organization (2018) WHO Road Traffic Injuries Fact Sheet. Retrieved February 24, 2018, from http://www.who.int/mediacentre/factsheets/fs358/en/

Xu, C., Liu, P., Wang, W., & Li, Z. (2012). Evaluation of the impacts of traffic states on crash risks on freeways. Accident Analysis & Prevention, 47, 162-171.

Yan, X., Radwan, E., & Abdel-Aty, M. (2005). Characteristics of rear-end accidents at signalized intersections using multiple logistic regression model. Accident Analysis & Prevention, 37(6), 983-995.

CHAPTER II

Sound Insulation Evaluation: A Comparative Study between a Brick Wall and a Concrete Wall Using Octave 8.3.0 Program

Ehab FARHAN[1]

1.Introduction

Noise seriously affects human health, as it can result in many health problems. Hearing loss, whether permanent or temporary, is among the major negative effects of prolonged exposure to noise. In addition, continuous exposure to high levels of noise is linked to chronic high blood pressure and an increased risk of strokes, especially when exposure to sudden sounds such as explosions, which sometimes leads to death(Al-Ahmadi & Abd, 2017). Sound is

[1] 1Ehab Farhan, Kütahya Dumlupınar University, Institute of Graduate Education, Department of Civil Engineering, ehab.farhan@ogr.dpu.edu.tr. Orcid id - 0009-0006-7087-6667.

a disturbance as it travels through a medium, as it consists of a series of disturbances and compressions that travel in surrounding physical media. Sound reaches the ear and is felt. Sound waves resulting from the vibration of an object in the air are a series of changes in air pressure, caused by the movement of vibrating particles from their fixed position. The sense of sound is through the ear, as the number of waves that the ear can sense per second varies between 20 and 20,000 hertz. The change in pressure that the ear can sense as sound ranges between 20 x 10^-6 and 20 newtons per square meter. Accordingly, pressure below the minimum cannot be heard, while excessive pressure can cause internal damage to the ear, especially if it exceeds the maximum (Kormer, 1974).

Acoustic design is essential in the design process in general and especially when it comes to designing specialized halls. It appears that neglecting this aspect leads to poor sound clarity in most built halls, and this particularly causes problems in classrooms. There are several factors that affect the sound level, including noise sources and the acoustic properties of wall and ceiling materials (Al-Mamouri & Al-Mutairi, 2015). The process of noise isolation is the ability of materials to reduce the level of sound pressure by taking into account the sound source, the transmitting medium, and the receiver. This effect is measured by a ratio between the Sound ability before penetrating the material and after penetrating it, and this ratio is known as the noise reduction(Gong X, 2012). Sound insulation is considered one of the important criteria in the engineering design of buildings due to its direct impact on human comfort. In recent years, increased interest has been observed in reducing the impact of noise sources resulting from increased means of transportation and the use

of mechanical equipment in energy production (Al-Ali, 2004). When sound waves collide with a certain barrier, part of these waves is reflected, another part is absorbed, and part of them is transmitted to the other side of the barrier. The sound insulation value expresses the difference between the sound intensity generated by a specific source on one side of the barrier and the sound intensity transmitted to the other side, and this difference is expressed in a logarithmic unit. Sound intensity is measured in (dB) and is called decibels, named after Graham Bell (Al-Ali, 2004). The sound absorption coefficient of structural materials depends on the properties of the material itself such as its nature and density as well as the thickness of the barrier and the sound frequency. (Table 1) provides information about the sound absorption coefficient of some construction materials (Al-Dawaf, 1978).

Porosity is considered one of the most important properties that plays a vital role in the efficiency of sound absorption by materials. Large and continuous pores are what allow sound energy to seep through and play an effective role in the sound absorption process. As a result, lighter weight aggregate is more effective at absorbing sound than denser aggregate (Carlson, 1956). When the structure contains pores this makes air movement through it possible, which enhances the effectiveness of sound absorption. This is through the conversion of sound energy into heat through friction, as the presence of gaps also affects the relationship between sound insulation and Cutter density, as gaps increase the effectiveness of sound insulation (Neville, 1981).

Octave originated around 1988 as a complementary software to accompany an undergraduate-level textbook on chemical reactor

design, co-authored by James B. Rawlings from the University of Wisconsin-Madison and John G. Ekerdt from the University of Texas. Initially designed with specialized tools for solving chemical reactor design issues, the project shifted its focus due to identified limitations, aiming to develop a more versatile tool. Evolving into GNU Octave, it is now recognized as a high-level language primarily designed for numerical computations. The software offers a user-friendly command line interface for numerically solving linear and nonlinear problems, conducting various numerical experiments, and is largely compatible with Matlab. Octave also serves as a batch-oriented language and includes robust tools for tasks such as solving numerical linear algebra problems, locating roots of nonlinear equations, integrating ordinary functions, manipulating polynomials, and solving ordinary differential and differential-algebraic equations (Eaton, 2012).

The main objective of this study is to contribute to environmental impact assessment by finding the results of sound insulation of a brick wall and a concrete wall and comparing them with each other. It also determines the environmental impact of using different building materials and moving towards the most environmentally sustainable materials.

Table (1) *The sound absorption coefficient of some construction materials (Al-Dawaf, 1978).*

Sound absorption coefficient			**Materials**
Frequency (Hz)			
2024	512	128	
0.023	0.017	0.012	Clay bricks
0.049	0.030	0.024	Concrete bricks
0.020	0.015	0.010	Kashi flooring
0.020	0.027	0.035	Glass

0.040	0.025	0.013	The whiteness of the plaster
0.015	0.010	0.010	Marble and glazed kashi
0.054	0.060	0.039	Ficus

2. Materials and Method

In this study, the Octave program was used to calculate the sound insulation values of the brick wall and the concrete wall, which is an open source programming language. Octave has several notable features, including a widely recognized programming language that makes it easy to write advanced programs and perform complex mathematical operations with ease. The octave is widely used in scientific research, engineering, and mathematics. The Octave program provides an easy-to-use programming interface that helps researchers perform accurate mathematical calculations and complex data analyzes efficiently. Simply put, Octave is a valuable and essential tool for anyone who needs to perform advanced mathematical calculations and rigorous analyzes in science and engineering.

A function was created in the Octave program to calculate the sound insulation values of the brick wall and the concrete wall (Fig.1), assuming the following inputs:

1. Material Properties for the Brick Wall: This section defines the material properties for the brick wall, including its density, thickness, speed of sound in the brick, and absorption coefficient for the brick.

2. Material Properties for the Concrete Wall: This part defines the material properties for the concrete wall, including its density, thickness, speed of sound in the concrete, and absorption coefficient for the concrete.

3. Source and Receiver Positions: This section defines the distances from the sound source to the walls and from the walls to the receiver

4. Calculating the characteristic impedance of air: The code calculates the characteristic impedance of air using the density of air and the speed of sound in the air.

5. Calculating the characteristic impedance of bricks: The code calculates the characteristic impedance of the brick by multiplying the density of the brick with the speed of sound in the brick.

6. Calculating the characteristic impedance of concrete: Likewise, the code calculates the characteristic impedance of concrete by multiplying the density of the concrete with the speed of sound in the concrete.

7. Calculate the reflection coefficient at the source side for both walls: This part calculates the reflection coefficient at the source side for both brick and concrete walls taking into account the characteristic impedances and air resistance.

8. Calculate the reflection coefficient at the receiving side for both walls: The code calculates the reflection coefficient at the receiver side of both walls, taking into account the characteristic impedances and air resistance.

9. Calculate Absorption Loss for Both Walls: This section computes the absorption loss for both the brick and concrete walls based on their respective absorption coefficients.

10. Calculate Transmission Loss for Both Walls: The code calculates the transmission loss for both walls by considering the reflection coefficients and absorption losses, incorporating the material properties and thicknesses.

```
octave:1> % Define material properties for the brick wall
octave:1> brick_density = 1920; % Density of brick (kg/m^3)
octave:2> brick_thickness = 0.2; % Updated thickness of the brick wall (m)
octave:3> brick_sound_speed = 343; % Speed of sound in brick (m/s)
octave:4> brick_absorption_coefficient = 0.03; % Absorption coefficient for brick (unitless)
octave:5> % Define material properties for the concrete wall
octave:5> concrete_density = 2400; % Density of concrete (kg/m^3)
octave:6> concrete_thickness = 0.2; % Thickness of the concrete wall (m)
octave:7> concrete_sound_speed = 3200; % Speed of sound in concrete (m/s)
octave:8> concrete_absorption_coefficient = 0.02; % Absorption coefficient for concrete (unitless)
octave:9> % Define the source and receiver positions
octave:9> source_distance = 1; % Distance from the sound source to the walls (m)
octave:10> receiver_distance = 1; % Distance from the walls to the receiver (m)
octave:11> % Calculate the characteristic impedance of air
octave:11> air_density = 1.225; % Density of air (kg/m^3)
octave:12> air_sound_speed = 343; % Speed of sound in air (m/s)
octave:13> air_impedance = air_density * air_sound_speed;
octave:14> % Calculate the characteristic impedance of the brick
octave:14> brick_impedance = brick_density * brick_sound_speed;
octave:15> % Calculate the characteristic impedance of the concrete
octave:15> concrete_impedance = concrete_density * concrete_sound_speed;
octave:16> % Calculate the reflection coefficient at the source side for both walls
octave:16> reflection_coefficient_source_brick = (brick_impedance - air_impedance) / (brick_impedance + air_impedance);
octave:17> reflection_coefficient_source_concrete = (concrete_impedance - air_impedance) / (concrete_impedance + air_impedance);
octave:18> % Calculate the reflection coefficient at the receiver side for both walls
octave:18> reflection_coefficient_receiver_brick = (air_impedance - brick_impedance) / (air_impedance + brick_impedance);
octave:19> reflection_coefficient_receiver_concrete = (air_impedance - concrete_impedance) / (air_impedance + concrete_impedance);
octave:20> % Calculate the absorption loss for both walls
octave:20> absorption_loss_brick = -20 * log10(1 - brick_absorption_coefficient);
octave:21> absorption_loss_concrete = -20 * log10(1 - concrete_absorption_coefficient);
octave:22> % Calculate the transmission loss for both walls
octave:22> transmission_loss_brick = 20 * log10(1 / abs(1 - reflection_coefficient_source_brick * reflection_coefficient_receiver_brick) * exp(-4 * pi * brick_absorpti
on_coefficient * brick_thickness / brick_sound_speed));
octave:23> transmission_loss_concrete = 20 * log10(1 / abs(1 - reflection_coefficient_source_concrete * reflection_coefficient_receiver_concrete) * exp(-4 * pi * concr
ete_absorption_coefficient * concrete_thickness / concrete_sound_speed));
octave:24> % Display the results
octave:24> disp('Sound Insulation Coefficient for Walls:');
Sound Insulation Coefficient for Walls:
octave:25> disp(['Brick Wall Thickness 0.2 meters: ', num2str(transmission_loss_brick + absorption_loss_brick), ' dB']);
Brick Wall Thickness 0.2 meters:
octave:26> disp(['Concrete Wall Thickness 0.2 meters: ', num2str(transmission_loss_concrete + absorption_loss_concrete), ' dB']);
Concrete Wall Thickness 0.2 meters:
```

Figure (1) *The function was created on the Octave 8.3.0 program in order to calculate the sound insulation values of a brick wall and a concrete wall.*

3. Result

It was found that when the solution was performed using the function that was created in the Octave 8.3.0 program (Fig.2). Assuming that the thickness of the wall consisting of brick and concrete wall is (0.2) meters, the distance from the sound source to the wall is (1) meter, and the distance from the wall to the receiver is (1) meter. After extracting the results using the function that was created on the Octave 8.3.0 program for the sound insulation coefficients for both the brick wall and the concrete wall, while determining the wall thickness for each material, the results were as follows (Table 2). This function allows comparing the sound insulation properties of a brick wall and a concrete wall, taking into account the properties of the different materials and their thickness, in addition to the source and receiver distances.

```
octave:1> % Define material properties for the brick wall
octave:1> brick_density = 1920; % Density of brick (kg/m^3)
octave:2> brick_thickness = 0.2; % Updated thickness of the brick wall (m)
octave:3> brick_sound_speed = 343; % Speed of sound in brick (m/s)
octave:4> brick_absorption_coefficient = 0.03; % Absorption coefficient for brick (unitless)
octave:5> % Define material properties for the concrete wall
octave:5> concrete_density = 2400; % Density of concrete (kg/m^3)
octave:6> concrete_thickness = 0.2; % Thickness of the concrete wall (m)
octave:7> concrete_sound_speed = 3200; % Speed of sound in concrete (m/s)
octave:8> concrete_absorption_coefficient = 0.02; % Absorption coefficient for concrete (unitless)
octave:9> % Define the source and receiver positions
octave:9> source_distance = 1; % Distance from the sound source to the walls (m)
octave:10> receiver_distance = 1; % Distance from the walls to the receiver (m)
octave:11> % Calculate the characteristic impedance of air
octave:11> air_density = 1.225; % Density of air (kg/m^3)
octave:12> air_sound_speed = 343; % Speed of sound in air (m/s)
octave:13> air_impedance = air_density * air_sound_speed;
octave:14> % Calculate the characteristic impedance of the brick
octave:14> brick_impedance = brick_density * brick_sound_speed;
octave:15> % Calculate the characteristic impedance of the concrete
octave:15> concrete_impedance = concrete_density * concrete_sound_speed;
octave:16> % Calculate the reflection coefficient at the source side for both walls
octave:16> reflection_coefficient_source_brick = (brick_impedance - air_impedance) / (brick_impedance + air_impedance);
octave:17> reflection_coefficient_source_concrete = (concrete_impedance - air_impedance) / (concrete_impedance + air_impedance);
octave:18> % Calculate the reflection coefficient at the receiver side for both walls
octave:18> reflection_coefficient_receiver_brick = (air_impedance - brick_impedance) / (air_impedance + brick_impedance);
octave:19> reflection_coefficient_receiver_concrete = (air_impedance - concrete_impedance) / (air_impedance + concrete_impedance);
octave:20> % Calculate the absorption loss for both walls
octave:20> absorption_loss_brick = -20 * log10(1 - brick_absorption_coefficient);
octave:21> absorption_loss_concrete = -20 * log10(1 - concrete_absorption_coefficient);
octave:22> % Calculate the transmission loss for both walls
octave:22> transmission_loss_brick = 20 * log10(1 / abs(1 - reflection_coefficient_source_brick * reflection_coefficient_receiver_brick) * exp(-4 * pi * brick_absorpti
on_coefficient * brick_thickness / brick_sound_speed));
octave:23> transmission_loss_concrete = 20 * log10(1 / abs(1 - reflection_coefficient_source_concrete * reflection_coefficient_receiver_concrete) * exp(-4 * pi * concr
ete_absorption_coefficient * concrete_thickness / concrete_sound_speed));
octave:24> % Display the results
octave:24> disp('Sound Insulation Coefficient for Walls:');
Sound Insulation Coefficient for Walls:
octave:25> disp(['Brick Wall Thickness 0.2 meters: ', num2str(transmission_loss_brick + absorption_loss_brick), ' dB']);
Brick Wall Thickness 0.2 meters: -5.7469 dB
octave:26> disp(['Concrete Wall Thickness 0.2 meters: ', num2str(transmission_loss_concrete + absorption_loss_concrete), ' dB']);
Concrete Wall Thickness 0.2 meters: -5.8443 dB
```

Figure (2) Extracting the sound insulation values of the brick wall and the concrete wall using the function created on the Octav8.3.0 program.

Table (2) *Results of sound insulation values for the brick wall and the concrete wall extracted using the function created on the Octave 8.3.0 program.*

Wall type	**Sound insulation values (dB)**
Brick wall	-5.7469
Concrete wall	-5.8443

4. Discussion

The sound insulation values of the brick wall (-5.7469 dB), while the sound insulation values of the concrete wall (-5.8443 dB). These results indicate that the sound insulation of a concrete wall is better compared to a brick wall.

This is due to:

1. Material Density: Concrete is usually denser than brick, which means it has a higher capacity to block sound transmission. Concrete's density allows it to better absorb and impede sound waves.

2. Speed of Sound in the Material: The speed of sound in concrete is typically higher than in brick. This means that sound travels more slowly through concrete, which helps reduce transmission.

3. Sound Absorption Coefficient: Concrete often has a lower ability to absorb sound compared to brick. This means that sound reflects less and absorbs less in concrete, helping to direct sound outward rather than absorbing and transmitting it.

5. Conclusion

Sound insulation is a technique used to reduce or prevent the transmission of sound from one area to another. It is employed to create a quieter and more comfortable environment by minimizing the impact of noise. Sound insulation is crucial in various settings, including residential, commercial, and industrial spaces. In this study a function was created using Octave 8.3.0 program to calculate sound insulation values for a brick wall and a concrete wall. It was found that the sound insulation values of the brick wall were (-5.7469 dB), while the sound insulation values of the concrete wall were (-5.8443 dB). These results indicate that the sound insulation of concrete wall is better compared to brick wall. This is because concrete is denser and has a higher speed of sound than brick, which makes it better at preventing sound transmission. However, they have less sound absorption capabilities, which results in less sound absorption and reflection, ultimately directing sound outwards.

References

Al-Ali, L. (2004). *Basic Physics for All University Majors* (First Edition). Kuwait: Kuwait University Press.

Al-Dawaf, Y. (1978). *Construction of Buildings and Construction Materials* (Fifth edition). Baghdad: Dar Al-Hikma

Al-Mamouri, H., & Al-Mutairi, M. (2015). The effect of sustainable characteristics on the acoustic moderation of classrooms. *Babylon University Journal of Engineering Sciences, 23*(1), 16-26

Al-Ahmadi, Q., & Abd, M. (2017). Sound insulation ability of some types of concrete blocks. *Tikrit Journal of Engineering Sciences, 24*(2), 45-53.

Carlson, C. C. (1956). Light weight aggregates for concrete masonry units. *ACI Journal Proceedings*, *52*(5), 491-498.

Eaton, J. (2012). GNU Octave and reproducible research. *Journal of Process Control*, *22*(8), 1433-1438.

Gong, X. (2012). *Vibration and acoustic performance of in-plane honeycomb sandwich panels* (Master's thesis). Clemson University.

Kormer, A. (1974). *Building materials and components*. Moscow: Mir Publishers.

Neville, A. M. (1981). *Properties of Concrete* (Third Edition). London: Longman Publishing.

CHAPTER III

The Role of Pedestrian Faults in Traffic Accidents and Solution Suggestions

Nuriye KABAKUŞ[1]
Ahmet Kamil KABAKUŞ[2]

1. Introduction

Traffic accidents are one of the most serious problems of modern urban life. The unpreventable increase in road traffic accidents as a result of ever-increasing vehicle ownership has made road safety a major concern worldwide. Approximately 1.19 million people die each year as a result of road traffic accidents (WHO, 2023). In addition, the increase in vehicle ownership and traffic congestion caused by population density in urban areas have created significant safety issues, especially for pedestrians. Therefore, the

[1] Asst. Prof.., Ataturk University, Faculty of Applied Sciences, Department of Emergency Aid and Disaster Management, Erzurum/Türkiye, Orcid: 0000-0002- 8479-6733, nsirin@atauni.edu.tr

[2] Assoc. Prof.., Ataturk University, Faculty of Economics and Administrative Sciences, Department of Management Information Systems, Erzurum/Türkiye, Orcid: 0000-0003-3209-0672, kkabakus@atauni.edu.tr[1] Lecturer, Dr., Recep Tayyip Erdogan University, Department of Civil Engineering, Rize/Türkiye, Orcid: 0000-0002-4534-3686, adnan.kiral@erdogan.edu.tr

study of pedestrian faults and the measures to be taken in this area play a critical role in the development of traffic safety policies.

Pedestrian faults in traffic accidents can be attributed to various factors that increase the risk of accidents and severity of injuries. Studies have highlighted several key reasons for pedestrian-vehicle accidents. These include illegal crossing of traffic lanes, speeding, adverse weather conditions like rainy days, slippery roads, lack of timely braking, and visual impairments (Yang et al., 2022). Additionally, distractions among pedestrians have been identified as a significant factor contributing to severe injuries, with distracted pedestrians having a higher probability of suffering severe injuries compared to those who are not distracted (Febres et al., 2021). Moreover, the vulnerability of pedestrians in road traffic accidents is exacerbated by the failure to adhere to existing traffic rules by both pedestrians and drivers (Hb et al., 2020). Pedestrian faults, such as disobeying traffic rules and ignoring red signals, have been associated with a considerable number of accidents (Olszewski et al., 2016). Furthermore, the analysis of pedestrian accidents in various locations has considered factors such as pedestrian characteristics, driver characteristics, accident time, location, weather conditions, road surface, illumination, vehicle characteristics, and speed limits, all of which can contribute to pedestrian faults leading to accidents (Al-Omari & Obaidat, 2013).

Factors like age also play a role in pedestrian accidents, with studies indicating that elderly pedestrians may be more prone to causing accidents, especially at night and during reverse collisions (Chen et al., 2023). Additionally, the built environment features, such as on-street parking, narrow travel lanes, and intersections,

have been found to influence the occurrence of pedestrian accidents (Congiu et al., 2019). They also identified moving vision obstructions as a critical factor in vehicle-pedestrian crashes and emphasized the importance of environmental factors in pedestrian safety (Miao et al., 2016). Pedestrian risk behaviors are the focus of this research to identify comprehensive accident prevention strategies and improve pedestrian safety on roads (Narváez et al., 2019).

In conclusion, pedestrian faults in traffic accidents are multifaceted and influenced by a combination of pedestrian behavior, environmental factors, and interactions with drivers and road conditions. Understanding these factors is crucial for developing effective strategies to improve pedestrian safety and reduce the incidence of accidents.

This study aims to examine the role of pedestrian faults in traffic accidents in Türkiye. Data on pedestrian traffic accidents were collected and analyzed, and the types of pedestrian faults and their contribution to accidents were evaluated. The study presents the causes of pedestrian accidents and the effects of pedestrian faults in these accidents and presents a comparative analysis of pedestrian faults in fatal and injury accidents.

2. Data

The traffic accident statistics used in this study include traffic accidents with injuries and fatalities that occurred in Türkiye between 2015 and 2019. These traffic accident statistics were obtained from the General Directorate of Security through a data request. Within the scope of the research, it was aimed to create a

data set for the last five years, but the decrease in mobility due to the Covid-19 pandemic led to a decrease in traffic accidents (Kabakuş and Şahvelet, 2022). In order not to affect the results of the study and to reflect the reality, the dataset was created using five-year traffic accident statistics from the period before the Covid-19 outbreak. Table 1 shows pedestrian faults in fatal and injury accidents.

Microsoft Excel and SPSS software were used to organize the data in accordance with the purpose of the study.

Table 1. Pedestrian faults

Pedestrian Faults	**Description**
PF1	Crossing the road under the influence of alcohol
PF2	Failure to take precautionary measures to prevent collision in low visibility day and night
PF3	Failure to comply with passing rules where there are no crossings and intersections
PF4	Failure to obey traffic rules when crossing the road
PF5	Not stopping at the scene of an accident, not taking necessary precautions
PF6	Acting in a way that endangers traffic on the roadway
PF7	Entering the roadway
PF8	Not driving on the left side of the roadway
PF9	Throwing or spilling anything on the road in a way that makes traffic difficult and making similar gestures
PF10	Failure to comply with other traffic safety rules
PF11	Failure to obey traffic lights and signs
PF12	Using drugs or recreational substances

3. Results

In this study, the pedestrian faults causing fatal and injury traffic accidents in Turkey between 2015 and 2019 are analyzed. Table 2 shows the percentage contribution of driver, pedestrian, passenger, road and vehicle faults to traffic accidents.

Table 2. Faults that cause accidents involving death or injury (TSI, 2024)

Year	Driver fault	Pedestrian fault	Passenger fault	Road fault	Vehicle fault	Total
2015	%89,3	%8,8	%0,4	%0,9	%0,6	210 498
2016	%89,6	%8,7	%0,4	%0,8	%0,5	213 149
2017	%89,9	%8,5	%0,4	%0,7	%0,5	213 325
2018	%89,5	%8,4	%0,9	%0,6	%0,6	217 898
2019	%88	%8,2	%1,3	%0,5	%2	204 538

The statistics in Table 2 make it clear that the biggest cause of traffic accidents is driver faults. From 89.3% in 2015 to 88% in 2019, it still represents the highest percentage. Pedestrian at fault varied between approximately 8.2% and 8.8% during the analyzed period. This shows that pedestrians also play an important role in road accidents. The share of passenger faults in road accidents is one of the lowest and varied between 0.4% and 1.3% over the analyzed years.

Especially in 2018 and 2019, it increased to 0.9% and 1.3%, indicating that passenger safety should not be ignored. Road faults have a relatively low share in road accidents, ranging between 0.5% and 0.9%. However, improving road conditions and increasing maintenance can contribute to reducing accidents. The rate of vehicle faults increased by up to 2% in 2019. This increase once again highlights the importance of vehicle maintenance and inspections. Regular maintenance and inspections are critical to reduce vehicle faults.

Figure 1 shows the distribution of pedestrian faults in fatal traffic accidents in Turkey between 2015 and 2019. The impact of each pedestrian fault on fatal crashes is analyzed. No fatal crashes

were recorded due to PF1 (0.0%). However, alcohol use is often a potential risk factor as it can affect attention and reflexes. PF2 with a total of 29 accidents and a rate of 2.8%, can cause fatal accidents due to pedestrians not taking adequate precautions in low visibility conditions. This includes factors such as inadequate lighting or failure to use reflectors. PF3 is the most common fault with a total of 332 accidents and 32.2%. This shows that pedestrians' disobeying traffic rules by crossing uncontrolled points is the most common factor causing fatal accidents. With a total of 81 accidents and a rate of 7.8%, PF4 contributes significantly to fatal accidents when pedestrians do not obey traffic rules while crossing the road. PF5 is rare, with only 1 accident and a rate of 0.1%, but can still have serious consequences. PF6 is a serious risk factor for pedestrians behaving dangerously on the road with a total of 147 accidents and 14.2%. PF7 is a widespread problem with a total of 143 accidents and 13.9%. Pedestrians entering the carriageway may require a sudden reaction from drivers, which can lead to fatal accidents. PF8 is a less common fault with a total of 18 accidents and 1.7%, but pedestrians not using the left-hand side of the road also poses a risk. PF9 is an important factor with a total of 114 accidents and a rate of 11.0%. Behaviors such as throwing or spilling things on the road can distract drivers and lead to accidents. PF10 with a total of 56 accidents and a rate of 5.4%, pedestrians' failure to comply with general traffic safety rules can cause fatal accidents. PF11 is a widespread problem with a total of 111 accidents and a rate of 10.8%. Failure of pedestrians to obey traffic lights and signs is an important cause of accidents. No fatal accidents were recorded due

to PF12 (0.0%). However, the use of drugs or recreational substances is a potential risk as it can impair attention and reflexes.

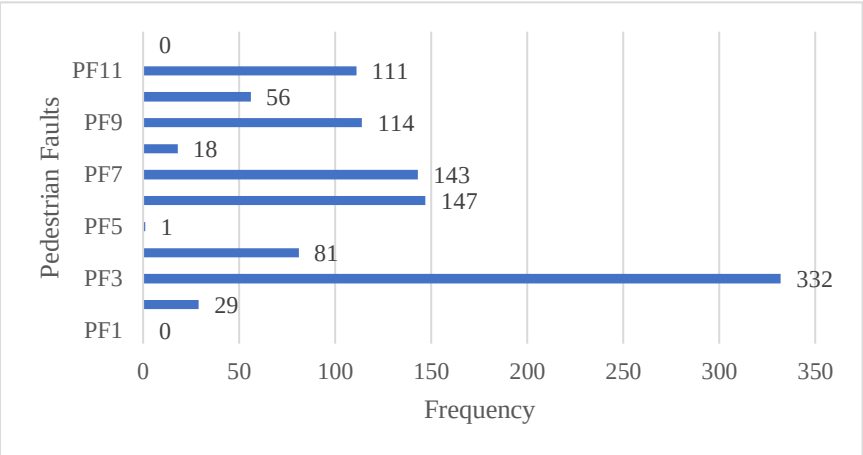

Figure 1. Distribution of pedestrian faults in fatal traffic accidents in Türkiye between 2015-2019

Figure 2 shows the distribution of pedestrian faults in injury traffic accidents in Turkey between 2015 and 2019. Injury accidents caused by PF1 were recorded 11 in these years. PF2 with a total of 1179 accidents and a rate of 1.6% is an important factor in injury accidents due to not taking adequate precautions in low visibility conditions. PF3 with the highest percentage, totaling 26851 accidents and 35.8%, this category is the most common fault of pedestrians causing injury accidents. Uncontrolled use of crossing points by pedestrians accounts for the majority of accidents. With a total of 7304 accidents and a rate of 9.7%, PF4 is an important risk factor for pedestrians not obeying traffic rules while crossing the road. PF5 is recorded with 95 accidents and a rate of 0.1%. However, failure to take precautions at the scene of an accident can lead to

serious consequences. PF6 with a total of 14610 accidents and a rate of 19.5%, dangerous behavior of pedestrians on the roadway is an important cause of injury accidents. PF7 with a total of 5028 accidents and a rate of 6.7%, pedestrians entering the roadway is also an important factor causing injury accidents. PF8 with a total of 901 accidents and a rate of 1.2%, this fault is less common but still poses a significant risk. PF9 with a total of 5815 accidents and a rate of 7.7%, can jeopardize traffic safety when pedestrians throw or spill things on the road or perform similar actions. PF10 with a total of 3498 accidents and a rate of 4.7%, pedestrians not obeying general traffic rules is also an important risk factor for injury accidents. PF11 with a total of 9669 accidents and a rate of 12.9%, failure to obey traffic lights and signs, is also a common fault of pedestrians in injury accidents. 1 injury accident was recorded due to PF12**.**

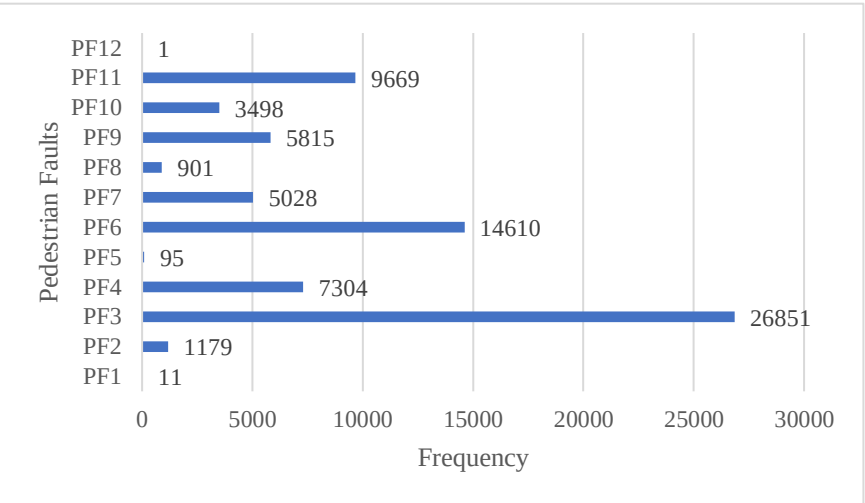

Figure 2. *Distribution of pedestrian faults in injury traffic accidents in Türkiye between 2015-2019*

The ranking of pedestrian fault in fatal traffic accidents in 2015-2019 is as follows: PF3, PF6, PF7, PF9, PF11, PF4, PF10, PF2, PF8, PF5, PF12 and PF1. Pedestrian fault ranking in injury traffic accidents: PF3, PF6, PF11, PF4, PF9, PF7, PF10, PF2, PF8, PF5, PF1 and PF12.

4. Conclusion and Suggestions

In both fatal and injury accidents, PF3 and PF6 pedestrian faults take the first two places. This shows that these two defects are the most common pedestrian defects in traffic accidents. Awareness-raising and education campaigns should be increased especially for these defects. The PF11 pedestrian fault ranks 5th in fatal accidents and 3rd in injury accidents. This shows that PF11 is more prevalent in injury crashes, but also plays an important role in fatal crashes. PF7 ranks 3rd in fatal accidents, but drops to 6th in injury accidents. Similarly, PF9 ranks 4th in fatal accidents and 5th in injury accidents. While these defects are common in both types of accidents, they play a more prominent role in fatal accidents. PF4 ranks 6th in fatal accidents and 4th in injury accidents. This shows that the PF4 defect is more prominent in injury accidents. PF10 has a similar ranking in both types of accidents (7th place in fatal accidents and 7th place in injury accidents). This fault has an average prevalence in both types of accidents. Faults PF2, PF8, PF5 have similar rankings in both types of accidents and generally occur with average or lower frequency. PF2 and PF8 rank 8th and 9th in both fatal and injury crashes. Pedestrian faults PF1 and PF12 are ranked last in both types of accidents.

Various strategies and measures can be taken to reduce pedestrian faults, improve pedestrian safety and minimize traffic

accidents. These measures should range from education to infrastructure improvements. We can list the solutions to reduce pedestrian faults:

- Provide traffic safety education for pedestrians in schools and community centers. Organize seminars and training programs for adults and children to teach safe pedestrian behaviour. Public service announcements on pedestrian safety should be broadcast on television, radio and social media to raise public awareness. In addition, informative brochures and posters on pedestrian safety should be prepared and distributed to the public.
- Pedestrian crossings should be made more prominent and safer. Crosswalk lighting should be increased and crosswalk markings should be more prominent. In addition, speed humps and crosswalk signals should be used at pedestrian crossings.
- Pedestrian overpasses and underpasses should be constructed in areas with heavy traffic. These crossings will enable pedestrians to cross the road safely.
- In city centers and areas with heavy pedestrian traffic, pedestrian routes should be widened and made safer for pedestrians. Barriers and railings can be used to improve pedestrian safety.

- Compliance with traffic rules at pedestrian crossings and on pedestrian roads should be strictly monitored. Penal sanctions can be imposed if pedestrians do not obey traffic rules. Traffic signaling at pedestrian crossings should be operated correctly and effectively. Pedestrians should be ensured to cross safely by using pedestrian buttons at pedestrian crossings.

- Pedestrian safety can be improved by using smart traffic lights and pedestrian detection systems. Traffic flow can be optimized by using sensors and cameras in areas with high pedestrian density. Mobile applications can be developed to show safe routes for pedestrians. Warning systems that can be installed on mobile devices can be used to improve pedestrian safety.

- Municipalities and local governments should play an active role in pedestrian safety. Local governments should be encouraged to invest in pedestrian safety projects.

The above-mentioned measures to reduce pedestrian defects will be important steps in improving pedestrian safety. Education and awareness-raising campaigns, infrastructure improvements, strict enforcement and the use of technology, as well as community cooperation, will play a critical role in the success of this process. These strategies will not only reduce pedestrian offenses, but also significantly improve overall traffic safety.

In conclusion, traffic accident statistics show that drivers bear the greatest responsibility for preventing accidents. However, it is of great importance for traffic safety to examine other causes of accidents in detail and to discuss measures to be taken to reduce these causes. This approach provides valuable guidance for the formulation and implementation of traffic safety policies.

Acknowledgments

The authors are very grateful to the General Directorate of Security for providing the traffic accidents data.

References

Al-Omari, B. and Obaidat, E. (2013). Analysis of pedestrian accidents in irbid city, jordan. *The Open Transportation Journal*, 7(1), 1-6. https://doi.org/10.2174/1874447801307010001

Chen, Y., Yuan, R., Wei, J., & Li, S. (2023). Research on the influencing factors of elderly pedestrian traffic accidents considering the built environment. *International Review for Spatial Planning and Sustainable Development*, 11(1), 44-63. https://doi.org/10.14246/irspsd.11.1_44

Congiu, T., Sotgiu, G., Castiglia, P., Azara, A., Piana, A., Saderi, L., … & Dettori, M. (2019). Built environment features and pedestrian accidents: an italian retrospective study. *Sustainability*, 11(4), 1064. https://doi.org/10.3390/su11041064

Febres, J., Saldaña, M., Herrera, S., & Herrero, S. (2021). Pedestrians' injury severity in traffic accidents in spain: a pedestrian actions approach. *Sustainability*, 13(11), 6439. https://doi.org/10.3390/su13116439

Hb, K., Prasad, H., & Ks, G. (2020). Pattern of pedestrian injuries during road traffic accidents in autopsied cases at belgaum institute of medical sciences, belagavi. *International Journal of Forensic Medicine*, 2(2), 04-07. https://doi.org/10.33545/27074447.2020.v2.i2a.23

Kabakuş, N., & Şahvelet, M. N. (2022). The Positive Effect Of Covid-19: The Reduction In Traffc Accidents. Editors: Assoc. Prof. Mehmet Sinan BAŞAR Assoc. Prof. Atif BAYRAMOGLU, 47.

Miao, M., Yang, Y., & Liang, Y. (2016). Pedestrian crash risk assessment and intervention. *Advances in Mechanical Engineering*, 8(7), 168781401665329. https://doi.org/10.1177/1687814016653296

Narváez, Y., Sierra, V., Cárdenas, F., Ramos, L., González, B., Martínez, J., … & Aranda, O. (2019). Road risk behaviors: pedestrian experiences. *Traffic Injury Prevention*, 20(3), 303-307. https://doi.org/10.1080/15389588.2019.1573318

Olszewski, P., Osińska, B., & Zielińska, A. (2016). Pedestrian safety at traffic signals in warsaw. *Transportation Research Procedia*, 14, 1174-1182. https://doi.org/10.1016/j.trpro.2016.05.188

TSI (2024). *Highway traffic accident statistics*. (Accessed from https://data.tuik.gov.tr/Search/Search?text=kaza%20istatistikleri&dil=1 on 09/06/2024).

WHO (2023). *Road traffic injuries*. (Accessed from https://www.who.int/news-room/fact-sheets/detail/road-traffic-injuries on 10/06/2024).

Yang, J., Lai, Y., Shi, H., & Chen, Y. (2022). Analysis of the causes of pedestrian-vehicle traffic accidents based on bayesian networks. https://doi.org/10.21203/rs.3.rs-2286561/v1

CHAPTER IV

Seismic Response Control of Buildings Using Viscous-Based Devices*

Adnan KIRAL[1]
Zeliha TONYALI[2]

Introduction

The seismic design of buildings continues to evolve. There are two driving factors for this evolution. The first one is associated with more reliability and higher safety levels for densely populated city centres located in earthquake-prone areas. The second one is that economical limitations tighten the need to optimise craftsmanship and resources.

[1] Lecturer, Dr., Recep Tayyip Erdogan University, Department of Civil Engineering, Rize/Türkiye, Orcid: 0000-0002-4534-3686, adnan.kiral@erdogan.edu.tr
[2] Assistant professor, Recep Tayyip Erdogan University, Department of Civil Engineering, Rize/Türkiye, Orcid: 0000-0002-6637-7949, zeliha.tonyali@erdogan.edu.tr
* This chapter is derived from the first author's PhD thesis (Adnan KIRAL) submitted to the Department of Automatic Control and Systems Engineering at the University of Sheffield, United Kingdom. 01 September 2022.

The current building-design methodology is based on the ductility criterion. One advantage of this approach compared to the older, strength-based design, is that the forces in the structure are limited, which reduces the resistance demand and ultimately the size of structural elements. The deformations of the system are limited by the increased dissipation of seismic energy through controlled damage at pre-defined zones of the structure. Even though this design methodology achieves more efficient use of materials, resulting in lighter structures, it leads to high repair costs after a ULS earthquake. Also, the primary function of the main structural elements (e.g., columns and beams) is to maintain the integrity of the structure under earthquakes (i.e., the job of structural elements is either to dissipate energy or keep the integrity of the system for occupants' safety), so it is difficult to optimise their energy dissipation capacity. Therefore, the current design methodology may not be an optimal solution (see, [1-3]).

A possible solution, which is called structural control, has been studied for some time for both retrofitting of existing and design of new buildings. The main aim of this solution is to reduce the seismic response, which could prevent/or, at least, limit structural damage under severe earthquakes. Structural control systems, which can be classified as passive, active and semiactive systems, can lower the seismic response either by neutralising the seismic forces directly or by introducing additional elements designed specifically to dissipate seismic energy and/or change the dynamic properties of the structure during the earthquake.

Structural control systems can:

- Increase energy dissipation,
- Improve reliability (the elements can be standardized and produced in an industrial setting),
- Have low-cost repairs after an earthquake; but
- Increase initial costs

Each type of structural control has advantages and disadvantages. Active and semi-active control systems require advanced technological resources, such as energy supply, sensors, controllers, and devices that will generate forces in the structure [4]. Relatively simple passive control systems, which can be based on a variety of mechanisms [5], such as viscous (see [6-9]; Figure 1.1a), viscoelastic (see [8], [10-13]; Figure 1.1b), yielding (see [8], [14-19]; Figure 1.1c), or friction (see [8], [15], [20-22]; Figure 1.1d), can decrease the seismic response of the building and reduce damage (or even prevent under small ground excitations) in the main structural elements, such as beams, braces, or columns.

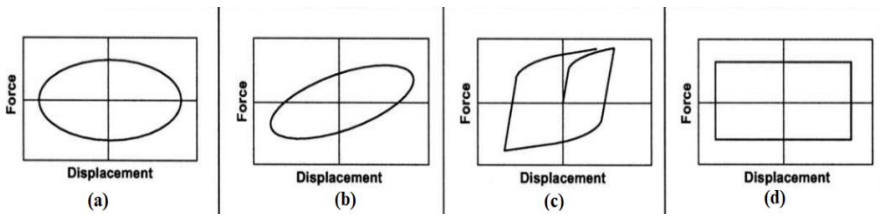

Figure 1.1. *Hysteretic behavior of (a) viscous, (b) viscoelastic solid, (c) metallic and (d) friction damper*

The application of any structural control mechanisms (e.g., active, semiactive, or passive) on moment resisting frame structures can however increase total base shear and foundation demand, which

are the concern of vibration control of the design of buildings or retrofit applications.

For example, Passive Viscous Damper (PVD), which is one of the commonly used damping devices**,** can add damping without increasing base-shear only for low-damping applications (i.e., in cases when the main structure remains linear elastic, which only happens for low level earthquake acceleration inputs). For high-level of structural damping, which is the case for most structures designed for severe earthquakes on the basis of a traditional performance-based seismic design and retrofit philosophy, where the main structure is expected to develop larger deformations and non-linear response, it is inevitable for PVDs to increase base shear and foundation demand [23-27]. This bounds the wide use of PVDs in new structures and retrofits.

Adaptable passive control approaches (sometimes called smart control; active, semi-active etc.,) have also been widely investigated as systems for improving the performance of passive control. By changing the configuration of the chambers inside Viscous Damper (VD) and filling it with different viscous fluids, one can modify both the passive viscous damping exponent and its coefficient during manufacturing [26].

In 1972, an active control approach, which was intended to be an alternative to traditional passive damping devices, was proposed by Yao (Yao, 1972) to improve the dynamic structural response. Altering damping inputs and device behaviour in response to changes in structural dynamics was the advantage of that control as well as showing an increase in robustness compared with passive

solutions. Nevertheless, such control needs larger power input to be practical in the need of actively producing large seismic mitigation forces.

Active control devices and their algorithms can be also complicated and could raise concerns about their robustness (in terms of energy requirements and algorithms under ground excitations) over the long term [28]. As a result, demanding significant costs for operation and adding complexity into vibration control of structural frames is inevitable for active controls.

As a solution, a semiactive system which is a combination of active and passive control systems requires a small external power source for its operation [26]. Semi-active control device function continues its operation as a passive device, even in case of a power failure [26]. The semi-active devices do not add energy to the system rather they store or absorb the vibration energy resulting from an excitation. They cannot, therefore, destabilize the structural frames [29], [30]. The semi-active control system can only alter the control action of a structure by changing the damping [31-32] or stiffness of the system [33].

It was already discussed that additional PVDs in non-linear structures or generally in structures with a high level of damping would likely increase base shear and foundation demand. Such increases would reduce the ability to use PVD (Passive Viscous Damper) in structural retrofitting applications without significant added cost.

Apart from potential semiactive control devices in literature (see [26], [34-38]), which provide damping forces in all four

quadrants of a viscous damper, there is also an ongoing research interest in manipulating the force-displacement hysteresis curve of the damper (Figure 1.2a) to achieve design objectives such as reducing drift without increasing base shear [30], increasing energy dissipation of the damper [31-32] or effective shock absorbers for vehicles [39-40]. The force-displacement loop can be reshaped by either decentralised semiactive control [30-32], or mechanically, by a passive damper [30], [40]. Reshaping the hysteresis loop has attracted interest of researchers in the field of control systems in earthquake engineering, as well as of vehicle researchers for shock absorbers [39-40].

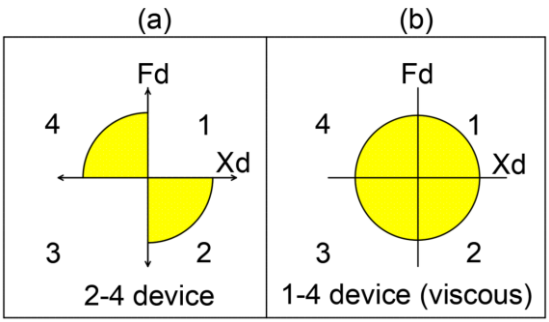

Figure 1.2. *Force- displacement relation of a conventional passive linear viscous damper*

Reshaped viscous dampers (Figure 1.2a) offer unique abilities similar to those seen for less robust and more complicated semi-active stiffness-based devices. The manipulated force-displacement relationship of the viscous dampers delivers an outstanding and appealing solution for reducing seismic response, with minimal risk of structural or foundation damage, which makes them convenient for more economic retrofit, as well as new designs. Unlike the passive control, the reshaped hysteresis loop doesn't

increase base shear since damper forces and columns forces do not occur at the same time.

A smart control (e.g., semiactive), which can reduce inter-storey drifts of a building, but reduce the base shear or/ doesn't increase base shear of the structure, could be a promising approach for mitigating structural damage during severe earthquakes.

Literature review of viscous-based control

Structural control systems, which can be classified as passive, active and semiactive systems, reduce the seismic response either by neutralising the seismic forces directly or by introducing additional elements designed specifically to dissipate seismic energy and/or change the dynamic properties of the structure during the earthquake.

Structural control systems (i) increase energy dissipation, (ii) improve reliability (the elements can be standardized and produced in an industrial setting), and (iii) reduce the cost of repairs after an earthquake; but (iv) they increase the initial costs

Each type of structural control has advantages and disadvantages. Active and semi-active control systems require advanced technological resources, such as energy supply, sensors, controllers, and devices that will generate forces in the structure [4].

2.1. Passive control

Passive control systems dissipate the energy that enters the system in an earthquake by yielding of materials, frictional sliding, or compression of fluids. The main advantages of passive control systems are that they do not need any external power source for their

control operations, they have simple working mechanisms, they absorb a significant amount of seismic energy from the structures, and they require little maintenance after installation [13], [26]. In a passive control system (PCS), the control forces applied to the building only depend on the structural motion [41]. Modern buildings are designed to dissipate energy through nonlinear deformations, the added cost of passive control systems needs to be justified by significant improvements in performance. Existing studies show that this can only be done by relatively extensive parametric studies for each structure, although there are some promising studies [2-3], that use sophisticated optimisation techniques to establish simple rules for designing passive systems.

Active control systems

Active control systems dissipate the energy of structures utilizing additional actuators based on acceleration, velocity, displacements, etc. measured by the sensors in vibration systems. Active control systems used in civil engineering applications raise considerable uncertainty (which is largely due to implementation issues) such as nonlinearities in both physical properties and disturbances, a limited number of actuators and sensors, complexities in the dynamics of the actuators, the scale of the forces and energy required for their operations (which can be quite large) [26], [42-43].

Semiactive control

Semiactive (SA) systems which are a combination of active and passive control systems requires a small external power source for its operation [26], as they use the movement of the building to

develop the control forces, with small external energy needed only to control the operation of the device [26]. As an active control system, it monitors the feedback from the control system and creates necessary command signals [44]. Control forces which are only engaged to deliver the resistive forces [36] initially act to oppose the motion and are improved through suitable algorithms. A semi-active control device continues its operation as a passive device, even in a power failure [26], [45-46]. The design and construction of an SA control system can be done even after installation. Note that the semi-active control system can only alter control action of a structure through damping (see [30]) or stiffness characteristics of the system (see [29]).

As follows are the mechanical properties and description of the smart-fluid damper (semi-active): A semi-active fluid viscous damper was proposed by Symans et al. [26], as a simple conversion of a standard passive damper, "*by drilling two ports in the cylindrical housing and connecting them with steel tubing and a control valve (see Figure 2.1). The amount of fluid which can pass through the external path is determined by the orifice opening within the control valve*." [26].

According to Symans and Constantinou [26], variable damping coefficients can be estimated as follows (see eq. 2.1):

$$C(v) = C_{min} + (C_{max} - C_{min})\exp(-\mu v n) \qquad (2.1)$$

where C(v) is the damping coefficient which is a function of command voltage v. μ and n are constant. The damper can generate any value within these C_{max} and C_{min} bounds.

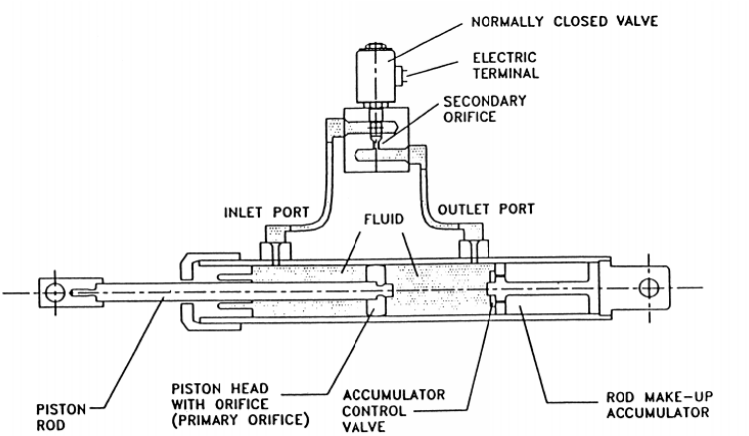

***Figure 2.1**: A Semiactive fluid damper [26]*

The general schematic diagram of a semi-active control system is given in Figure 2.2. This control system was first introduced in civil engineering structures by Hrovat et al. [45].

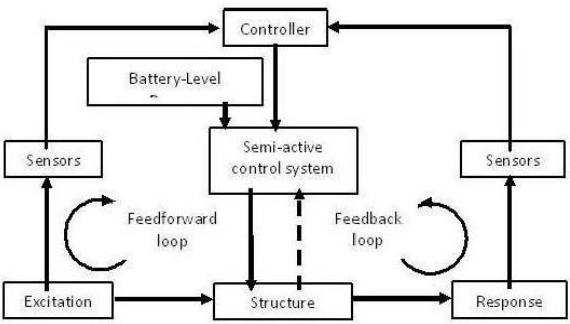

***Figure 2.2**. Schematic diagram of the semi-active control [45]*

Proposing an optimal control force to suppress building vibration has been an ongoing interest for engineers for many years. Many different control methods under different circumstances have been offered. However, none of them could be widely used in civil engineering design since each building needs different design

requirements for each type of building such as hospital, museum, school, skyscraper etc**.** Yet, in order to suppress the vibration over a wide frequency region, FVDs are often adopted in the structural systems to achieve a better system vibration performance [26]. Also, many researchers have studied the effects of viscous damping placed to different floors of buildings to examine the behaviour of SDOF systems (e.g., [47-48]).

Fluid viscous damper for seismic control

FVD which is known as one of the most commonly used passive damping devices was firstly applied for artillery rifle in 1897 [49]. In 1980s, it gained popularity in armies and navies of many countries; nevertheless, it was not publicly broadcasted due to the secretive nature of the research [50]. Fluid viscous dampers, which were manufactured at that time, were mostly based on the viscous effect between metal plates in the damper as depicted in Figure 2.3a. Due to viscosity dependent behaviour of the damper, it was highly sensitive to the working environment and the temperature. The fully developed FVD technology was declassified and made available for public practice in the late 1980s [51]. The developed fluid viscous dampers, which offered high damping capacity and wide range of manufacturing options, paved the way for many commercial applications such as bridges, buildings etc. Soong and Constantinou [52] proposed a modern fluid viscous damper (Figure 2.3b), which was widely embraced by mechanical and civil engineering structural applications. In this modernized FVD, the vibration energy is dissipated by the compressible silicone fluid which flows through the damper orifices and generates the resistance force. The modified damping principles of FVD by the help of late developments paved

the way for having a stable behaviour in a complex working environment [43]. These boosted the Fluid viscous dampers' acceptance in civil engineering and practical mechanical systems.

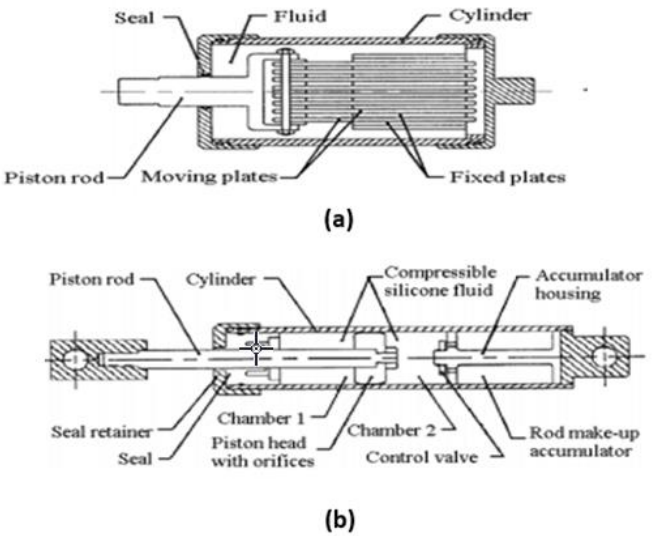

Figure 2.3*. (a) Fluid viscous damper, (b) modern FVD [52]*

FVD is deemed to be the least space-intensive and the most cost-effective approach in the vibration control design of a system after a few decades of research followed in many theoretical and experimental studies [26], [43]. Some of the advantages of FVD are (see [43]):

1. Due to being out of phase with shear stresses and primary bending in a structure, FVD can be used to reduce both deflections and internal shear forces in a building structure for low damping applications.

2. FVD (passive) is self-sustaining and doesn't need to have the power to perform during excitation
3. FVD works at a fluid pressure level of important magnitude, which makes the dampers small, compact and easy to install.
4. Compared with other passive damping devices, fluid viscous dampers are cheaper, require less maintenance and are easier to install, which reduces the cost of the structure.
5. As a result of its successful use in large-scale applications for over 30 years, it gained trust in the military, civil structural engineering, and aerospace industries.
6. Ever since the increased demand to preserve commercial and public structures, such as sensitive instruments, mechanical components, nuclear reactors, and structural installations, under wind loadings, ground motions (e.g., earthquake), shocks and impact loads, FVD is widely employed by a wide range of engineering (mechanical, civil structural and aerospace).
7. Several different types of installation modes for FV damping devices have been developed and are in progress to meet the engineering demand with a cost-effective and sustainable approach. Some of these examples are shown in Figure 2.4.

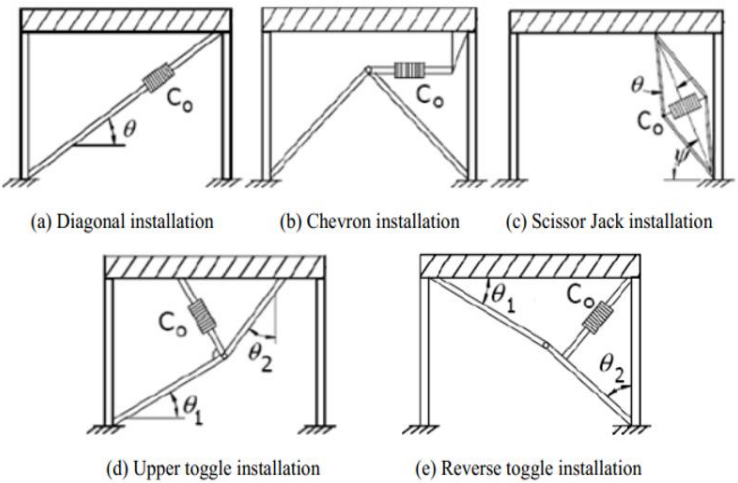

Figure 2.4*. Typical installation modes of FV damping devices [53]*

The resistive damping force F_d generated by a fluid viscous damper with brace stiffness can be theoretically expressed by Maxwell modelling (eq. 2.2).

$$F_d = C_d * \dot{\delta}^a_{damper} = K_{brace} * \delta_{brace}\ ,\ \delta_{total} = \delta_{damp} + \delta_{brace} \quad (2.2)$$

where $\dot{\delta}$ is the relative velocity between the two ends of the damper. C_d and a are the damping coefficient and velocity exponent respectively. δ_{brace} and δ_{damp} are brace and dashpot displacement respectively. Figure 2.5 shows the relationship between the relative velocity of typical fluid viscous dampers and the damping force under different values of a.

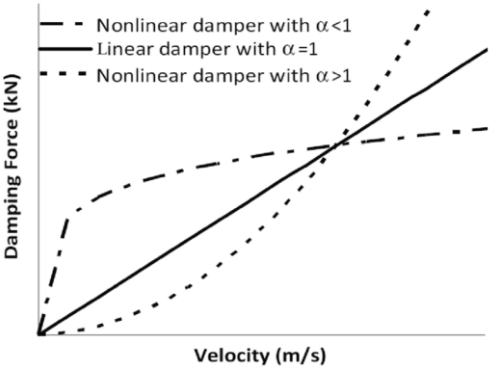

***Figure 2.5**. Force-velocity relationship of viscous damper [54]*

When the damping exponent (a) is larger or smaller than 1, the damper's dynamic characteristic is nonlinear, as the damping force acts in the opposite direction to that of the relative velocity between two ends of the damper itself. The damper's dynamic characteristic is otherwise linear (a=1). Through changing the configuration of the chambers inside the damper and filling with different viscous fluids, one can modify the viscous damping exponent and its coefficient. To meet the design requirements, fluid viscous dampers' dynamic characteristic can be modelled either as nonlinear or linear [54].

Traditional Design vs. Fluid Viscous Damper

To show the superiority of FVDs over the traditional vibration control methods, the resulting benefits of fluid viscous dampers must surpass those of the traditional design methods. Hence, the performance requirements for the structure regarding the desired response during and after an earthquake is vitally important in the decision. The energy dissipation of conventional seismic design is dependent on the inelastic response of its structural

components. Quantifying an element's hysteretic behaviour requires quantifying its displacement between stories. The conventional seismic design anticipates having an inelastic deformation to some extent after some earthquakes. However, the integrity of the structure cannot be compromised.

After the Northridge earthquake, scientists started to question the traditional connection details for maintaining structural integrity. Even though a large number of research studies in connection detailing of structural components has been conducted, rehabilitation may still be required depending on the extent of inelastic deformation [55]. Fluid viscous dampers enable the structure to remain elastic, while FVDs themselves satisfy the necessary damping for dissipation of the energy in the structure during ground motions. FVDs can achieve much higher damping forces than conventional structures without leading to large drifts of building structures during seismic events [26]. Applying FVDs would require a higher cost despite the benefit of eliminating repair costs after an earthquake. Viscous damper (VD) can be a futuristic solution to environmentally friendly building design by designing a deficient dual frame (bare frame + VD) for the sake of consuming less steel or concrete materials in a structure. To discuss FVDs with one of potential vibration control methods, if a brace application is selected, it would decrease the fundamental period (T) of the building. As a result, in cases where the structure is designed for high intensity near-field earthquakes with short predominant periods, the stiffer braced structures may provoke resonant behaviour. In addition, brace would increase axial forces in columns.

Passive FVD applications

The first use of FVDs in the seismic protection field was the Arrowhead Regional Medical Centre in the United States of America. 186 dampers were installed in the building parallel with rubber base isolation bearings to absorb quake energy [51]. After the Loma Prieta earthquake, Vincent Thomas Bridge was retrofitted to control the deformation of the suspended trusses with full-scale nonlinear fluid viscous dampers [56]. Another example of FVD applied is the Rion-Antirion Bridge project in Greece. NFVD (Nonlinear Fluid Viscous Damper) with lower-than-one power damping characteristic parameter was utilised to control displacements caused by an earthquake [57]. A considerable number of experimental and theoretical studies were conducted to investigate linear and nonlinear fluid viscous damper behaviour for a various number of structural engineering applications. A study conducted by McNamara et al. [58] aimed to investigate the vibration isolation performance of a 39-storey office building subjected to wind loadings and compare with other potential vibration isolation devices. They proved that FVDs were deemed the most cost-effective and the least space-intensive on the office building, which is followed by the installation of diagonal and toggle braces on several floors. A new design procedure for supplemental FVDs in practical bridge structures is also introduced to control the vibration during ground motions [59].

De Domenico et al [60] discuss nine different damper placement methodologies along with building heights in their review paper. They include iterative methods and simple methods. The

damper placement methods (which were selected from Figure 2.6) are:

- Sequential search algorithm (SSA) (which is classified as repetitive methodology)
- Uniform distribution (UD) (which adopts that the damping constants are identical at every storey)
- Storey-shear-proportional-distribution (SSPD) (it suggested to distribute the FVDs in proportion to the design story shears)
- Storey-shear-strain-energy (SSSE) distribution (it was offered to distribute the FVDs in proportion to the storey shear strain energy)
- Storey-shear-strain-energy-to-efficient-storeys (SSSEES) distribution (modification of SSSE was used for shear strain energy is larger than the average story shear strain energy)
- Stiffness-proportional distribution (SPD) (using Rayleigh damping constant)
- Gradient-based search methods (it employed the displacement transfer function)
- Fully-stressed analysis/redesign procedure (This method employs an iterative procedure to maximize the effect of the dampers on the performance index parameter)

- Optimal control theory (it targeted to minimize a performance cost function)
- Genetic algorithm (GA) (it automatically assumed different starting points and perform the search sequentially without computing any gradient)

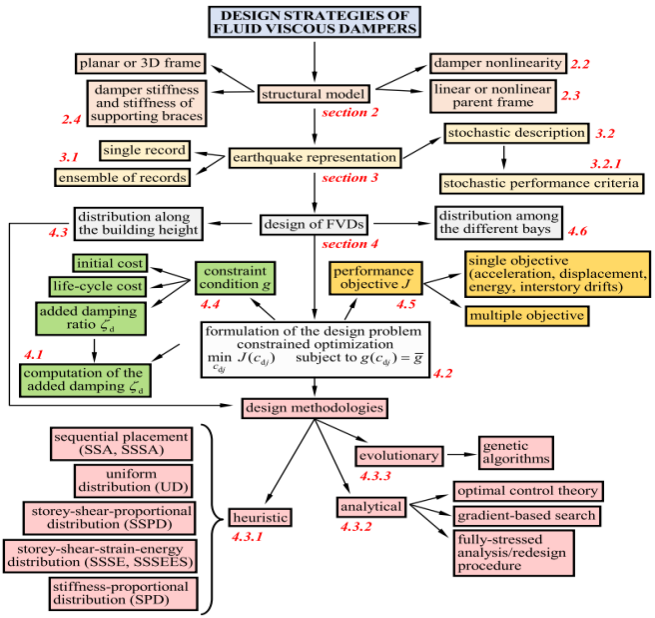

***Figure 2.6**. Design strategies of fluid viscous dampers [60]*

The design methodologies mentioned above assumed that the parent frame has a *linear elastic behaviour*. The nonlinearity of the frame response (considering buildings experiencing inelastic deformations or assuming a yielding structure) was included in the design of FVDs by some studies from the relevant literature (see [61-63]). Lavan et al. suggested the concept of weakening and damping, which tries to weaken the columns of structure (allowing nonlinearities in the structure) and add damping (with viscous

damper) to the structure for the sake of reducing acceleration (by reducing column forces) and displacement of the system (by using the advantage of viscous damper since it is out of phase with column forces). Lavan and Dargush presented a novel Genetic Algorithm (GA) for multi-objective seismic design optimization (acceleration and displacement). The algorithm is used for the concept of weakening and damping. Attard proposed a gradient-based optimization algorithm in nonlinear steel frame. An optimal damping ratio was computed in all modes of vibration. Whenever the damping ratio changes were negligible, the objectives were achieved.

Those nonlinear frame applications considered either damping ratio-based distribution or weakening of structure. All these aforementioned studies simply try to propose an optimal damping coefficient distribution in buildings, while achieving their design objectives.

In order to formulate effective design strategies in codes (e.g., EC8, ASCE), more work must be done in this field, and it would be desirable to incorporate more contributions into them. In fact, only the US structural code [64] and recently EC8 [65] provide specific recommendations for simplified structural analysis and design of dampers in buildings, but not sufficient information for an easy and rapid damper design [66].

The modal damping ratio associated with supplemental FVDs can be used to assess and quantify the effectiveness of damper distributions in buildings. The simplified formula proposed in the FEMA 356 [64] provisions, which is recalled here (see eq. 2.3), can

be used in a preliminary stage of analysis and design to determine the viscous damping ratio of the added FVDs.

$$\zeta_{\mathrm{d}} = \frac{T_1}{4\pi} \frac{\sum_{j=1}^{n_{\mathrm{d}}} c_{\mathrm{d}j} f_j^2 \left(\phi_{1j} - \phi_{1j-1}\right)^2}{\sum_{i=1}^{n} m_i \phi_{1i}^2} = \frac{T_1}{4\pi} \frac{\boldsymbol{\phi}_1^T \mathbf{R}^T \mathbf{D} \mathbf{R} \boldsymbol{\phi}_1}{\boldsymbol{\phi}_1^T \mathbf{M} \boldsymbol{\phi}_1} \tag{2.3}$$

where $\boldsymbol{\phi}_1$ is the first eigenvector of the undamped building structure (such that $\mathrm{K}\boldsymbol{\phi}_1 = \mathrm{M}\boldsymbol{\phi}_1 \omega_1^2$), and $T_1 = 2\pi/\omega_1$ is the fundamental period.

With the use of damping correction factors, Eurocode 8 [65] also determines the damping ratio (ζ) for achieving the desired performance level. In Cl. 3.2.2.2 [65], EC8 provides a relationship (Eq. 2.4) between the total damping ratio and the damping correction factor.

$$\eta = \sqrt{\frac{10}{5+\zeta}} \geq 0.55 \tag{2.4}$$

By calculating the amount of supplemental damping needed, damper coefficients and damper placement can be determined after.

Passive Viscous Damper (PVD) can add damping without increasing base-shear for only low-damping applications (i.e., under small-earthquake accelerations). For high-level of added damping, which is the case for most structures designed for severe earthquakes on the basis of a traditional performance-based seismic design and retrofit philosophy, where the main structure is expected to develop larger deformations and non-linear response under large earthquake accelerations, it is inevitable for PVDs to increase base shear and foundation demand (see [23-27]). This limits the wide use of PVDs in new structures and retrofits. It is worth mentioning that to lessen

structural element yielding under earthquakes, base shear ought to be reduced as much as possible in a building design.

Therefore, adaptable passive control approaches (e.g., active, semi-active etc.,), which can offer smaller inter-storey drifts than corresponding passive control systems, but reduce /or doesn't increase the base shear, could be a promising approach for mitigating structural damage during severe earthquakes. Semiactive controls, for example, that could manipulate force-displacement loops of viscous dampers (by removing forces in some quadrants; motion away from equilibrium) when applied to a frame, would not require strengthening of columns and foundation and thus reduce structural damage by preventing base shear increase.

Semiactive FVD applications

To improve the performance of the conventional passive FVDs, after some experimental works, a study [26] stated that the semi-active fluid viscous damper (SAFVD) with variable characteristics performed better than passive control. SAFVDs offers some benefits to the system by offering adaptability during earthquakes (with variable characteristics), requiring a small power source, and having the potential of stabilizing the structure (due to velocity-dependent behaviour). The first use of SAFVDs in seismic control of a linear MDOF building was published by Kurata et al. [37] in the 1990s. The other applications of SAFVDs were introduced in vibration control of bridges [38]. Low-rise linear base-isolated structures equipped with SAFVDs were also studied [35]. The study stated that the semiactive control performed better than passive viscous damper. Another application of the semi-active fluid viscous dampers was conducted for an asymmetric 3-D high-rise

linear building under some single earthquakes [67]. The research concluded that the semi-active system reduced torsional effects of irregular tall building compared with uncontrolled structure. Oliveira et al. [68] have investigated a linear-SDOF structure equipped with semi-active fluid viscous dampers. They showed that the effectiveness of the semiactive control for passive and active systems. The same study was extended for a base isolated SDOF structure equipped with SAFVD. The investigation ended with similar results [68]. Ho et al. [36] have conducted an experimental study for linear-MDOF system against a long-period ground motion. They confirmed the effectiveness of SAFVDs against passive linear fluid viscous damper. i.e., By utilizing semiactive control, low acceleration transmissibilities can be achieved around the structural natural frequency and higher ground motion frequencies as commonly observed during Japanese earthquakes.

Apart from all semiactive control devices in literature [26], [34-37], which provide damping forces in all four quadrants, there is also an ongoing research interest in manipulating the force-displacement hysteresis curve of a damper to achieve design objectives such as reducing drift without increasing base shear (see [30]) or increasing energy dissipation of the damper (see [31-32]).

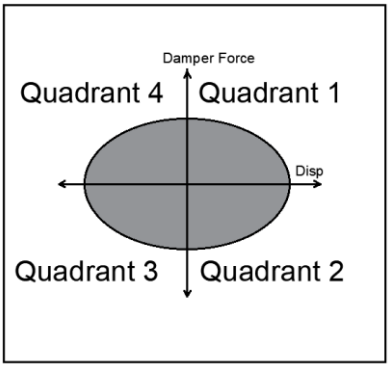

Figure 2.7*. Traditional force-displacement relation of fluid viscous damper*

The force-displacement loop (Figure 2.7) can be reshaped by either decentralised semiactive control [30-32], or mechanically, by a passive damper [30], [40]. By adding dampers (such as viscous dampers) to the building frame, the maximum base shear can be increased substantially, which in practice would require stronger foundations and columns. Reshaping the hysteresis loop (having forces in only quadrants 2 and 4) has attracted interest of researchers in the field of control systems in earthquake engineering due to not increasing base shear while reducing drifts, as well as of vehicle researchers for shock absorbers [39-40], [69].

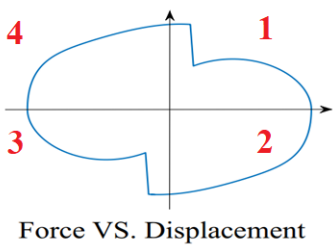

Figure 2.8. *Force-displacement relation of a shock-absorber for a vehicle [40]*

A variable damping viscous device, which can just adjust the level of damping, was first reported in NCEER-95-0011 [26]. In this device there was no individual control of specific quadrants of the hysteresis loop, but rather just change of damping in all four quadrants.Figure 2.9 shows the changes of the hysteretic loop and the changes of the control signal (and the resulting damper force) in time.

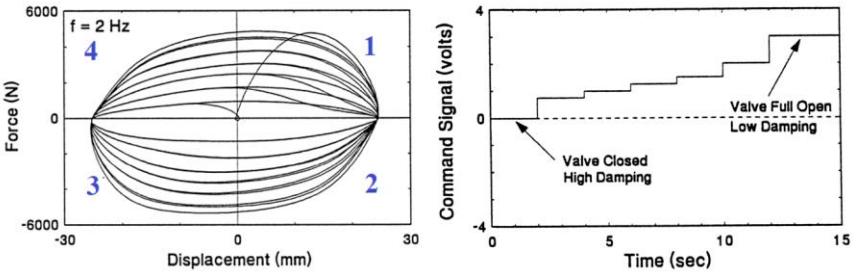

Figure 2.9. *Typical force- displacement loops for variable damper- from report NCEER 95-0011*

Tsopelas and Constantinou [70] developed a passive device, which was called fluid restoring force/damping. It operates only in quadrants 1 and 3, by introducing spring and viscous damping force in the device (Figure 2.10). However, as expected, these devices add damper forces at increasing displacements, in parallel with the increase of the restoring forces in the main structure, therefore increasing the total shear of the system.

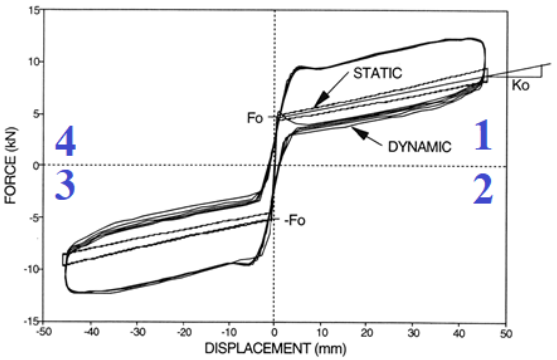

Figure 2.10 *The response of the device from report NCEER 94-0014*

The force-displacement relation of a device, and thus the entire structure, can be manipulated by either a readily reshaped (passive) device response or by direct control of the damping coefficient depending on the movement of the dampers in each direction, by a decentralized semiactive control strategy (e.g., [30-32]). The following examples discuss re-shaped hysteresis loops achieved by semiactive control. A resettable device, which is essentially a combination of hydraulic (or pneumatic) and spring elements in which the un-stretched spring length can be reset, is a semi-active approach to managing structural response energy. This means that a semiactive resettable device doesn't alter the damping of the structure but changes the stiffness of the structure [29], [33], [71]. The semiactive control devices based on the concept of variable stiffness are complex**,** increase the base shear (for Figure 2.11b and Figure 2.11c) and cannot generate very large control forces which are often required for seismic control of buildings.

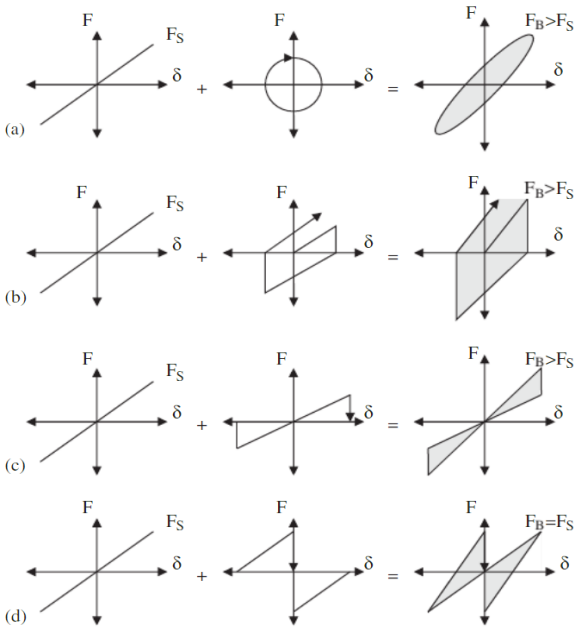

Figure 2.11. Resettable semi-active device [33]: Schematic hysteresis for (a) viscous damping; (b) a 1–4 device; (c) a 1–3 device; and (d) a 2–4 device. Quadrants are labelled in the first panel, and FB=total base shear, FS=base shear for a linear, undamped structure. FB > FS indicates an increase due to the additional damping

Viscous-based energy dissipation devices are well-known to be robust and provide significant forces (see [26]) when they are compared with complex stiffness devices (see [29], [33], [71]) or force-based devices (see [72-73])

Thus, presenting significant advantages over other devices, a fluid viscous damper is ideal for manipulating the force-displacement loop. Up to date however, there are only a few semiactive control systems that can provide viscous damping in selected quadrants.

A semiactive control of conventional viscous damper for building applications was proposed in 2003 by Kurino et al. [32]. Here the opening of the on/off valve is switched by a signal from a controller. Such control law simply locks the damper in quadrants (1 and 3) and opens the valve in quadrants 2 and 4 (Figure 2.12a). However, owing to experiences in the Great East Japan Earthquake of 2011, the demand for a more efficient control device in high-rise buildings was reported. In 2019, Fukuda and Kurino [31] updated their previous Maxwell-type viscous damper model with a Voight model, which was achieved by attaching an auxiliary oil tank to a conventional viscous damper (Figure 2.12b). These two studies [31-32] were only meant to increase energy dissipation of a conventional viscous damper by reshaping its hysteresis loop in selected quadrants (1 and 3). However, such control strategy can lead to an increase in maximum base shear of the building, which, in practice, would likely require strengthening of columns and foundations.

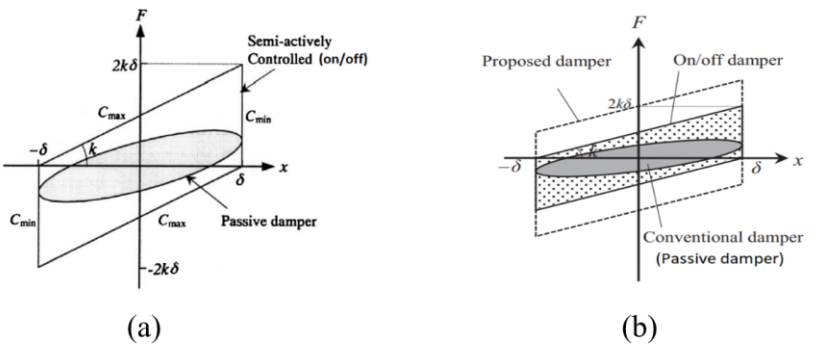

***Figure 2.12**. Force-displacement relation of semiactive damper under harmonic motion; (a) [32], (b) [31]*

Reducing damping force in quadrants 1 and 3, but increasing that in 2 and 4, when the restoring forces in the main structure are reducing, would be a promising response control strategy as it would lead to reduction of the total shear forces in the building. In a recent study [30] the authors adopted a decentralized semiactive control approach to investigate different control laws (1-4, 2-4 and 1-3; Figure 2.13) of a Single Degree of Freedom System (SDOF) subjected to a set of ground motions.

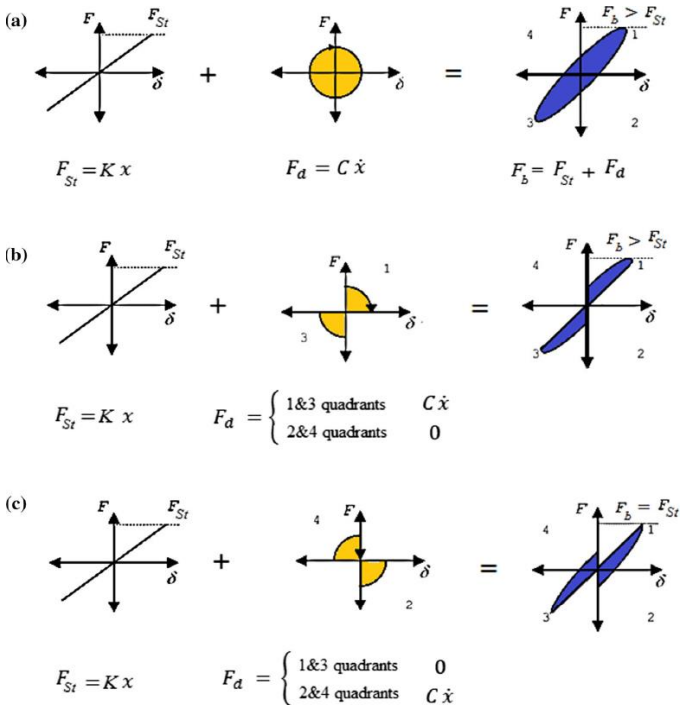

Figure 2.13*. Schematic hysteresis for (a) 1–4 device, (b) 1–3 device, and (c) 2–4 device. Fb = total base shear, FSt = base shear for a linear, un-damped structure. Fb > FSt indicates an increase in the total base shear due to the additional damping force* [30]

Conclusion

The outcomes of this chapter provided important insight into the area of enhancing the seismic performance of structures with viscous damper controls. The use of damping devices is a promising strategy for reducing seismic damage to buildings, and they are particularly effective at improving the response of existing, potentially deficient buildings. When applied to moment-resisting frames (MRF), they generally reduce the drifts but increase the total base shear and acceleration and thus increase the risk of damage to contents (due to greater acceleration) and foundations (due to larger total base shear). However, when used as an alternative to a passive viscous damper, the increase in shear forces and accelerations can be controlled, and the deformations of the structure can be reduced without exceeding the shear force limits by considering semiactive control systems.

Acknowledgements

First author: The first author also acknowledges that this research was only made possible by a fully supported PhD scholarship (2018–2022; Turkish law no.1416) provided by the Ministry of National Education of Türkiye (Turkey).

References

[1] A. Kiral and Z. Tonyali, “The February 6, 2023, Kahramanmaras-Turkiye Earthquakes: Seismo-Tectonic Evaluations and Effects on Reinforced Concrete Buildings,” in *Ege 8th International Conference on Applied Sciences*, Izmir, 2023, pp. 1–12.

[2] D. Domenico and I. Hajirasouliha, “Multi-level performance-based design optimisation of steel frames with nonlinear viscous dampers,” *Bull. Earthq. Eng.*, vol. 19, pp. 5015–5049, 2021.

[3] N. Nabid, I. Hajirasouliha, D. Escolano Margarit, and M. Petkovski, “Optimum energy based seismic design of friction dampers in RC structures,” *Structures*, vol. 27, no. February, pp. 2550–2562, 2020, doi: 10.1016/j.istruc.2020.08.052.

[4] H. C. Quintana and M. Petkovski, “Optimum performance of structural control with friction dampers,” *Eng. Struct.*, vol. 172, pp. 154–162, 2018, doi: 10.1016/j.engstruct.2018.06.017.

[5] M. C. Constantinou, A. S. Whittaker, Y. Kalpakidis, D. M. Fenz, and G. P. Warn, “Performance of seismic isolation hardware under service and seismic loading,” the University at Buffalo, State University of New York, 2007. [Online]. Available: http://mceer.buffalo.edu

[6] S. Akcelyan, D. G. Lignos, T. Hikino, and M. Nakashima, “Evaluation of Simplified and State-of-the-Art Analysis Procedures for Steel Frame Buildings Equipped with Supplemental

Damping Devices Based on E-Defense Full-Scale Shake Table Tests," *J. Struct. Eng.*, vol. 142, no. 6, pp. 1–17, Jun. 2016.

[7] Y.-Y. Lin, K.-C. Chang, and C.-Y. Chen, "Direct displacement-based design for seismic retrofit of existing buildings using nonlinear viscous dampers," *Bull. Earthq. Eng.*, vol. 6, no. 3, pp. 535–552, Aug. 2008, doi: 10.1007/s10518-008-9062-9.

[8] Y. M. Parulekar and G. R. Reddy, "Passive Response Control Systems for Seismic Response Reduction: A State-Of-The-Art Review," *Int. J. Struct. Stab. Dyn.*, vol. 9, no. 1, pp. 151–177, 2009, [Online]. Available: www.worldscientific.com

[9] Y. Xie, J. Zhang, and W. Xi, "Effectiveness evaluation and optimal design of nonlinear viscous dampers for inelastic structures under pulse-type ground motions," *Earthq. Eng. Struct. Dyn.*, vol. 47, no. 14, pp. 2802–2820, Nov. 2018.

[10] A. R. Ghaemmaghami and O. S. Kwon, "Nonlinear modeling of MDOF structures equipped with viscoelastic dampers with strain, temperature and frequency-dependent properties," *Eng. Struct.*, vol. 168, no. 7, pp. 903–914, 2018, doi: 10.1016/j.engstruct.2018.04.037.

[11] W.-H. Lin and A. K. Chopra, "Earthquake response of elastic SDF systems with non-linear fluidviscous dampers," *J. Eng. Mech.*, vol. 129, 2003, doi: 10.1061/ASCE0733-93992003129:6597.

[12] J. Xu and J. Li, "Stochastic dynamic response and reliability assessment of controlled structures with fractional derivative model of viscoelastic dampers," *Mech. Syst. Signal*

Process., vol. 72–73, pp. 865–896, May 2016, doi: 10.1016/j.ymssp.2015.11.016.

[13] A. Kıral and A. Gurbuz, "Using supplemental linear viscous dampers for experimentally verified base-isolated building: Case study," *J. Struct. Eng. Appl. Mech.*, vol. 7, no. 1, pp. 34–50, Mar. 2024, doi: 10.31462/jseam.2024.01034050.

[14] I. D. Aiken, D. K. Nims, A. S. Whittaker, and J. M. Kelly, "Testing of Passive Energy Dissipation Systems," *Earthqauke Spectra*, vol. 9, 1993.

[15] J. E. Martínez-Rueda, "On the evolution of energy dissipation devices for seismic design," *Earthq. Spectra*, vol. 18, no. 2, pp. 309–346, 2002, doi: 10.1193/1.1494434.

[16] K. C. Tsai, H. W. Chen, C. P. Hong, and Y. F. Su, "Design of Steel Triangular Plate Energy Absorbers for Seismic-Resistant Construction," *Earthqauke Spectra*, vol. 9, 1993.

[17] A. S. Whittaker, V. V Bertero, C. L. Thompson, and L. J. Alonso, "Seismic Testing of Steel Plate Energy Dissipation Devices," *Earthqauke Spectra*, 1991.

[18] M. Tehranizadeh, "Passive energy dissipation device for typical steel frame building in Iran," *Eng. Struct.*, vol. 23, pp. 643–655, 2001.

[19] M. Bayat and G. R. Abdollahzade, "Analysis of the steel braced frames equipped with ADAS devices under the far field records," *Lat. Am. J. Solids Struct.*, vol. 8, pp. 163–181, 2011.

[20] L. D. Aiken, J. M. Kelly, and A. S. Pall, "Seismic response of a nine-story steel frame with friction damped cross-

bracing," in *ninth world Conf. Earthq. Eng.*, Tokyo Kyoto, Japan, 1988.

[21] J. Enrique Martinez-Rueda and A. S. Elnashai, "A novel technique for the retrofitting of reinforced concrete structures," *Eng. Struct.*, vol. 17, no. 5, pp. 359–371, 1995.

[22] A. S. Pall and C. Marsh, "Response of Friction Damped Braced Frames," *J. Struct. Div.*, vol. 108, 1982.

[23] A. Filiatrault, R. Tremblay, and A. Wanitkorkul, "Performance evaluation of passive damping systems for the seismic retrofit of steel moment-resisting frames subjected to nearfield ground motions," *Earthq. Spectra*, vol. 17, no. 3, pp. 427–456, 2001.

[24] W. H. Lin and A. K. Chopra, "Asymmetric one-storey elastic systems with non-linear viscous and viscoelastic dampers: Earthquake response," *Earthq. Eng. Struct. Dyn.*, vol. 32, no. 4, pp. 555–577, Apr. 2003, doi: 10.1002/eqe.237.

[25] H. K. Miyamoto and J. P. Singh, "Performance of Structures with Passive Energy Dissipators," *Earthq. Spectra*, vol. 18, no. 1, pp. 105–119, 2002.

[26] M. D. Symans and M. C. Constantinou, "Development and Experimental Study of Semi-Active Fluid Damping Devices for Seismic Protection of Structures, Technical Report NCEER-95-0011," 1995. [Online]. Available: Technical Report NCEER-95-0011

[27] R. Vargas and M. Bruneau, "Effect of Supplemental Viscous Damping on the Seismic Response of Structural Systems

with Metallic Dampers," *J. Struct. Eng.*, 2007, doi: 10.1061/ASCE0733-94452007133:101434.

[28] P. I. Kogut and G. Leugering, "Optimal L1-Control in Coefficients for Dirichlet Elliptic Problems: W-Optimal Solutions," *J. Optim. Theory Appl.*, vol. 150, no. 2, pp. 205–232, Aug. 2011, doi: 10.1007/s10957-011-9840-4.

[29] J. G. Chase *et al.*, "Re-shaping hysteretic behaviour using semi-active resettable device dampers," *Eng. Struct.*, vol. 28, no. 10, pp. 1418–1429, Aug. 2006, doi: 10.1016/j.engstruct.2006.01.011.

[30] N. K. Hazaveh, G. W. Rodgers, J. G. Chase, and S. Pampanin, "Reshaping structural hysteresis response with semi-active viscous damping," *Bull. Earthq. Eng.*, vol. 15, no. 4, pp. 1789–1806, 2017, [Online]. Available: Netherlands

[31] R. Fukuda and H. Kurino, "Highly efficient semi-active oil damper with energy recovery system," *Japan Archit. Rev.*, vol. 2, no. 3, pp. 238–249, 2019, [Online]. Available: Japan

[32] H. Kurino, J. Tagami, K. Shimizu, and T. Kobori, "Switching Oil Damper with Built-in Controller for Structural Control," *J. Struct. Eng.*, vol. 129, no. 7, pp. 895–904, 2003.

[33] K. J. Mulligan, J. G. Chase, J. B. Mander, G. W. Rodgers, and R. B. Elliott, "Nonlinear models and validation for resetable device design and enhanced force capacity," *Struct. Control Heal. Monit.*, vol. 17, no. 3, pp. 301–316, Apr. 2008, doi: 10.1002/stc.298.

[34] M. Dan and M. Kohiyama, “System identification and control improvement of a semi-active-controlled base-isolated building using the records of the 2011 Great East Japan Earthquake,” in *Safety, Reliability, Risk and Life-Cycle Performance of Structures and Infrastructures - Proceedings of the 11th International Conference on Structural Safety and Reliability, ICOSSAR*, 2013.

[35] H. P. Gavin and U. Aldemir, “Optimal Control of Earthquake Response Using Semiactive Isolation,” *J. Eng. Mech.*, vol. 131, no. 8, pp. 769–775, 2005.

[36] C. Ho, Y. Zhu, Z. Q. Lang, S. A. Billings, M. Kohiyama, and S. Wakayama, “Nonlinear damping based semi-active building isolation system,” *J. Sound Vib.*, vol. 424, pp. 302–317, 2018, doi: 10.1016/j.jsv.2018.03.023.

[37] N. Kurata, T. Kobori, M. Takahashi, N. Niwa, and H. Midorikawa, “Actual Seismic Response Controlled Building with Semi-Active Damper System,” 1999.

[38] W. N. Patten, J. Sun, G. Li, J. Kuehn, and G. Song, “Field Test of An Intelligent Stiffener For Bridges At The I-35 Walnut Creek Bridge,” *Earthq. Eng. Struct. Dyn.*, vol. 28, pp. 109–126, 1999.

[39] C. T. Lee and B. Y. Moon, “Study of the simulation model of a displacement-sensitive shock absorber of a vehicle by considering the fluid force,” *Proc. Inst. Mech. Eng. Part D J. Automob. Eng.*, vol. 219, no. 8, pp. 965–975, Aug. 2005, doi: 10.1243/095440705X34685.

[40] S. Nie, Y. Zhuang, Y. Wang, and K. Guo, “Velocity & Displacement-Dependent Damper: A Novel Passive Shock Absorber Inspired by the Semi-Active Control,” *Mech. Syst. Signal Process.*, vol. 99, pp. 730–746, Jan. 2018.

[41] O. Yoshida and S. J. Dyke, “Seismic Control of a Nonlinear Benchmark Building Using Smart Dampers,” *J. Eng. Mech.*, 2004, doi: 10.1061/ASCE0733-93992004130:4386.

[42] K. C. Chang, M. L. Lai, T. T. Soong, D. S. Hao, and Y. C. Yeh, “Seismic Behavior and Design Guidelines for Steel Frame Structures with Added Viscoelastic Dampers,” 1993.

[43] P. Guo, “Damping System Designs using Nonlinear Frequency Analysis Approach,” Department of Automatic Control and Systems Engineering, Faculty of Engineering, University of Sheffield, 2012.

[44] T. K. Datta, “A state-of-the-art review on Active Control of Structures,” *ISET J. Earthq. Technol.*, vol. 40, no. 1, pp. 1–17, 2003.

[45] D. Hrovat, P. Barak, and M. Rabins, “Semi-Active versus Passive or Active Tuned Mass Dampers for Structural Control,” *J. Eng. Mech.*, vol. 109, no. 3, pp. 691–705, 1983, doi: 10.1061/(asce)0733-9399(1983)109:3(691).

[46] T. A. Z. Rahman, A. As’arry, and N. A. A. Jalil, “Active Vibration Control of a Flexible Beam Structure Using Chaotic Fractal Search Algorithm,” *Procedia Eng.*, vol. 170, pp. 299–306, 2017, doi: 10.1016/j.proeng.2017.03.033.

[47] Z. Q. Lang, P. F. Guo, and I. Takewaki, “Output frequency response function based design of additional nonlinear viscous dampers for vibration control of multi-degree-of-freedom systems,” *J. Sound Vib.*, vol. 332, no. 19, pp. 4461–4481, 2013, doi: 10.1016/j.jsv.2013.04.001.

[48] I. Takewaki, “Optimal Damper Placement for Minimum Transfer Function,” *Earthq. Engng. Struct. Dyn*, vol. 26, pp. 1113–1124, 1997.

[49] D. P. Taylor and M. C. Constantinou, “Fluid viscous dampers in applications of seismic energy dissipation and seismic isolation,” 2010. [Online]. Available: www. taylordevices. com

[50] D. P. Taylor and M. C. Constantinou, “Development and testing of an improved fluid damper configuration for structures having high rigidity,” in *Proceedings of the 69th Shock and Vibration Symposium*, 1996.

[51] R. J. McNamara, D. P. Taylor, and P. Duflot, “Fluid Viscous Dampers to reduce Wind-induced Vibrations in Tall Buildings,” 2005. [Online]. Available: http://www.taylordevices.eu/pdfs/tall-building_1.pdf

[52] T. T. Soong and M. C. Constantinou, *Passive and Active Vibration Control in Civil Engineering*, vol. 345, no. May. 1994. doi: 10.1007/978-3-7091-3012-4.

[53] M. C. Constantinou, P. Tsopelas, W. Hammel, and A. N. Sigaher, “Toggle-Brace-Damper Seismic Energy Dissipation Systems,” *J. Struct. Eng.*, vol. 127, no. 2, pp. 105–112, 2001.

[54] A. Gherbi and M. Belgasmia, “Use of fluid viscous dampers in structural control: a case study,” *Int. J. Forensic Eng.*, vol. 4, no. 2, p. 119, 2018, doi: 10.1504/ijfe.2018.10019980.

[55] A. Hwang, “Practical Application Issues for the Structural Engineer,” Massachusetts Institute of Technology, 1998.

[56] H. B. Yun *et al.*, “Comparison of modeling approaches for full-scale nonlinear viscous dampers,” *JVC/Journal Vib. Control*, vol. 14, no. 1–2, pp. 51–76, 2008, doi: 10.1177/1077546307079396.

[57] S. Infanti, P. Papanikolas, G. Benzoni, and M. G. Castellano, “Rion-Antirion Bridge : Design And Full-Scale Testing,” 2004.

[58] R. J. McNamara, C. D. Huang, and V. Wan, “Viscous-damper with motion amplification device for high rise building applications,” in *Structures Congress 2000: Advanced Technology in Structural Engineering*, 2000. doi: 10.1061/40492(2000)123.

[59] J. S. Hwang and Y. S. Tseng, “Design formulations for supplemental viscous dampers to highway bridges,” *Earthq. Eng. Struct. Dyn.*, vol. 34, no. 13, pp. 1627–1642, 2005, doi: 10.1002/eqe.508.

[60] D. De Domenico, G. Ricciardi, and I. Takewaki, “Design strategies of viscous dampers for seismic protection of building structures: A review,” *Soil Dyn. Earthq. Eng.*, vol. 118, no. 1, pp. 144–165, Mar. 2019, doi: 10.1016/j.soildyn.2018.12.024.

[61] T. L. Attard, “Controlling All Interstory Displacements in Highly Nonlinear Steel Buildings Using Optimal Viscous Damping,” *J. Struct. Eng.*, vol. 133, no. 9, pp. 1331–1340, 2007.

[62] O. Lavan, G. P. Cimellaro, and A. M. Reinhorn, “Noniterative Optimization Procedure for Seismic Weakening and Damping of Inelastic Structures,” *J. Struct. Eng.*, vol. 134, no. 10, pp. 1638–1648, 2008, doi: 10.1061/(asce)0733-9445(2008)134:10(1638).

[63] O. Lavan and G. F. Dargush, “Multi-objective evolutionary seismic design with passive energy dissipation systems,” *J. Earthq. Eng.*, vol. 13, no. 6, pp. 758–790, 2009, doi: 10.1080/13632460802598545.

[64] FEMA-356, “American Society of Civil Engineers, Fema 356 Prestandard and Commentary for the Seismic Rehabilitation of Building,” *Rehabilitation*, no. November, 2000.

[65] CEN Eurocode 8, “CEN (European Committee for Standardisation). Eurocode 8: design of structures for earthquake resistance. General rules, seismic actions and rules for buildings. EN1998-1:2004. (EN 1998-1, Brussels; 2004),” 2004.

[66] G. Alotta, L. Cavaleri, M. Di Paola, and M. F. Ferrotto, “Solutions for the Design and Increasing of Efficiency of Viscous Dampers,” *Open Constr. Build. Technol. J.*, vol. 10, no. 1, pp. 106–121, 2016, doi: 10.2174/1874836801610010106.

[67] S. Pourzeynali and T. Mousanejad, “Optimization of Semi-Active Control of Seismically Excited Buildings Using Genetic Algorithms,” *Trans. A Civ. Eng.*, vol. 17, no. 1, 2010.

[68] F. Oliveira, M. A. Botto, P. Morais, and A. Suleman, “Semi-active structural vibration control of base-isolated buildings using magnetorheological dampers,” *J. Low Freq. Noise Vib. Act. Control*, vol. 37, no. 3, pp. 565–576, 2017, doi: 10.1177/1461348417725959.

[69] C. T. Lee and B. Y. Moon, “Simulation and experimental validation of vehicle dynamic characteristics for displacement-sensitive shock absorber using fluid-flow modelling,” *Mech. Syst. Signal Process.*, vol. 20, no. 2, pp. 373–388, Feb. 2006, doi: 10.1016/j.ymssp.2004.09.006.

[70] P. Tsopelas and M. C. Constantinou, “NCEER-Taisei Research Program on Sliding Seismic Isolation Systems for Bridges: Experimental and Analytical Study of a System Consisting of Sliding Bearings and Fluid Restoring Force/Damping Devices,” 1994.

[71] G. W. Rodgers, J. B. Mander, J. G. Chase, K. J. Mulligan, B. L. Deam, and A. Carr, “Re-shaping hysteretic behaviour - Spectral analysis and design equations for semi-active structures,” *Earthq. Eng. Struct. Dyn.*, vol. 36, no. 1, pp. 77–100, 2007, doi: 10.1002/eqe.624.

[72] L. M. Jansen and S. J. Dyke, “Semiactive Control Strategies for MR Dampers: Comparative Study,” *J. Eng. Mech.*, vol. 126, no. 8, pp. 795–803, 2000.

[73] F. C. Ponzo, A. Di Cesare, A. Telesca, A. Pavese, and M. Furinghetti, “Advanced modelling and risk analysis of rc buildings with sliding isolation systems designed by the italian seismic code,” *Appl. Sci.*, vol. 11, no. 4, pp. 1–16, 2021, doi: 10.3390/app11041938.

CHAPTER V

Bearing Loads Due to Natural Rock and Concrete Blocks in Hypothetical Towered Structures

Mehmet Kemal GOKAY[1]

1.Introduction

Understanding certain engineering facts sometimes could be more reasonable when the facts are defined in different manners. Vertical stresses formed due to the weight of dimensioned natural rock (marble, granite etc.) blocks or unreinforced concrete blocks are conceptually dealt with to define strength requirements of the surface monuments if these rock blocks are used to form tower-like monumental surface structures by put each of them over another to form the towers. Conceptions forwarded here aimed to enhance engineering thinking in civil and rock engineering through rock mechanics contexts. Vertical stresses formed due to the weight of

[1] Dr., Konya Technical University, Mining Eng. Dept., Konya/Turkey, Orcid: 0000-0003-3792-9414, mkgokay@gmail.com

dimensioned massive natural rock blocks and dimensioned massive artificial, man-prepared, rock (concrete) blocks with no reinforcements are analysed logically here if they are configured to form tower like surface structures. In the conception, it is aimed to visualise the stresses differences in the levels (floors) of the formed towers and their influences on the strength behaviours (long term) of natural rocks and concrete blocks.

Actually, in civil and rock engineering concepts, the forwarded stress-strength relations are basic steps to be followed through engineering standard testing procedures. However, it is conceptually supplied here also that there are certain facts that should also be considered to understand stress & strength relations of massive solid materials used for engineered constructions located in/on earth crust. Supplying assumptional cases in this approach need to put limitations on the complexity of the stress conditions for the blocks considered. Those limitations were accepted logically here to focus on only vertical stress differentiation at different levels of the towers due the upper layers' weights.

2.Individual Massive Natural Rock Blocks

When we think about the earth crust which is formed from molten lava in different kinds of rock masses. Due to structural features of their origin differences and tectonic activities of earth, it is difficult to find large scale massive, (without any discontinuities), rock masses. However, a few rock mass types have provided more massive rock characteristics at certain of their reserves. Experiences gained in dimensioned-stone constructions for surface structures through ancient civilisations, lead to build bigger monumental structures by using certain types of rock types. Thus, rocks are even cut in bigger sizes & one pieces to form monumental status for their

usage. Rock masses' massive characteristics were one of the main decision factors in their mining operations. Massive red granite rock mass had been selected by ancient Egyptians to cut large prismatic, monumental, rock blocks, (they are called as obelisks), (Brier, 2021). Other large rock block usages were found through the archaeological remnants at Baalbek, Lebanon. They are three large horizontally lying limestone rock blocks, *[each has 19x4.2x3.6m, (metre), sizes, and around 825 tons, (metric tons), weight]*. These rock blocks, (Trilithon), put to their place purposely to "form part of the podium of the Temple of Jupiter Baal at Baalbek", *(Baalbek complex in Heliopolis Syriaca 16BC-AD60).* Actually, there are 3 more large blocks left at the limestone quarry site at Baalbek, and due to their dimensions and estimated weights of these three Roman monoliths, they are known also with their names as; the "*Stone of the Pregnant Woman*" (length *20.31-20.76m*; width *4.0m* at the base, and *4.14-5.29m* at the top; height *4.21-4.32m*; weight around *1000 tons*), the "*Stone of the South*" (length *19.5-20.5m*; width *4.34-4.56m*; height *4.5m*; weight around *1242 tons*), and the "*Forgotten Stone*" (length *19.6m*; width *6.0m*; height *5.5m*; weight around *1650 tons*), (Aaron, 2016; Wikipedia, 2024a). Baalbek monolithic limestone rock blocks supply examples of vertical stress levels that originated due to the massive individual rock block cut for surface structures. If there was a change to use the largest of these Baalbek blocks, (the *Forgotten Stone*), for an ancient surface structure, it might have caused around *14 ton/m^2* vertical stress on its base area (*6x19.6m* if it was arranged horizontally lying). The value could have been about *50 ton/m^2* (if it was erected vertically on its smaller rectangular base area of *6x5.5m*). Hypothetical concern in this study is the considerations of strength features of large monumental natural rock blocks by

estimation of their dead-load related impacts (vertical stresses) while all the other influencing factors on their stabilities are accepted as neutral (no impactcept).

When archaeological remnants and current documents are assessed for the usage of largest rock block dimensions, the other most certain sample group has the huge rock blocks known as "obelisk". Obelisks had been individually cut from their massive rock mass in quarries, (Egypt), by hand-tools to supply monumental massive rock structures. These massive column-like rock blocks were erected in Egypt by Egyptian emperors in early historic times. Some of them, then shipped to different cities like Rome, Istanbul, Paris, Newyork, London, (Lewis, 1984). When obelisks' dimensions and weights are in consideration, their foundations & base layers could also be thought as long-lasting bearing capacity test locations with dead-loads of the erected obelisks. Since the standard bearing-capacity tests for foundations of surface structures are performed in short periods of time with increasing-load procedures, long-term bearing capacity considerations for; *i)* the foundation of the obelisks and, *ii)* the rock materials of the obelisks under constant dead-loads are accepted in this work as a conceptual subjects of curiosity.

Archaeological information related with obelisks have included mostly historical concerns but also covered their size issues as well. Childress (2019) supplied dimensional and weight related data of some of the obelisks located in different parts of the world. He mentioned one of the obelisks erected at Karnak, (Egypt), by Thutmose-I (reigned 1493-1482 BC) has *24m* height. This massive rock monument has a square base area *(1.8x1.8m)* in dimensions and *143 tons* in weight. Another obelisk was shipped to the Piazza San Giovanni in Laterano (Rome, Italy) from Karnak, (Egypt). It was

originally erected by reigns of Pharaohs Thutmose-III (reigned 1479-1426 BC) and Thutmose-IV (reigned 1400–1390 BC) at Karnak. This obelisk's height was originally *32m* and it has a square base with *2.7x2.7m* in dimensions. Childress (2019) wrote that it tapers to a square top with sides of *1.88m*. This obelisk was shipped to Rome (Italy) from Alexandria (Egypt) in AD 357. It was reported that its weight was originally around *413 tons*. It collapsed in 5th Century AD and stayed in mud for a long time (in three pieces). It was re-erected around the 1580's with *4m* shorter in length with around *300 tons* in weight (Wikipedia, 2024b).

There are some other obelisks moved from Egypt, and two of them were the pair obelisks. One of these was shipped to the Central Park, (New York, US), and the other was moved to the Thames embankment, (London, UK), in the 19th Century (Lewis, 1984; Wikipedia, 2024b). These pair obelisks were dedicated at Heliopolis (Cairo, Egypt) by Thutmose-III, and they were cut from red granite rocks with *21.2m* heights. Their base areas are almost square with *2.36x2.33m* in dimensions. Each of these pair obelisks is *180 tons* in weight. One of the archaeologically important obelisks was re-erected in Istanbul, (Turkey), by Roman emperor Theodosius by shipping it from Egypt in 390 AD. Its original height was *29m* and weight was around *380 tons*. The lower parts of the obelisk were weathered and crushed, after re-erecting, its height became *19.46m* and its new weight is about *200 tons*. (the obelisk monument in Istanbul has *24.77m* in height with its pedestal, (Polat & Saygili, 2020). Hoseyni etal., (2022) pointed also to the information supplied by Traquair & Wace (1909) and Crkvenjakov (2016) for the obelisk in Istanbul including sizes of 5 different layers of its pedestal part, (Fig.1). These layers, starting from the bottom are; a) Limestone rock

slabs in 2 layers were put over each other. Their dimensions are *7.1x7.1x0.5m* and *6.8x6.8x0.6m*, b) Lower pedestal marble block *3.8x3.8x1.9m*, c) Combined rock layer (marble-red granite) *0.5m* in height, d) Upper marble block *2.9x2.9x2.4m*, e) Small sized 4 metal (bronze) blocks, each has *0.4x0.4x0.5m* in dimensions. The obelisk pyramidal rock block which was cut from red granite rock mass in Egypt was then put on these 4 bronze blocks over its pedestal in Istanbul. It has a pyramidal volumetric shape with *2.3x2.3m* base area dimensions. The square area at the top of this obelisk is *1.4x1.4m* in dimensions.

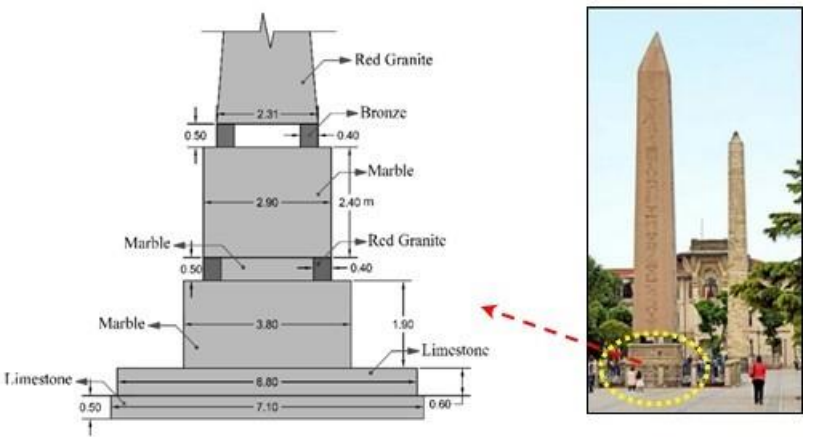

Figure 1: a) Dimensions of pedestal parts of the obelisk in Istanbul (Hoseyni, etal., 2022). b) Obelisk of Istanbul, (Britanica, 2024).

In modern times, another obelisk which is "The Obelisk of Ramses II" was found at "San Elhagar" in Egypt, Saleh, etal., (2023) wrote that this obelisk, "*was found broken into two pieces and separated from the base*". After restoration works, it was re-erected and will be opened for visit in 2024 at the entrance piazza of the Grand Egyptian Museum, Giza, Cairo, Egypt.

3.Blocks, Columns & Slabs Dimensioned for Concept-Tower

After collecting information about historical monuments including huge massive rock block(s), the data related with their dimensions and weights have been used to estimate their downward pressures (vertical stresses) on their bottom layers (foundations). In the conceptual samples offered below, two plans were provided for the hypothetical surface structures; one form was offered to visualise massive natural rock monuments and the other was offered to simulate high rise monumental structures. These structures are planned to be formed by using massive marble (density: *2.71 ton/m*^{3}) rocks and C30 type concrete (density: *2.50 ton/m*^{3}, without reinforcements). For this approach, assume that massive in-situ marble rock reserve is cut purposely into form; Marble blocks (*3x3x3m*), Marble columns (*0.6x0.6x2.85m*), and Marble slabs (*3x3x0.15m*), (Fig. 2).

Similarly, concrete blocks, columns and slabs are prepared through C30 standard procedures, which could be taken into account as "artificial" (man-made) rock materials. Monumental surface tower structures aimed to be built (conceptually) are presented in Fig. 3. Massive (marble & concrete) individual blocks here are dimensioned to get *"Solid-volume"* of *27m*^{3}. Similarly, *"Column-cornered-volume"* defined through 4 individual solid-columns and one solid-ceiling-slab. The weights and vertical compressive stresses *(originated due to their massive solid structural elements)* at the base areas of these two volume types are given in Fig. 2.

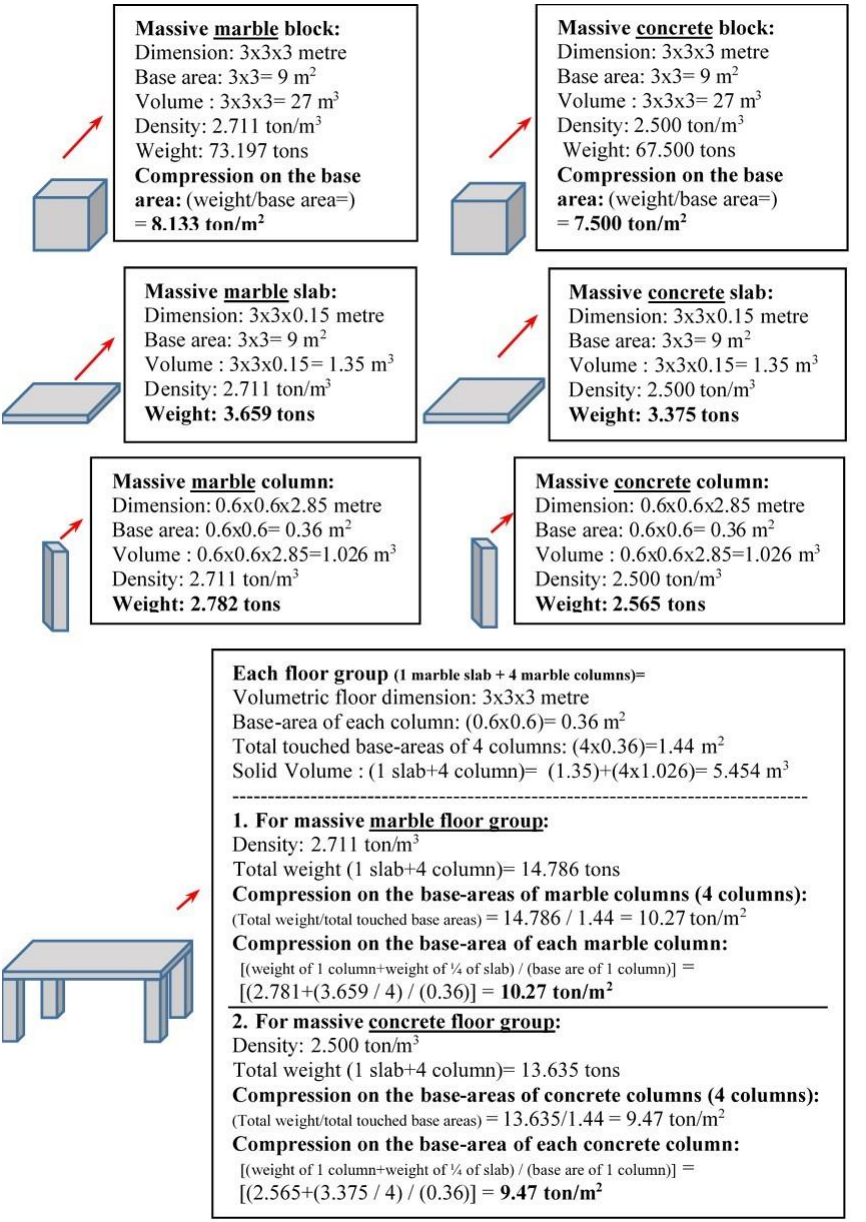

Figure 2: Massive marble & concrete structural elements planned to be used in the selected conceptual set-ups.

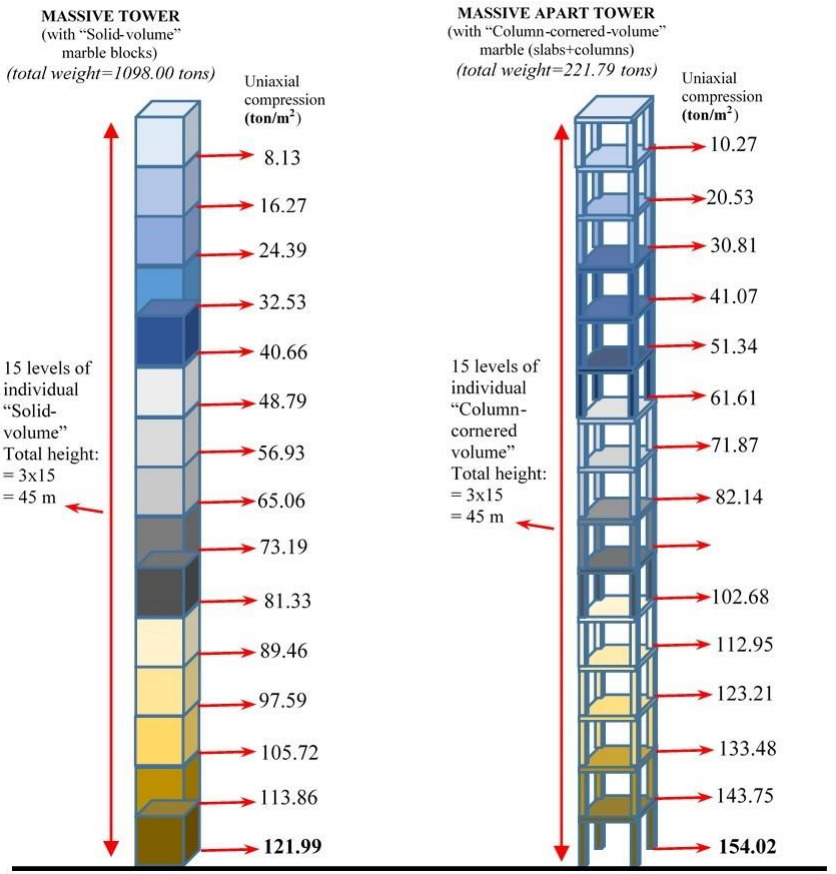

Figure 3: Vertical stresses formed at the base of each massive marble structural volume at the conceptual tower set-ups.

4.Conceptual Tower Set-ups

Individual volumes considered in this approach are then put over each other vertically to simulate conceptual man-made structural monumental towers. Illustrative sketches supplied in Fig. 3 present these two tower forms. Obelisks were erected in Egypt in history, some of them were shipped to different parts of the world and re-erected there. Thus, negative and positive external impacts on these obelisks' stabilities have included all types of natural and

social factors. On the other hand, the conceptual towers under consideration are accepted as being influenced only by gravity (their own dead-loads). All the other influences including; live loads, snow & ice loads, rain loads, flood loads, wind loads, earthquake loads, earth pressure, any other loads are excluded from this concept together with all types of natural and social impacts. Individual structural ”Solid-volumes” and “Column-cornered- volumes” are assumed positioned stand-still at their locations in the conceptual towers by their weight and their overloads transferred through them. Thus, there is no additional adhesives or mechanical connection mechanisms to be considered. Since the only consideration is the earth-gravity, decisions related with the bearing- load values are supplied accordingly. The weight of conceptual, (spectral), massive marble tower, (Fig.3), (with Solid volume marble blocks) is *1098 tons*, (the weight of a massive apart tower with Column-cornered-volumes is *221.79 tons*). The weight of obelisks, especially the heavy ones, could then be compared with the weight of the conceptual marble & concrete towers given in Fig. 3.

According to documents, the heaviest obelisk was named as the “Unfinished obelisk” and it had been under rock cutting operations at the quarry (Aswan, Egypt) when it was left unfinished. Its height was planned to be *41.75m*. Its weight would be around *1090 tons*, if its mining (cutting) operation had been managed to be finished. The second largest obelisk is the “Lateran obelisk” in Rome, Italy, and its weight was originally *413 tons*. After re-erecting operations for this monument, the lateran obelisk’s weight decreased to *300 tons* due to its collapsing & crushing of some of its parts, (Wikipedia, 2024a). Then, if vertical stress formed under its base area (*2.7x2.7m*) is calculated, it is around *41.15 ton/m*^{2}. Similarly,

the red granite obelisk located in Istanbul has around *200 tons* in weight. The base area of this obelisk is *2.3x2.3m*, that means the vertical stress formed at its base area is about *37.81 ton/m^2* (if it would be put on directly on the upper marble block of its pedestal, Fig.1). However, it was preferred to put this obelisk on the upper pedestal marble block through 4 small metal (bronze) pieces (each has base area dimensions of *0.4x0.4m*) at the obelisk's square base corners. Thus, if it is considered that, quarter of the obelisk's weight is carried by one of these small metal blocks (sharing the weight of the obelisk equally among them), then the vertical stress transferred downward through each of them should be around *312.50 ton/m^2*. Vertical stress values formed due to the largest obelisk in Rome and the obelisk in Istanbul are two examples of vertical stresses that originated due to dead-loads of the monumental large rock blocks.

The concept under consideration here can be extended to have huge scale monumental structures (look like modern high-rise buildings), as sketched in Fig. 4 by combining the supplied individual marble & concrete conceptual towers (Fig. 3) side by side. In these combined structures presented in Fig. 4, individual marble & concrete towers with "Solid-volumes" and "Column-cornered-volumes" are assumed to be erected side by side without touching each other. One of the combined structural forms presented in Fig. 4 is called a "Massive tower" and it has *9x12x45m* in dimensions. There are *(3x4)*, 12-individual "Solid-volume" at each level. Then "Massive tower" presented in Fig.4 has totally *(12x15)*, 180 indivudual Solid-volumes of massive marble. It can also be conceptualised as a new monumental "Massive-tower-group" with 1000 "Massive-tower" presented in Fig. 5. By keeping the height as *45m*, this conceptual "Massive-tower-group" could have a huge

monumental structures with *45x9x12000m* (or *45x90x1200m*, *45x900x120m*, *45x450x240m*) in dimensions which include *180,000* "Solid-volumes" of massive marble blocks. Total volume of them is *4,860,000m*^{3} with a total base area of *108,000m*^{2}, it looks like a huge massive marble reserve (Fig, 5) at earth crust. If the volumetric mass described here is a single rock reserve isolated from surrounding rocks, then vertical stress formed due to this marble reserve (*with supplied total volume and the total base area values*) on its base area is expected around *121.99 ton/m*^{2}. It is assumed here that the targeted marble reserve at the marble quarry is positioned at the surface, thus there is no additional marble layer (or any other materials) over this prismatic reserve illustrated in Fig.5. In different cases where the reserves are under certain additional layers of extra rock masses, their dead-loads should also be added to calculations which increase the vertical stress conditions as well. Actually, conception followed here includes towered structures standing side by side without touching each other. Therefore, their vertical load concentrations always stay similar for different levels in their structure beside how many of them are grouped to form huge volumetric monuments or reserve-like structures. Vertical load concentration calculated for the base area of the described single reserve is similar to the presented vertical load concentration at the bottom of the ground level of the "Massive tower" set-up with the "Solid volume" marble blocks (Fig.3). This hint also presents the importance of the 3D stress conditions in the earth crust. Considerations of vertical stress state for monumental towers like obelisks form circumstances of stress conditions excluding horizontal stresses. In actual stress-strain distribution conditions of earth crust, thinking only the vertical stress levels for underground/surface structures are not good enough to

evaluate rock behaviours surrounding the engineering projects. Mine & rock engineers have already experienced the earth pressures over galleries, tunnels, and excavated open spaces which can not directly be correlated with excavations' depths. R*ock load height* criteria, (Terzaghi, 1946), and supplied evaluations in basic rock engineering context, (Barton, etal., 1974; Osgoui, 2007) are accepting, certain height (rock load height) over the underground space which governs the effective dead-load over the excavation roof. The remaining part of the depth *(over the "rock load height" part)* conclusively is not effective on the excavated underground space at all. Thus confined 3D stresses directed through them are redistributed to the sides of the excavation as a secondary stress field.

At this point, the following thought is also being taken into account to analyse the stress influence situations. "If there is an opportunity and isolation of overburden rock layers over an underground excavation *(assume that volumetric underground space dimension 3x3x3m, with a roof area of 3x3m)* is possible then prismatic volume *(with a dimension of 3x3xdepth of excavation down to its roof in metres)* of overburden rock layers could be separated from the surrounding rock masses for their dead-load effects on *3x3m* targeted excavation's roof area. In this conception, if the vertical loads are taken only the applicable influence, (excluding all the other influencing factors including horizontal stresses), vertical stress which is originated and transferred downward through isolated overburden rock volume presents the case like it was illustrated in Fig.3 for the massive tower of marble blocks. Thus, without supplying any touching solid rock masses around an underground excavation, vertical loads concentrated over the roof area of the excavation are total vertical stress transferred

through isolated overburden rock volume which has no opportunity to hang due to horizontal stresses, and no possible bearing (load transferring) connections to distribute its weight surrounding rock masses of the targeted excavation. Therefore, it is assumed that all the weight of the isolated overburden rock volume is concentrated on the supplied *3x3m* sized roof area of the targeted underground excavation.

Horizontal stresses can also be considered as mechanical features which aid to grip the rock mass blocks at their location by pressing the blocks in horizontal directions. This could also be conceptualised like carrying 3 or more separate light weight & small sized food boxes by two hands applying only horizontal pressure from the side boxes. In earth crust, horizontal stresses are also the influencers of the rock fracturing and rock masses' deformations, but they also have an important impact in these rock masses' vertical displacements. Therefore, according to rock mass conditions (including discontinuities), horizontal stresses act with vertical stress to accelerate or decelerate the displacement of any considered rock blocks towards the engineered excavations. When the vertical & horizontal stresses in earth's crust are in consideration, their in-situ differentiations were studied when there were opportunities as it was mentioned by McGarr & Gay (1978).

Horizontal stress distribution in earth crust is important design factors of underground excavations like the vertical stress levels. Realising 3D stress redistribution (arching) procedures at the roof strata of underground excavations has depended on the following basic factors; *a)* State of 3D stress conditions before the excavation, *b)* Mechanical and structural properties of the rock masses surrounding the excavations, *c)* Shape and size of the

excavations, *d)* Supports types used for the excavations, *e)* Structural rock features (discontinuities) located near sides, *f)* Other excavations influencing the targeted ones, etc. That means, assumption leads to the isolation of the overburden rock volume, *(like prismatic volume by eliminating its connection from surrounding rock masses)*, and definitely removes most of the design factors defined above. The rock load height criteria supplied by Terzaghi (1946) is explaining the different cases of overburden strata descriptions and their overburden load transferring characteristics. (If the roof strata have good strength & structural property, they can act well and they have transferred overburden loads to the surrounding rock masses more properly. That means they may produce lower "rock load height" over the excavations. If the overburdened rocks are weaker in strength, the "rock load height" is then higher over the targeted excavations).

Combined structures could also be handled through "Column-cornered-volumes" as it is presented in Fig. 4 as "Massive apart tower". This combined structure has (3x4) 12 indivudual monumental apart towers which each of them has 15 floors. In the concept, these individual towers are located side by side without touching each other like the "Massive tower" case. Therefore, vertical stresses calculated and presented in (Fig. 3 and 4) for the columns located at different floors (levels) of the structures are the same values for each individual "Column-cornered-volume" marble tower. Stress values at different levels of towers arranged through

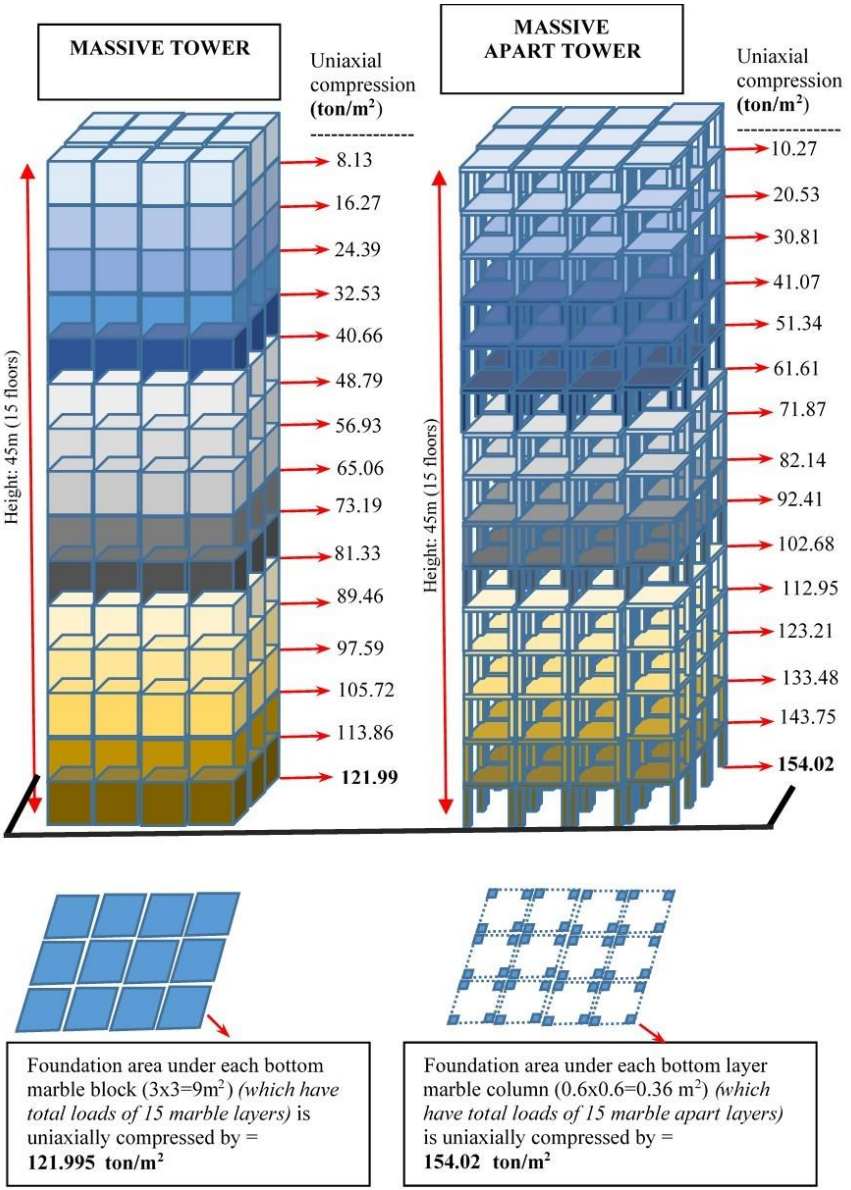

Figure 4: Combined tower concept where individual massive marble towers are combined to form the structures without any touching attachment among them.

massive marble “Solid-volumes” and “Column-cornered-volumes” are getting decreased as the selected floor is approaching the top levels of the towers, (Fig.3 and 4). Actually, if the conceptual towers are totally connected to each other and they are not isolated from the surrounding rock masses, then, in-situ horizontal stress values should also be considered in analyses. Then, all the 3D stress conditions at each level of the two conceptual towers (Combined massive towers, and Combined massive apart towers) become different (in either advantageous or disadvantageous manners) then the conditions presented in Fig. 3 and 4.

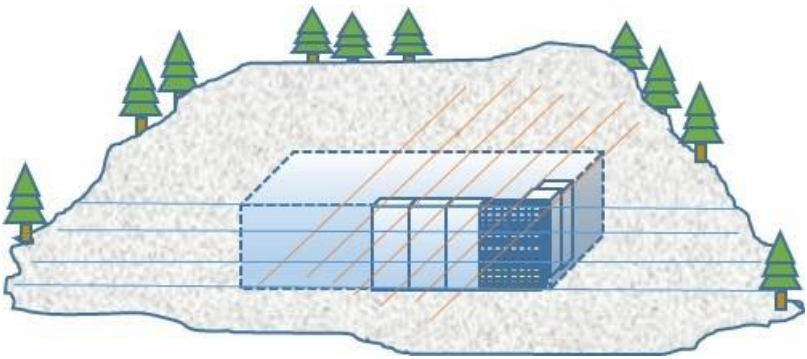

Figure 5: Massive marble rock which could possibly be mined out through a marble pit if the reserve is convenient. Otherwise separate pits are used to get marble blocks, columns and slabs.

5.Influence of Time on the Strengths of Marble Blocks & Columns

The strength of solid materials can be determined through uniaxial and triaxial compressive strength tests in addition to strength tests against tensile, bending, etc., forces. Since the load bearing characteristics of marble blocks & columns are important in the proposed concept here. Uniaxial compressive strength, UCS, values of marble materials are planned to be determined in different

phases of this conceptual approach. Getting the strength quality of the marble blocks and columns just after their cut from marble reserves is the first step in this concept. But the UCS values for the marble materials at the quarry should be sampled through the materials located just nearside of the cut blocks. The mine out marble blocks should not be damaged for any physical rock test sampling procedures (no drill-hole). While these marble blocks are cut to provide blocks, columns and slabs from marble quarries, building operations of planned conceptual towers (Fig. 3) might be continued according to the engineered plans. Time of these tower constructions may take a few mounts (or years) according to the total number of blocks, columns and slabs required and their convenient supply availability. When the individual or combined towers are finished, it should be borne in mind that marble blocks & columns staying at the first floors (just over the foundations) are under more vertical stress values with respect to the ones at top floors.

After several years, what can be the UCS value conditions for the marble blocks & columns at these conceptual towers. The blocks and columns are theoretically under dead-loads of over marble layers here. These loads are long-lasting static (constant) loads without any unloading & loading circumstances in time. This loading condition is similar to the case for the UCS tests procedure under long-lasting static loads. The strength values (for marble materials) are expected to be decreased due to the static long-time loading periods when it is compared to the standard UCS test values. This mechanical behaviour is described in engineering research as the creep behaviour of the solid materials. Paraskevopoulou, (2016) performed a thesis study where evaluation of the creep behaviours of the rocks were also considered. Paraskevopoulou, etal., (2017)

then mentioned the studies of; Singh, 1975; Aydan, etal., 1993; Einstein, 1996; Malan, etal., 1997; Hudson and Harrison, 1997; Hagros, etal., 2008; Brantut, etal., 2013; and Paraskevopoulou, (2016) for the studies concerning on "time-dependency of rock under load". Engineering activities in/on rock masses have forced design engineers to evaluate mechanical properties of rocks. After realising importance of the rock & soil mechanics, some approaches developed in the solid mechanic context have then been employed also for rock materials. As it was indicated by Paraskevopoulou, (2016) the theory of creep studied for metals (Weaver 1936) was also facilitated to analyse rock strength behaviours under long- lasting loading circumstances. Paraskevopoulou, etal., (2017) noted also that laboratory rock testing data analyses had been performed by several researchers to define influences of time on rock strength conditions. Innocente, etal. (2021) wrote that there are a few more "time dependent" rock behaviours other than creep, they are; swelling, squeezing, consolidation, stress relaxation, time-dependent dilatancy, and stress corrosion. In this content, Frenelus, etal., (2022) added also that rocks' creep behaviours are influenced by different external & inner factors which are; "mainly hydraulic pressure, stress level, water content, temperature, damage, and time-to-failure".

Creep behaviours of natural rocks, (Marble for the conceptual towers considered here; Red granite for the obelisk of Istanbul; Limestone for the Forgotten stone of Baalbek monolith) and concrete should also be considered for their long-lasting load carrying properties. Therefore, UCS values obtained for natural rocks where the rock blocks and columns are mined out (just after mining stages) should be compared & re-evaluated through their

creep behaviour. Because after years of usage at their load carrying positions, (as members of monumental towers), natural rocks at these monuments have still been their obligations to stand dead-loads applying on them vertically. Different values of vertical stresses have been expected at different layers of the monuments. These differences will most probably influence the creep behaviours of the rock and concrete blocks & columns in different manners. If the loading and unloading phases of monumental natural rock (red granite, limestone, etc.) towers are in consideration, the cases should be started by evaluating in-situ stress-strain conditions of the quarries where these huge rock blocks cut out. The case for the obelisk in Istanbul can conceptually be figured as it is presented in Fig. 6. The source rock formation is red granite in Aswan, Egypt; this rock formation has its origination and structural features occurred in geological eras. Rock masses in earth crust could be overburdened by other rocks, they may be fractured, folded, thrusted, etc. Their overburdened layers may also be weathered together with some parts of their layers as well.

Geological researches about any rock types at certain targeted earth locations can be conducted to explain certain basic structural features that happened in geological eras. The first 2 phases (a & b) in Fig. 6 illustrated the rock mass related structural features of red granite. After cutting the obelisk rock block from the actual rock reserve, (Fig.6c presents similar rock cutting case for another unfinished obelisk in Egypt), the next engineering question arose; If there are any locked strains in the obelisk rock due to 3D in-situ loading conditions in geological eras, how long time needed for these strains to be relieved after the obelisks are cut at the

quarries. These relaxation features could impact the integrity of the obelisks according to their mechanical strength features.

It should not be forgotten that stress-strain conditions of source rock masses have differentiated in 3D manner in geological eras. After erecting monumental rock blocks like obelisks, their own weight influenced the targeted rock positions (inside them) according to the dead-load over them. Bottom layers of the monumental obelisks for instance must stand the dead-loads of the whole bodies of them, *[This load would be 1090 tons for "the Unfinished obelisk" case, Aswan-Egypt; and it would be 413 tons for "the Lateran obelisk" case, (Rome, Italy)].* Since these

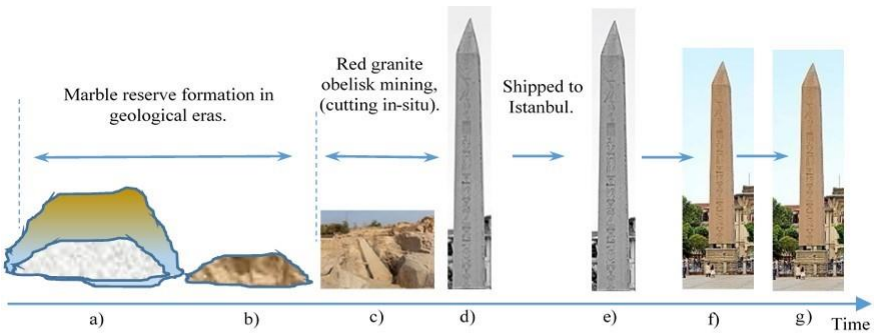

Figure 6: Major phases of the obelisks in Istanbul, Turkey, under consideration. [a&b) geological time periods, c) Obelisk cutting step like the "Unfinished obelisk", d) Erected in Egypt during Thummose-III, e) Shipped and re-erected in Istanbul AD 390, f) The obelisk image currently, g) The same obelisk in future].

monumental massive rock blocks (obelisks) were moved to other locations (including haulage in land and shipping over the sea etc.), the vertical stresses in them experienced unloading-loading phases again after their first monumental positioning in Egypt. The figure sections from Fig.6d to Fig. 6g illustrate these cases for the obelisk in Istanbul. As it was summarized before, the obelisk rock in Istanbul

had been cut from a red granite quarry at Aswan and erected in Karnak, Egypt, *(during 18th dynasty of Egypt. It is also called the obelisk of Pharaoh Thutmose-III 1479-1425 BC).* If this obelisk had not been moved to Istanbul. Since it was erected by Thutmose-III in Egypt, (Wikipedia, 2024a), the total duration of "vertical loading" would be around 3475-3500 years. Thus, it could be a representative of one of the *"long-term vertical loading compressive strength tests with static, dead-load, conditions".* But, this change was lost when the obelisk was shipped to Istanbul.

Actually, vertical strain variation in rock masses could be differentiated due to local 3D stress conditions which have close relation to earth crust tectonic forces and gravity effects in geological eras. Conceptual loading & unloading circumstances of the specific rock masses at certain locations in earth crust might influence engineering projects realised in/on them due to their long-term 3D stress-strain conditions. Essentially, locked strains in the rock blocks which had been cut from special targeted rock masses are always ready to be released from them in time. This could be realised in short or long time periods which needs further studies to be cleared out according to the rock mass types and behaviours.

6.Strengths of Marble Block & Column Include Drill-Hole

Conceptions assumed in this study include two marble towers (Fig. 3). Conceptually, before construction of these towers, handling of the marble blocks, columns and slabs from the mine site covers their strength related circumstances. These considerations should be continued after handling of the conceptual towers, because dead-loads related load bearing-capacity limits of marble & concrete materials have influenced design procedures of these towers. Their vertical stress-strain behaviours in short-time and long-time *(creep)*

should both be included in these conceptual towers' design activities. It is certain that rock and concrete materials have their creep behaviours and they may produce extra deformations before their UCS values are reached. Thus, if rock engineers would like to analyse load-bearing capacity of the marble blocks, columns, and slabs at the conceptual tower structures after several decades of their construction, there will certainly be in dense engineering decisions & disputes cases. Determination of bearing-capacity values for the the bottom layers of all obelisks, all columns & beams of man-made surface/underground structures have similar decision environment. The concept includes determination of bearing-capacity values of load-carrying structural elements, preferably without disturbing physical intactness of them. The measurement methods first in consideration include remote recognition of the parametric differentiation in these columns and obelisks. Electrical resistivity, magnetic sensitivities, electro-magnetic and seismic wave accessibilities are the common physical properties which have already been used in related remote-testing instruments. Moreover, there is also drill-hole sampling methodology to test the carrot samples obtained from the rock & concrete blocks, columns, or slabs, (Fig.7). Actually, drilling a hole damages the physical intactness of them. In order to collect a comprehensive data set, repeating the drilling carrot holes in different parts of the rock blocks, columns, and slabs will cause more damage to their wholeness. Uzbas&Gokay (2023) summarized features of drill-hole testing analyses & studies performed for rock and concrete samples. They pointed out the negative influences of drill-hole methodology even though they are filled with expandable concrete mortars. After years of usage, strength testing of the structural elements by drill-hole carrot

samples may come into consideration among the other available options (even with its obstacles). It should be borne in mind that, even if the filling of the drilled hole with expandable enhanced quality concrete mortars was realised, the defected blocks, columns, or slabs can not be the same ones as they were before the drilling operations. Elastic modulus & UCS values represented by stress-strain curves of the aged concretes at the columns of constructions direct their behavioural matches with the filling materials' similar characteristics. Any difference in the comparisons causes modes of fracture initiation and propagations, (Uzbas&Gokay, 2023).

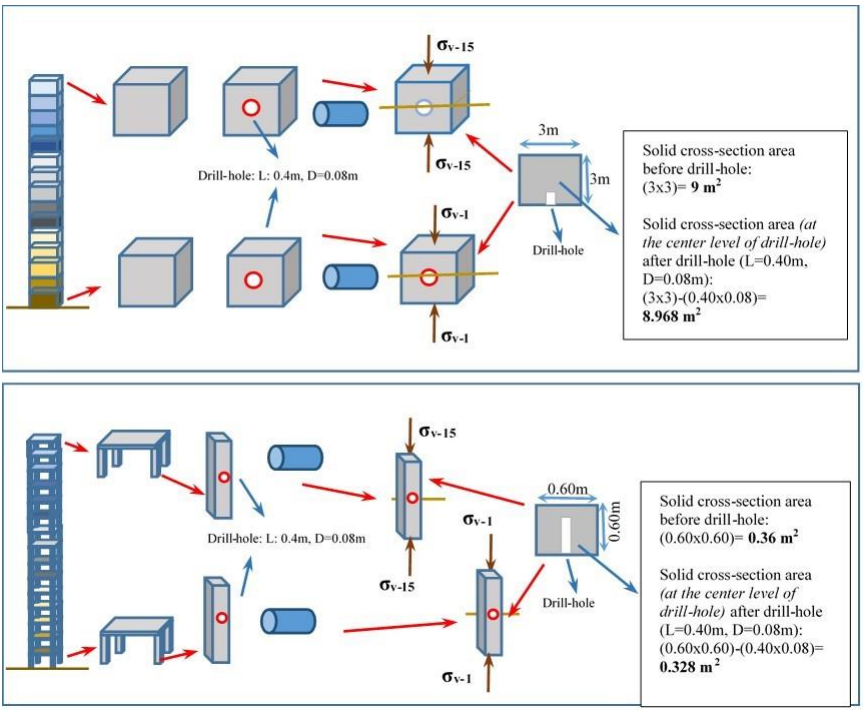

Figure 7: Drill-hole sampling features which could conceptually be performed at massive marble blocks and massive marble columns.

7.Conclusions

Mechanical properties of massive rock and concrete materials can be determined by laboratory testing according to ISRM suggested methods. However, in mining and civil engineering applications, there are numerous load-bearing structural-elements which should unceasingly bear upper layers' loads. These loads are mostly static, (dead-loads), and applied through long-lasting periods. Thus creep properties of rocks (around the mining activities) and concrete types (at civil engineering structures) are the important decision factors in design works. Providing conceptual tower cases in this work was aimed to promote engineering creativities in decision conditions. Long-lasting loading cases for the samples of natural rock blocks (obelisks, monolithic huge rock blocks, dimensioned stones etc.) and concrete columns were described here in sketched figurative manners to visualise the static load concept. Conceptual towers which are assumed to be built by isolated marble blocks, columns, and slabs from surrounding stress fields help to understand rock-load-height and impacts of horizontal stresses in actual 3D stress-field conditions. The qualities of rock & concrete materials which are defining the UCS, elastic modulus, and creep behaviours of them have their influences also on their long-term stress-strain behaviours. After years of usage, if bearing-capacity differentiation controls are needed for load-carrying blocks, columns, slabs, and pillars (in civil and mining engineering applications), remote testing methods were preferred to protect intactness of the structures. Research on remote sensing instruments to predict more reliable strength properties of rock masses & structural concretes together with more comprehensive creep behaviour reasoning for rocks & concrete types will direct the near

future developments in stability controls for underground spaces *(mine galleries. tunnels, shelters, shopping centers, social-cultural-sport centres, living units, etc.)* and surface structures *(houses, apartments, bridges, dams, etc.).*

References

Aaron, A. (2016) Moving the stones of Baalbek–The wonders of Roman engineering, Webpage: (https://gilgamesh42.wordpress.com/2013/04/25/moving-the-stones-of-baalbek-the-wonders-of-roman-engineering/), Posted on Apr. 25th, 2016, Fleeing Nergal, Seeking Stars, Retrieved in May 2024.

Aydan, O., Akagi, T. and Kawamoto, T. (1993) The squeezing potential of rocks around tunnels; theory and prediction.

J. Rock Mech. Rock Eng., 26, 2, pp137-163.

Barton, N., Lien, R. and Lunde, J. (1974) Engineering classification of rock masses for the design of tunnel support, *Rock Mechanics*, 6, pp189-236.

Brantut, N., Heap, M.J., Meredith, P.G. and Baud, P. (2013) Time-dependent cracking and brittle creep in crustal rocks: a review.

J. Struct. Geology, 52, pp17-43.

Brier, B. (2021) *Cleopatra's Needles, The Lost Obelisks of Egypt.* Bloomsbury Academic Press. UK, p238.

Britanica, (2024) Obelisk of Theodosius in the Hippodrome at Constantinople (now Istanbul), Web page: www.britannica.com/technology/hippodrome-architecture. Retrieved in Apr. 2024.

Childress, D.H. (2019) *Obelisks, Towers of power*, Advantures unlimited press, Kempton, Ilinois, US.

Crkvenjakov, V. (2016) The obelisk of Theodosius in Constantinople, *Axio*s, Skopje, Republic of Macedonia, 1, pp196.

Frenelus, W., Peng, H., and Zhang, J. (2022) Creepbehavior of rocks and its application to the long-term stability of deep roc tunnels, *Applied Sciences, MDPI*, 2022, 12, 8451, doi: 10.3390/app 12178451.

Hagros ,A., Johanson, E. and Hudson, J.A. (2008) Time dependency in the mechanical properties of crystalline rocks: A literature survey. Possiva OY, Finland.

Hoseyni, M., Dabanli, O., and Hejazi, M. (2022) Comparison of the structural behaviour of monolithic and masonry obelisks: Obelisk of Theodosius and Walled Obelisk in Istanbul, Engineering failure analysis. 142, 106744.

Hudson, J.A. and Harrison, J.P. (1997) Engineering rock mechanics-An introduction to the principles. Elsevier, Oxford.

Einstein, H.H. (1996) Tunnelling in difficult ground-swelling behaviour and identification of swelling rocks. J. Rock Mech. Rock Eng., 29, 3, pp113-124.

Innocente, J.C., Paraskevopoulou, C., and Diederichs, M.S. (2021) Estimating the long-term strength and time-to-failure of brittle rocks from laboratory testing, Int., J. Rock Mech. & Mining Sci. 147, 104900, doi: 10.1016/j.ijrmms.2021.104900.

Lewis, M.J.T. (1984) Roman methods of transporting and erecting obelisks, Trans. of the Newcomen Society, 56, 1, pp87-110.

Malan, D.F., Vogler, U.W. and Drescher, K. (1997) Time-dependent behaviour of hard rock in deep level gold mines. J. South Afr. Inst. Min. Metall., 97, pp135-147.

McGarr, A. and Gay, N.C. (1978) State of stress in the earth's crust, Ann. Rev. Earth Planet. Sci., 6, pp405-436.

Osgoui, R.R. (2007) Development of an elasto-plastic analytical model for design of grouted rock bolts in tunnels with particular reference to poor rock masses, *PhD Thesis,* The Graduate School of Natural & Applied Sciences, Middle East Technical University, Ankara, Turkey, p223.

Paraskevopoulou, C. (2016) Time-dependency of rocks and implications associated with tunnelling. *PhD. Thesis,* Dept. of Geo. Sci. and Geo. Eng., Queen's University, Kingston, Ontario, Canada

Paraskevopoulou, C., Perras, M., Diederichs, M., Loew, S., Lam, T., and Jensen, M. (2017) Time-Dependent Behaviour of Brittle rocks Based on Static Load Laboratory Tests, *Geotech Geol Eng*., doi:10.1007/s10706-017-0331-8.

Polat, G. and Saygili, O. (2020) Structural evaluation for the preservation of an ancient Egyptian obelisk in Istanbul, Turkey, *Bulletin of earth science, Yerbilimleri*, 41, 2, pp169-182.

Saleh, A.M., Mourad, S.A., Elanwar, H.H., Metwally, O.K., Zeidan, E., Adam, M.A., Ameen, M.F., Helal, K.R., Sholqamy, M.S., Allam, H.E., Ismael, M.A., Mostafa, K.A., Helal, H.M., Elbanhawy, A.Y., Grosse, C.U., Bakhoum, M.M., Farag, M.M., Matar, H.B., Eltobgy, H.H., Moharram, M.I., Marzouk, M.M., Metawie, M.S., Ali, M.R., Sayed, A.N., Mohamed, M.G., Elkarmoty, M.M., (2023) The restoration and erection of the world's first elevated obelisk, Scientific Reports, Nature portfolio,13, 2065.

Singh, D.P. (1975) A study of creep of rocks. *Int. J. Rock Mech. Sci.&Geomechics*, 12, pp271–276.

Terzaghi, K. (1946) *Rock defects and loads on tunnel supports.* in Rock Tunneling with Steel Supports, (eds R.V. Proctor

and T.L. White) 1, pp17-99. Commercial Shearing and Stamping Co. Youngstown, OH, US.

Traquair, R. and Wace, A.J.B. (1909) The base of the obelisk of Theodosius, *The journal of Hellenic studies,* 29, 1, pp60-69.

Uzbas, M. & Gokay, M.K. (2023), Influence of drill-holes on moulded column-like test samples' surface displacements: Digital image correlation analyses, *Chapter in; Innovative approaches in civil engineering, and management watershed-based water resources,* (Ed. Kumbasaroglu, A.), pp93-134, Bidge Publication, ISBN 978-625-6707-27-6, Ankara, Turkey.

Weaver, S.H. (1936) Creep curve of steel. *Trans. Am. Soc. Mech. Eng.*, LVIII, pp745–751.

Wikipedia, (2024a*)* Baalbek stones, Webpage: https://en.wikipedia.org/w/index.php?title=Baalbek_Stones&oldid=1193818487, Retrieved in May 2024.

Wikipedia, (2024b) Obelisk, Webpage: https://en.wikipedia.org/wiki/obelisk, Retrieved in May 2024..

CHAPTER V

Simulating the Behavior of Some Building Materials Using Octave 8.3.0 Program

Ehab FARHAN[1]

Introduction

The concept of building materials is the use of the appropriate material in appropriate construction, and it is revealed through tests, as the behavior of building materials changes as the external influence on them changes. The economic factor also plays a role in choosing building materials (Hamad, 2015).

[1] 1Ehab Farhan, Kütahya Dumlupınar University, Institute of Graduate Education, Department of Civil Engineering, ehab.farhan@ogr.dpu.edu.tr. Orcid id - 0009-0006-7087-6667.

Large quantities of steel plates are produced at a low cost and then used in construction and in various other industries. These steel plates are characterized by high flexibility, so that the parts produced can be solid and have a good strength-to-weight ratio (Marciniak et al., 2002). Wood is also considered one of the most widely used and oldest building materials, as it is used in construction and manufacturing because it is characterized by proportional resistance to tension and compression at the same time. It is also characterized by its abundance, light weight, poor conductivity of electricity, sound, and heat, and ease of formation (Salvadori, 1992; Attiya, 2008; Hamad, 2015). In addition, moving to renewable, carbon-storing building materials such as wood could be an important way to reduce climate change (F.A.O. United Nations, 2022). Concrete is used, which is a composite material consisting of various components, most of which consists of aggregate that combines together to form a solid mass through the cement paste surrounding it. This hardens through chemical reactions between cement and water, creating a solid structure with great compressive strength. To enhance specific properties of concrete some additives can be incorporated in small proportions (Imam, 2005; Saudi Arabia 104 Million, 2008).

The study used Octave 8.3.0, a high-level compiled language specifically designed for scientific computing. Octave provides solutions to linear and non-linear numerical problems with the possibility of providing scientific simulations, in addition to facilitating various numerical experiments. It has comprehensive graphical features for data visualization and manipulation. Although it is primarily used through an interactive command line interface, it also allows non-interactive software development. The Octave

language bears a striking resemblance to Matlab, allowing functions created in Octave to be used seamlessly in Matlab (Eaton, 2012; Lachniet, 2020).

The main objective of simulating the behavior of building materials using tools such as Octave is to better and more accurately understand and improve the performance and design of materials and structures, provide a means to test and analyze the behavior of materials under different conditions, and reduce the costs and risks associated with the design and implementation of engineering projects.

Materials and Method

Simulating the behavior of building materials is the process of analyzing and designing mathematical models that help us understand how materials interact with various factors in the environment and how their properties change over time. Using computer programs such as Octave is a powerful tool for creating mathematical models to simulate this behavior. In this study:

Let's assume we have a steel plate with the following parameters:

- Length of the plate (L) = 2 meters.
- Width of the plate (W) = 0.2 meters.
- Thickness of the plate (T) = 0.01 meters.
- Uniformly distributed load on the plate (q) = 1000 Newtons per meter.

We will use the Euler-Bernoulli theory for thin plates to calculate the plate's deflection:

W(x) = (q / (24 * E * I)) * x^2 * (L^2 - x^2)

Where:

- W (x) is the deflection of the plate at location xx.
- E is the Young's Modulus of steel.
- I is the moment of inertia of the plate.
- To calculate the deflection of the steel plate and plot the results using Octave 8.3.0, we will use the following function (Fig. 1).

```
octave:1> % Data
octave:1> L =               % Length of the plate (meters)
octave:2> W =               % Width of the plate (meters)
octave:3> T =               % Thickness of the plate (meters)
octave:4> q =               % Distributed load (Newtons per meter)
octave:5> E =               % Young's Modulus of steel (Pascals)
octave:6> % Calculate the moment of inertia I
octave:6> I = (W * T^3) / 12;
octave:7> % Calculate the plate deflection
octave:7> x = linspace(0, L, 100); % Divide the plate into small segments
octave:8> w = (q / (24 * E * I)) * (x.^2 .* (L^2 - x.^2));
octave:9> % Plot the deflection
octave:9> plot(x, w);
octave:10> xlabel('Location (meters)');
octave:11> ylabel('Plate Deflection (meters)');
octave:12> title('Plate Deflection under a Distributed Load');
octave:13> grid on;
```

Figure 1The function that was created on the Octave 8.3.0 program to calculate and plot the results of the steel plate deflection values.

Let's assume we have a wooden rod with the following parameters:

- •The original length of the wooden rod (L0) = 5 meters.
- •The coefficient of linear thermal expansion for wood (α) = 2.5 × 10^-6 per degree Celsius.

- •The temporal change in temperature (ΔT) over time (starting from 0 degrees Celsius and increasing by 10 degrees every second).

We want to calculate the change in the length of the wooden rod when temperature changes over time with a drawing. We can use the thermal expansion equation:

$\Delta L(t) = L0 * \alpha * \Delta T(t)$

Where:

- •ΔL (t) is the change in length at time t.
- •L0 is the original length of the rod.
- •α is the coefficient of linear thermal expansion.
- •ΔT (t) is the temporal change in temperature at time t.

We will use Octave 8.3.0 to calculate and plot the change in length of a wooden rod over time (Fig. 2)**.**

```
octave:1> % Data
octave:1> L0 =                % Original length of the wooden rod (meters)
octave:2> alpha =             % Coefficient of linear thermal expansion for wood (1/°C)
octave:3> time =              % Time array from 0 to 10 seconds with a 1-second increment
octave:4> delta_T =           % Temporal change in temperature over time (degrees Celsius)
octave:5>
octave:5> % Calculate the change in length over time
octave:5> delta_L = L0 * alpha * delta_T;
octave:6>
octave:6> % Plot the change in length over time
octave:6> plot(time, delta_L);
octave:7> xlabel('Time (seconds)');
octave:8> ylabel('Change in Length (meters)');
octave:9> title('Change in Length of the Wooden Rod over Time Due to Temperature Change');
octave:10> grid on;
```

Figure 2 The function was created in the Octave 8.3.0 program to calculate and plot the results of the change in the length of the wooden rod over time.

Let's assume we have a sample of concrete with the following parameters:

- Initial temperature (T0) = 25°C.
- Thermal conductivity of concrete (K) = 1.0 watts per meter Kelvin.
- Sample mass (m) = 10 kg.
- Specific heat capacity of concrete (C) = 0.8 watts per kelvin.
- Change in environmental temperature (ΔT) = 10°C.
- Time (t) starts at 0 and extends up to 60 minutes in 1-minute time steps.

We will use the heat transfer equation to calculate the temperature change of the concrete sample over time:

$$T(t) = T0 + (\Delta T / (m * c)) * (1 - e^{(-k * t / (m * c))})$$

Where:

•T(t) is the temperature at time t.

•T0 is the initial temperature.

•ΔT is the change in temperature.

•m is the mass of the sample.

•C is the specific heat capacity of concrete.

•K is the thermal conductivity.

•e is the natural number (approximately 2.71828).

We will use Octave 8.3.0 to calculate the change in temperature of the concrete sample over time and plot the results (Fig. 3).

```
octave:1> % Data
octave:1> T0 =               % Initial temperature (degrees Celsius)
octave:2> k =                 % Thermal conductivity (Watt/meter-Kelvin)
octave:3> m =                 % Mass of the sample (kilograms)
octave:4> c =                 % Specific heat capacity of concrete (Watt/Kelvin)
octave:5> delta_T =           % Temperature change (degrees Celsius)
octave:6> time =              % Time from 0 to 60 minutes with one-minute time steps
octave:7>
octave:7> % Calculate temperature over time
octave:7> T = T0 + (delta_T / (m * c)) * (1 - exp(-k * time / (m * c)));
octave:8>
octave:8> % Plot temperature over time
octave:8> plot(time, T);
octave:9> xlabel('Time (minutes)');
octave:10> ylabel('Temperature (degrees Celsius)');
octave:11> title('Temperature Change in Concrete Sample over Time');
octave:12> grid on;
```

Figure 3 The function that was created on the Octave 8.3.0 program to calculate and plot the results of the change in temperature of the concrete sample over time.

3. Result

After calculating the deflection of the steel plate and plotting the results using the Octave function 8.3.0 (Fig. 4) and (Fig. 5).

It was found that when a distributed load is applied to the steel plate, we see that the deflection value begins to increase until it reaches a certain point (peak point), and then the deflection value decreases after that.

```
octave:1> % Data
octave:1> L = 2;           % Length of the plate (meters)
octave:2> W = 0.2;         % Width of the plate (meters)
octave:3> T = 0.01;        % Thickness of the plate (meters)
octave:4> q = 1000;        % Distributed load (Newtons per meter)
octave:5> E = 2.1e11;      % Young's Modulus of steel (Pascals)
octave:6> % Calculate the moment of inertia I
octave:6> I = (W * T^3) / 12;
octave:7> % Calculate the plate deflection
octave:7> x = linspace(0, L, 100); % Divide the plate into small segments
octave:8> w = (q / (24 * E * I)) * (x.^2 .* (L^2 - x.^2));
octave:9> % Plot the deflection
octave:9> plot(x, w);
octave:10> xlabel('Location (meters)');
octave:11> ylabel('Plate Deflection (meters)');
octave:12> title('Plate Deflection under a Distributed Load');
octave:13> grid on;
```

Figure 4 This function calculates the deflection of the steel plate along its length and plots the results.

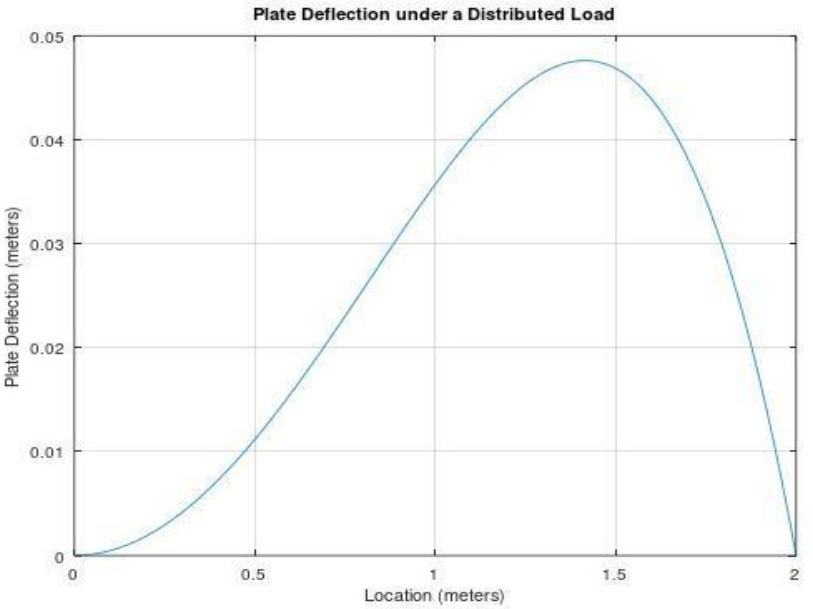

Figure 5 Simulating the deflection of a steel plate under the influence of a distributed load.

After calculating and plotting the change in the length of the wooden rod over time when exposed to increasing temperatures using a function in Octave 8.3.0 program (Fig. 6) and (Fig. 7).

It was found that exposing the wooden rod to increasing temperatures over time leads to an increase in the length of the wooden rod.

```
octave:1> % Data
octave:1> L0 = 5;              % Original length of the wooden rod (meters)
octave:2> alpha = 2.5e-6;      % Coefficient of linear thermal expansion for wood (1/°C)
octave:3> time = 0:1:10;       % Time array from 0 to 10 seconds with a 1-second increment
octave:4> delta_T = 10 * time; % Temporal change in temperature over time (degrees Celsius)
octave:5>
octave:5> % Calculate the change in length over time
octave:5> delta_L = L0 * alpha * delta_T;
octave:6>
octave:6> % Plot the change in length over time
octave:6> plot(time, delta_L);
octave:7> xlabel('Time (seconds)');
octave:8> ylabel('Change in Length (meters)');
octave:9> title('Change in Length of the Wooden Rod over Time Due to Temperature Change');
octave:10> grid on;
```

Figure 6 This function calculates the change in length of a wooden rod over time due to temperature changes and plots the results.

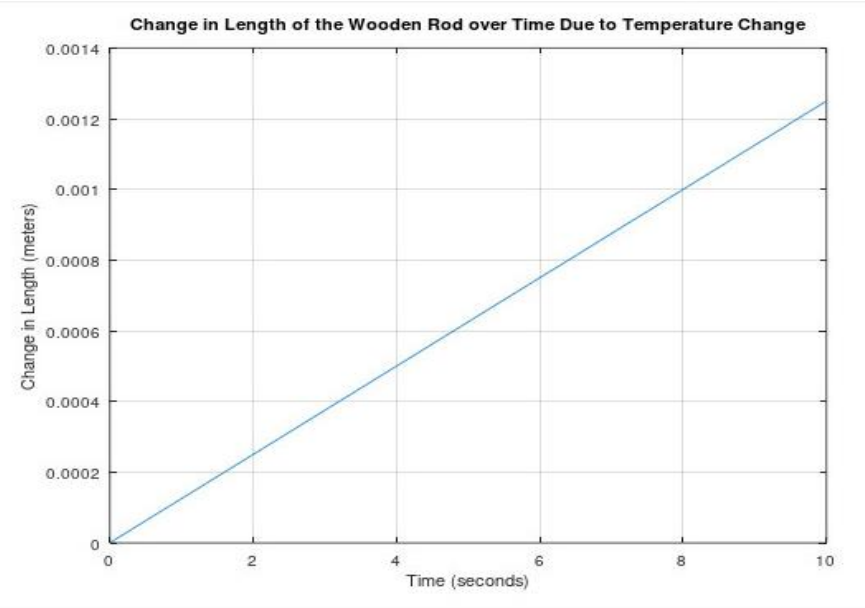

Figure 7 Simulating the change in length of the wooden rod over time due to temperature change.

After calculating the change in temperature of the concrete sample over time when exposed to increasing temperatures of the external environment and plotting the results using a function in the Octave 8.3.0 program (Fig. 8) and (Fig. 9).

It was found that when the temperature of the surrounding environment is higher than the temperature of the concrete sample, this will lead to the temperature of the concrete sample rising over time until it reaches the temperature level of the surrounding environment.

```
octave:1> % Data
octave:1> T0 = 25;           % Initial temperature (degrees Celsius)
octave:2> k = 1.0;            % Thermal conductivity (Watt/meter-Kelvin)
octave:3> m = 10;             % Mass of the sample (kilograms)
octave:4> c = 0.8;            % Specific heat capacity of concrete (Watt/Kelvin)
octave:5> delta_T = 10;       % Temperature change (degrees Celsius)
octave:6> time = 0:60;        % Time from 0 to 60 minutes with one-minute time steps
octave:7>
octave:7> % Calculate temperature over time
octave:7> T = T0 + (delta_T / (m * c)) * (1 - exp(-k * time / (m * c)));
octave:8>
octave:8> % Plot temperature over time
octave:8> plot(time, T);
octave:9> xlabel('Time (minutes)');
octave:10> ylabel('Temperature (degrees Celsius)');
octave:11> title('Temperature Change in Concrete Sample over Time');
octave:12> grid on;
```

Figure 8 This function calculates the temperature change in a concrete sample over time and plots the results.

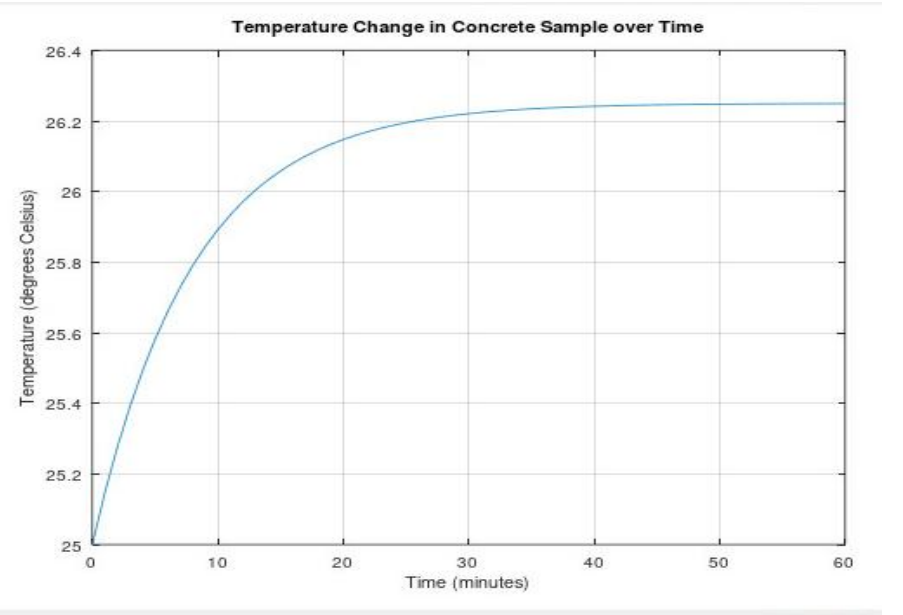

Figure 9 Simulating temperature change in concrete sample over time.

4. Discussion

When the distributed load is applied to the steel plate, we see that the value of the deflection begins to increase until it reaches a certain point (the peak point). Then the deflection value decreases after the peak point. This is because the steel plate begins to twist or bend in the opposite direction after exceeding the maximum bending peak.

Exposing the wooden rod to increasing temperatures over time leads to an increase in its length. This is due to a natural property known as “heat diffusion”. As the temperature of the external environment increases, expansion occurs in the wooden rod, which leads to an increase in its length due to the increased movement and spacing of the particles of the wooden material.

When the temperature of the surrounding environment is higher than the temperature of the concrete sample, this leads to an increase in the temperature of the concrete sample until its temperature reaches the level of the temperature of the surrounding environment over time. This is due to the thermal conductivity property of the material. That is, an increase in the temperature of the external environment leads to the transfer of heat to the concrete sample, and its temperature begins to rise until it stabilizes when it reaches the same temperature as the external environment.

5. Conclusion

Through the results of this study, it became clear after conducting a simulation of the behavior of a group of building materials using the Octave 8.3.0 program that:

When we place a distributed load on the steel plate, we notice that the deflection value gradually increases until it reaches a point

known as the peak point. After this point, the steel plate begins to twist or bend in the opposite direction, which leads to the deflection value beginning to decrease.

When the wooden rod is exposed to increasing temperatures over time, this leads to a change in its length. As high temperatures cause an increase in the length of the wooden rod as a result of its expansion. This is due to a natural property known as "heat diffusion" that increases the movement and spacing of molecules within the wood material.

When the external ambient temperature is higher than the temperature of the concrete sample. This will cause the temperature of the concrete sample to rise over time until it reaches the outside ambient temperature, at which point the temperature of the concrete sample will stabilize. This is due to the thermal conductivity property of the material.

References

Attia, A. (2008). *Technology of natural building materials*. Cairo: International House for Publishing and Distribution.

Eaton, J. (2012). GNU Octave and reproducible research. *Journal of Process Control*, *22*(8), 1433-1438.

Food and Agriculture Organization of the United Nations. (2022). *State of the world's forests.*

Hamad, S. (2015). *The effect of building materials on the choice of construction sentence (A case study of public buildings in Syria)*. Damascus University. Syria.

Imam, M. (2005). *Concrete properties - quality - tests*. Cairo: Al Noor Library.

Kingdom of Saudi Arabia. Technical and Vocational Training Corporation. General Administration for Curriculum Design and Development. (2008). *Civil technology specializes in the properties and tests of materials in 104 mdn.*

Lachniet, J. (2020). *Introduction to GNU Octave*. Wytheville, Virginia :Wytheville Community College.

Marciniak, Z., Duncan, J. L., & Hu, S. J. (2002). *Mechanics of sheet metal forming*. Oxford: Elsevier Science.

Salvadori, M. (1992). *The struggle against Earth's gravity from tents to skyscrapers*. Beirut: Dar Al Shorouk.


BİDGE